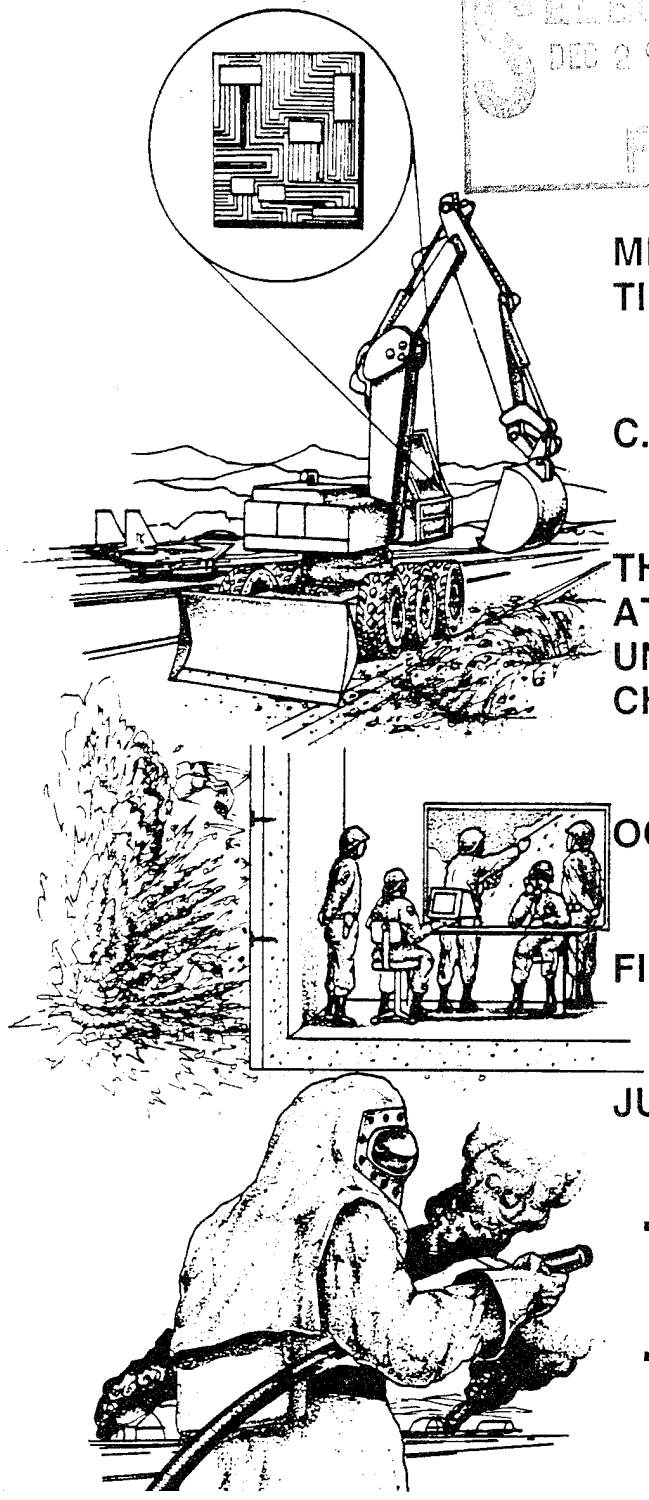

ESL-TR-91-17

MEASURE OF CREEP CHARACTERISTICS OF ASPHALT CONCRETE

C. LIU

THE UNIVERSITY OF NORTH CAROLINA
AT CHARLOTTE
UNCC STATION
CHARLOTTE NC 28223

OCTOBER 1995

FINAL REPORT

JULY 1988 - MAY 1991

APPROVED FOR PUBLIC RELEASE:
DISTRIBUTION UNLIMITED

ENGINEERING RESEARCH DIVISION
Air Force Civil Engineering Support Agency
Civil Engineering Laboratory
Tyndall Air Force Base, Florida 32403

NOTICE

PLEASE DO NOT REQUEST COPIES OF THIS REPORT FROM HQ AFCESA/RA (AIR FORCE CIVIL ENGINEERING SUPPORT AGENCY). ADDITIONAL COPIES MAY BE PURCHASED FROM:

NATIONAL TECHNICAL INFORMATION SERVICE
5285 PORT ROYAL ROAD
SPRINGFIELD, VIRGINIA 22161

FEDERAL GOVERNMENT AGENCIES AND THEIR CONTRACTORS REGISTERED WITH DEFENSE TECHNICAL INFORMATION CENTER SHOULD DIRECT REQUESTS FOR COPIES OF THIS REPORT TO:

DEFENSE TECHNICAL INFORMATION CENTER
CAMERON STATION
ALEXANDRIA, VIRGINIA 22314

DISCLAIMER NOTICE

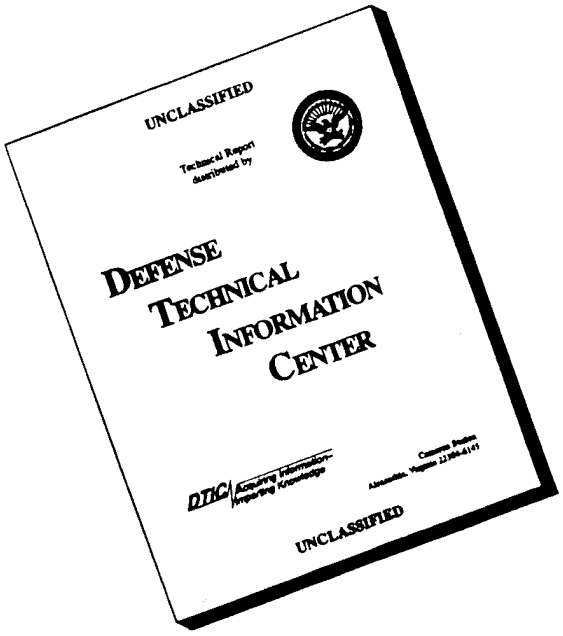

THIS DOCUMENT IS BEST QUALITY AVAILABLE. THE COPY FURNISHED TO DTIC CONTAINED A SIGNIFICANT NUMBER OF PAGES WHICH DO NOT REPRODUCE LEGIBLY.

REPORT DOCUMENTATION PAGE

Form Approved
OMB No. 0704-0188

1. AGENCY USE ONLY (Leave blank)	2. REPORT DATE	3. REPORT TYPE AND DATES COVERED
	October 1995	FINAL 1 JULY 1988 - 31 MAY 1991

4. TITLE AND SUBTITLE

MEASURE OF CREEP CHARACTERISTICS OF ASPHALT CONCRETE

5. FUNDING NUMBERS

PE 63723F
PR 2104
TA 30
WU 32

6. AUTHOR(S)

LIU, CHENG

7. PERFORMING ORGANIZATION NAME(S) AND ADDRESS(ES)

THE UNIVERSITY OF NORTH CAROLINA AT CHARLOTTE
UNCC STATION
CHARLOTTE NC 28223

8. PERFORMING ORGANIZATION REPORT NUMBER

9. SPONSORING / MONITORING AGENCY NAME(S) AND ADDRESS(ES)

AIR FORCE CIVIL ENGINEERING SUPPORT AGENCY
139 BARNES DRIVE
TYNDALL AFB FL 32403-5319

10. SPONSORING / MONITORING AGENCY REPORT NUMBER

ESL-TR-91-17

11. SUPPLEMENTARY NOTES

12a. DISTRIBUTION / AVAILABILITY STATEMENT

APPROVED FOR PUBLIC RELEASE
DISTRIBUTION UNLIMITED
AVAILABILITY SPECIFIED ON REVERSE OF FRONT COVER

12b. DISTRIBUTION CODE

13. ABSTRACT *(Maximum 200 words)*

THIS RESEARCH SOUGHT TO EVALUATE THE SHELL PROCEDURE AS A TOOL FOR PREDICTING RUTTING OF ASPHALT MIXTURES UNDER SIMULATED F-15 TRAFFIC. HALF THE ASPHALT MIXTURES USED FOR THE TEST SECTIONS WERE DESIGNED WITH MARSHALL PROCEDURES AND THE BALANCE WITH THE GYRATORY TESTING MACHINE. PREDICTIONS OF RUTTING OF BOTH MIXTURES WERE MADE WITH SAMPLES FROM THE PAVER AND FROM CORES EXTRACTED FROM THE MAT. CREEP CHARACTERISTICS WERE OBTAINED WITH UNCONFINED STATIC AND DYNAMIC TESTING IN THE LABORATORY.

ALTHOUGH THE RUTTING POTENTIAL OF ASPHALT MIXTURES USED IN THIS STUDY COULD BE QUALITATIVELY RANKED RELATIVE TO EACH OTHER, THE SHELL PROCEDURES, USING STATIC OR DYNAMIC TESTING, DID A MEDIOCRE JOB OF QUANTIFYING THE RUT DEPTHS PRODUCED IN THIS TEST. DYNAMIC TESTS TENDED TO UNDERESTIMATE THE RUT; STATIC TESTS OVER PREDICTED RUTTING OF THE GYRATORY-DESIGNED MIXTURES AND UNDERESTIMATED RUTTING OF MARSHALL MIXTURES. PREDICTION OF THE RUT DEPTH MAY BE ONLY OF ACADEMIC INTEREST, ANYWAY. THE REAL NEED IS TO PREVENT RUTTING.

14. SUBJECT TERMS

DESIGN OF ASPHALT MIXTURES
RUT PREDICTION
CREEP TESTING

15. NUMBER OF PAGES

123

16. PRICE CODE

17. SECURITY CLASSIFICATION OF REPORT	18. SECURITY CLASSIFICATION OF THIS PAGE	19. SECURITY CLASSIFICATION OF ABSTRACT	20. LIMITATION OF ABSTRACT
UNCL	UNCL	UNCL	

(The reverse of this page is blank.)

EXECUTIVE SUMMARY

The purpose of this study was to evaluate the Shell rut prediction model for asphalt layer under traffic of an F-15C/D fighter aircraft. To meet the objectives of this research, the Air Force Engineering and Services Center constructed flexible and composite pavement test sections for accelerated aircraft traffic. Half of the asphalt mixtures used on the subject test sections were designed with the gyratory testing machine developed by the Corps of Engineers. The conventional Marshall method was used to design the balance of test section mixtures.

The test sections were trafficked with two loadings, which were intended to simulate fully loaded and unarmed F-15C/D fighter aircraft, in a normal distribution transverse to the center line. The speed, transverse and longitudinal location, and dynamic loading of the traffic for each wheel load passing along with the temperature of the test sections during trafficking were recorded. The surface profile parameters used to quantify pavement damage under traffic were obtained with a Rainhart Profilometer. Only the true rut depth, which is the greatest measured displacement of the trafficked pavement surface from its original elevation, will be discussed in this report.

Two hundred and three asphalt concrete drilled cores and compacted specimens from various locations of the test sections at Tyndall AFB, Florida, were used to conduct this research. Shell unconfined, uniaxial static creep tests were performed on 177 drilled cores and compacted specimens. Twenty six drilled cores were subjected to unconfined, uniaxial dynamic creep tests. Data from both static and dynamic creep tests were used to develop creep curves which are characteristic of the permanent deformation behavior of the asphalt mixes tested. This can be achieved by expressing the results of the creep test as the stiffness modulus of the asphalt mix (S_{mix}) as a function of the stiffness modulus of the bitumen (S_{bit}). The result of the creep test were presented on a log-log plot of S_{mix} versus S_{bit}. The resulting characteristic curve is known as the creep curve.

Rut depth predictions based on both static and dynamic creep curves were made using the Shell procedure. Rut depth predictions were then compared with field rut measurements at various numbers of wheel passes. It is clear that rutting predictions based on dynamic creep curves tended to underestimate the rut depths actually developed in both gyratory and Marshall design mixtures. Furthermore, it appears that for this particular Marshall mixture, the rut depth predictions based on static creep curves seem to over-predict rutting for less than approximately 1000 wheel passes and under-predict rutting for more than 1000 wheel passes. On the other hand, for gyratory mix, rut depth predictions based on static creep curves tended to over estimate the rut depths actually developed in the field at all traffic levels.

(The reverse of this page is blank.)

PREFACE

This report was prepared by the University of North Carolina at Charlotte (UNCC), funded under Contract Number F08635-88-C-0206 by the Air Force Civil Engineering Support Agency, Civil Engineering Laboratory, Tyndall Air Force Base, Florida 32403-5319.

This report covers work performed between 1 July 1988 and 31 May 1991. The AFCESA/RD project officer was Jim Murfee.

This report has been reviewed by the Public Affairs Office and is releasable to the National Technical Information Service (NTIS). At NTIS, it will be available to the general public, including foreign nationals.

This technical report has been reviewed and is approved for publication.

JIM MURFEE, GS-13
Project Officer

FELIX T. UHLIK III, Lt Col, USAF
Chief, Air Base Systems Branch

EDGAR F. ALEXANDER, GM-14
Chief, Air Base Operability and
Repair Section

Accesion For	
NTIS CRA&I	☑
DTIC TAB	☐
Unannounced	☐
Justification	
By	
Distribution /	
Availability Codes	
Dist	Avail and / or Special
A-1	

(The reverse of this page is blank)

TABLE OF CONTENTS

LIST OF FIGURES

LIST OF FIGURES
(CONTINUED)

LIST OF FIGURES
(CONTINUED)

LIST OF FIGURES
(CONCLUDED)

LIST OF TABLES

LIST OF TABLES
(CONTINUED)

LIST OF TABLES
(CONCLUDED)

SECTION I

INTRODUCTION

A. OBJECTIVE

The objective of this research was to evaluate the Shell rut prediction model for asphalt layers under accelerated traffic of an F-15C/D fighter aircraft.

B. BACKGROUND

With increasing wheel load passes on a single wheel path, rutting in asphalt concrete develops gradually. It generally appears as a longitudinal depression in the wheel path. Rutting, or the permanent deformation of asphalt pavement, is caused by:

1. Traffic densification of paving mixes in the wheel paths,

2. Plastic deformation or lateral movement of asphalt material from below the wheel paths due to insufficient mix stability, and,

3. Wear or erosion of surface material under traffic.

A considerable amount of national research has been directed toward developing test systems which will predict rutting of flexible pavements, but nearly all of this has resulted in promotion of complicated analytical procedures and expensive laboratory apparatus and procedures (1). As the result of the recent research effort, several rut prediction models are available for flexible pavements. Some of them are (a) the Shell Procedure, (b) the VESYS Subsystem, (c) the Monismith, Barksdale and others, and (d) the Mechano-Lattice Method. All of them include analytical procedures for predicting permanent rut depth of the flexible pavement as well as laboratory tests of the asphalt mix which are used to assess the resistance of asphalt mix to permanent deformation. The Shell Procedure utilizes layer-strain concepts and is considered to be machanistic and empirical. It uses elastic theory to calculate stress distribution under a moving wheel. The Shell Method uses data from unconfined, uniaxial creep tests to predict rutting in the asphalt layer. The VESYS method characterizes the asphalt mixture by uniaxial repetitive loading compression tests. The Monismith, Barksdale and others use the repeated load triaxial compression test as does the Mechano-Lattice Method to characterize the asphalt mixture.

The Shell Procedure was used in this study to predict rutting in the asphalt layers. It has been evaluated over a 5-year period with favorable results by the North Dakota Highway Department and is generally considered to be relatively uncomplicated, inexpensive, and most easily adapted to existing laboratory equipment.

To meet the objectives of this research, the Air Force Engineering and Services Center prepared (Figure 1) flexible and composite pavement test sections for accelerated aircraft traffic. The flexible sections were comprised of 4-and 6-inch layers of asphalt concrete pavement over 12 inches of aggregate base and natural dune sand subgrade. The composite sections were 6 inches of asphalt mixture over 12 inches of Portland cement concrete. For the 6-inch sections, a 2-inch compacted lift was initially placed and compacted. This was followed by a tack coat and a final 4-inch compacted lift, which also paved the 4-inch sections. According to pavement type and method of compaction, each lane was divided into six test sections. Section number, type of underlaid base course, method of compaction and thickness of asphalt cement concrete for each section are listed in Table 1. All rut depth comparisons reported in this paper will refer to the 6-inch lift of asphalt concrete over Portland cement concrete.

Half of the asphalt mixtures used on the subject test sections were designed with the gyratory testing machine (GTM) developed by the Corps of Engineers at the Waterways Experiment Station, following the procedures of ASTM D 3387. The gyratory design for these test sections was accomplished with compaction pressure of 300 psi, an angle of gyration of 1 degree, and a gyratory stability index (GSI) determined from stabilities after 30 and 60 revolutions. The widely used 75-blow Marshall method (Military Standard 620A, Method 100) was used to design the balance of test section mixtures.

Traffic was applied while the temperature 3 inches deep in the asphalt ranged between 95 and 130 degrees F. The mean temperature at this depth was 104 degrees F during traffic. These test sections were trafficked with fighter aircraft wheel loadings of 29,500 and 19,500 lbs having tire inflation pressures of 355 and 195 psi, respectively. The two loadings, which were intended to simulate fully loaded and unarmed F-15C/D fighter aircraft, were applied, back and forth, in a normal distribution transverse to the centerline. The speed, transverse and longitudinal location, and dynamic loading of the traffic were recorded for each passing of traffic. The forward and reverse speeds of the loadcart averaged 13 and 9 mph, respectively. Only the results of the fully-loaded aircraft traffic on the composite sections will be presented in this report.

The surface profile parameters used to quantify damage under traffic were obtained with a Rainhart Profilometer and are defined in Figure 2. Only the true rut depth, which is the greatest measured displacement of the trafficked surface from its original elevation, will be discussed in this report.

Since the traffic was applied in an approximately normal distribution over 40 inches transversely, the number of actual applications causing the "true rut depth" could have been 20 to 40 percent of the total traffic. Figure 3 shows the relationship, for a typical test section location, between total passes of the location and effective passes over the "true rut" at that location.

Effective traffic is defined here as the application of any portion of the load wheel over the centerline of the "true rut".

C. SCOPE/APPROACH

The three phases of the study included: (a) performing static creep tests on 177 specimens and cores obtained from the test sections at Tyndall AFB, Florida, and collecting dynamic creep test data of 26 core samples also from Tyndall test sections. (The dynamic creep tests were performed at the Tyndall Laboratory and the data were furnished by the Air Force), (b) using the test data to predict rut depths at various levels of trafficking; the Shell model for predicting rutting in asphalt layers was used, (c) comparing the rutting predicting of the test sections and the field rut depth measurements. Figures and tables were separated from the text and were presented at the end of this report.

SECTION II

THE CREEP TEST

A. GENERAL

In 1978, the Shell International Petroleum Company published the Shell Pavement Design Manual for the structural design of asphalt pavements. Incorporated into their basic design procedure is a method of estimating the permanent deformation (i.e. rut depth) of the asphalt concrete pavements. In the method proposed, the deformation characteristics of an asphalt concrete pavement are assessed by means of an unconfined, uniaxial compression test on asphalt concrete specimens. This test is known as the creep test. The purpose of the creep test is to evaluate the deformation properties of an asphalt paving mix in terms of quantities which are independent of the external parameters of stress and temperature. This can be achieved by expressing the results of the creep test as the stiffness modulus of the asphalt mix (S_{mix}) as a function of the stiffness modulus of the bitumen (S_{bit}). The results of the creep test are represented on a log-log plot of S_{mix} vs. S_{bit}. The resulting characteristic curve is known as the creep curve. The creep curve is independent of operating parameters, such as stress, temperature, time of loading, etc., and may thus be regarded as a true mix characteristic. (1)

S_{mix} is defined as:

$$S_{mix} = \frac{\sigma_{mix}}{\varepsilon_{mix}} \qquad (1)$$

where:

σ_{mix} = stress applied to the specimen (N/m^2)
ε_{mix} = axial strain measured = $\Delta H/H_o$
ΔH = change in specimen height
H_o = initial height of specimen

The stiffness modulus of the bitumen (S_{bit}) is a function of temperature, loading time, the bitumen properties T_{800pen} and Penetration Index (PI). Values of S_{bit} are found using Van der Poel's nomograph (see Figure 4) for a given loading time and temperature.

B. STATIC CREEP TEST (1) (3) (4)

In the static creep test, cylindrical asphalt concrete specimens were subjected to a constant uniaxial compressive stress of $10^5 N/m^2$ (i.e. 14.5 psi) under unconfined condition. The specimen deformations are measured with either a dial gauge or an electric displacement transducer equipped with recording equipment. Standard reading times of 2, 5, 10, 15, 30, 45 and 60 minutes were

used (1). The time of wheel loading on any given point along the wheel path of flexible pavements is small compared to the time of loading on a test specimen in the static creep test. Van de Loo (1974) found that relatively low stress levels-within the linear range of materials (i.e. 14.5 psi or 100 kpa)-should be used in the static creep test. The detailed test information, such as required apparatus and supplies, dimensions of test specimen, test conditions, preparation of test specimen and description of test procedure were elaborated in Appendix A of this report.

C. DYNAMIC CREEP TEST (5)

In the dynamic creep test, cylindrical asphalt concrete cores were subjected to uniaxial repeated load (under unconfined condition) with a 1/2 Hz square wave pulse. The maximum axial stress shall be 100 kpa (i.e. 14.5 psi). The specimem deformations are measured at 10, 50, 100, 500, 1000 and 3600 load repetitions. The detailed dynamic creep test information, such as required apparatus and supplies, dimensions of test specimen, test conditions, preparation of test specimens and description of test procedure were elaborated in Appendix B of this report.

SECTION III

RUTTING PREDICTION - SHELL MODEL

A. GENERAL

The permanent deformation of an asphalt pavement depends on the pavement stress conditions, duration of stress application, the asphalt layer temperature and thickness, and the asphalt paving mix composition. To predict the rut depth that would develop in an asphalt pavement after a given number of wheel load applications, the asphalt layer is subdivided into several thinner sublayers, and the stress of each sublayer directly under the moving wheel load is then calculated using the elastic method. With the stress conditions at each sublayer and the results of unconfined, uniaxial laboratory tests (i.e., a creep curve), the total permanent deformation for a given number of wheel load applications is obtained by summing the products of the plastic strain at each sublayer and the corresponding sublayer thickness.

B. PROCEDURE

The Shell Procedure for estimating the permanent deformation of an asphalt concrete pavement consists of the following steps: (1) (4)

1. The asphalt layer is subdivided into thinner layers to account for the variations in temperature with depth and to account for differences in deformation properties of the respective asphalt mixes. The total asphalt layer thickness (h_1) may vary between 80 and 400 mm. Studies by Shell have led to the conclusion that a subdivision of the total asphalt layer (h_1) into the following sublayers is sufficiently accurate:

h_{1-1} = 40 mm (top sublayer)
h_{1-2} = 40 mm (middle sublayer)
h_{1-3} = h_1-80 mm (bottom sublayer)

Since field temperatures of asphalt sublayers were not available in this study, instead of using sublayers to calculate rut depth predictions, the entire layer of asphalt pavement and its mean temperature were used to estimate rut depth predictions.

2. The deformation characteristics of the asphalt mix are expressed in the form of a creep curve which relates the stiffness modulus of the mix (S_{mix}) to the stiffness modulus of the bitumen (S_{bit}). The creep test determines the stiffness modulus of asphalt paving mix (S_{mix}). The stiffness modulus of paving mix (S_{mix}) along with the stiffness modulus of bitumen (S_{bit}), which is determined by using Van der Poel's nomograph (see Figure 4), is plotted on a log-log graph. For the calculation of the permanent deformation, the Shell Laboratory assumed and verified that the relation S_{mix} - S_{bit}, derived from the creep test, is equal to $S_{mix,visc}$ - $S_{bit,visc}$. ($S_{mix,visc} = \sigma/\varepsilon_{perm}$; $S_{bit,visc}$ is the viscous or irrecoverable component

of the bitumen stiffness, which is responsible for the permanent deformation.) (6)

3. Next, the effective bitumen viscosity was determined. The bitumen viscosity depends on the asphalt temperature and on the properties of the bitumen (Penetration Index, T_{800pen}, etc.). The asphalt temperature is a function of the air temperature, which varies with the climate, the time of day, etc., and also with the location (depth) within the pavement. A nomogram (see Figure 5) can be used for determining effective bituminous viscosity.

4. The viscous component of the stiffness modulus of bitumen ($S_{bit,visc}$) is then determined. The basic equation (3) (7) for this is:

$$S_{bit.visc} = \frac{3}{\sum \frac{Wt_o}{VISC}} \qquad (2)$$

where:

W = number of wheel passes
t_o = loading time per wheel pass
VISC = bitumen viscosity (see Figure 5)

Loading time per wheel pass is a function of speed of a moving wheel and generally is assumed to be a constant. In this way, t_o can be placed before the summation sign in the Equation.

5. From the S_{mix}-S_{bit} characteristics, commonly known as creep curve, obtained from the creep test (see Step 2 above), we then read, the stiffness modulus of the asphalt paving mix (S_{mix}) for a value of S_{bit} which is equal to the value of $S_{bit,visc}$ determined in accordance with Step 4 above. These values are used directly in the estimation of permanent deformation.

6. Next, the effective stress under the moving wheel (σ_{eff}) should be determined. The term "effective stress" needs some further explanation. Under a moving wheel a complex stress situation occurs in an asphalt layer. The effective stress in a sublayer is dependent on the contact stress between tire and pavement and a number of parameters: geometry (ratio of radius of the entire contact area to the layer thickness), Poisson's ratio, and the ratios among the moduli of the various layers. To calculate the stress under the moving wheel, an elastic layer model BISAR was used in the Shell Laboratory because it was assumed that with the short loading times of the wheel ($t_o \approx 0.01$-0.1 second), asphalt behaves mainly elastically (3) (6). The effective stress was expressed as a portion of the contact stress (σ_o):

$$\sigma_{eff} = Z\,\sigma_o; \quad Z < 1 \qquad (3)$$

where:

Z = proportionality factor between effective stress and contact stress

Z was calculated as the ratio of the relative deformation ($\Delta H/H_0$) under the given conditions to the relative deformation under unconfined conditions (where $\sigma = \sigma_o$) (6)

$$Z = \frac{\Delta H/H_o}{\sigma/E} = \frac{\Delta H/H_o(E)}{\sigma} = \frac{\sigma_{eff}}{\sigma} \quad (4)$$

Where E = modulus of elasticity of the asphalt layer (i.e. S_{mix}) under the given conditions of loading time and temperature.

In other words, Z can alternatively be conceived to be the ratio of the relative reduction in layer thickness in the upper layer under the traveling wheel in the rutting test to the relative reduction in layer thickness of a specimen of the same material subjected to the creep test, under the same loading conditions as represented by σ_o (3). Shell does not use elastic theory to calculate pavement deformation, but only to determine the stress distribution under a moving wheel.

Proportionality Factor Z in the Shell Manual depends on six parameters: the subgrade modulus (E_3), thickness of the base layer (h_2), thickness of the bottom asphalt sublayer (h_{1-3}), and the stiffness moduli of the asphalt paving mix in the elastic behavior region for each sublayer (i.e. E_{1-1}, E_{1-2}, E_{1-3}). These variables are used to enter the "DATA TABLE Z" of the Shell Manual to find the appropriate Z factor (1) (4). The "DATA TABLE Z" of the Shell Manual consists of 96 pages with hundreds of tables, requiring six parameters to enter the table. However, Study Centre for Road Construction in the Netherlands (3) adopted a much simpler approach by using the BISTRO program to calculate the factor Z. The values of Z calculated with BISTRO have been plotted as a function of a/H_1 with E_2/E_1 as the parameter. (3) (7). (Here: a=radius of loaded area and H_1= layer thickness of asphalt concrete. E_2/E_1=the ratio of the moduli of elasticity of the respective layers). (See Figure 6). The Z factors used in this report were obtained from Figure 6.

7. The permanent deformation of each of the asphalt pavement sublayers is obtained by (3)

$$\Delta h = C_n \times h \times Z \times \frac{\sigma_o}{S_{mix}} \quad (5)$$

where:

Δh = rut depth

C_m = an empirical correction factor for the dynamic effect which depends on the mix type (see Table 2)

h = thickness of asphalt pavement sublayer

Z = proportionality factor (see Figure 6 and Step 6 above)

σ_o = contact pressure

S_{mix}= Stiffness Modulus of asphalt paving mix at

$S_{bit} = S_{bit,visc}$ (See Step 5 above)

The total asphalt pavement deformation is then a summation of the deformations of each sublayer.

SECTION IV

LABORATORY DATA AND EVALUATION

A. STATIC CREEP TEST DATA

One hundred and seventy-seven compacted specimens and drilled cores were tested for static creep characteristics. The results of static creep tests along with the stiffness moduli of asphalt paving mix (S_{mix}) vs the stiffness moduli of bitumen (S_{bit}) were tabulated in Tables 3 through 26. S_{mix} vs S_{bit} were also plotted in Figures 7 through 30. (They are known as creep curves.)

B. DYNAMIC CREEP TEST DATA

Twenty six drilled cores were tested for dynamic creep characteristics at Tyndall AFB Laboratory. The results of dynamic creep test which were furnished by the Air Force along with the stiffness moduli of paving mix (S_{mix}) vs the stiffness moduli bitumen (S_{bit}) were tabulated in Tables 27 through 34. S_{mix} vs S_{bit} were also plotted in Figures 31 through 38.

Dynamic creep vs static creep for fully loaded F-15 and unarmed F-15 drilled cores were plotted in Figure 39 through Figure 46.

C. OTHER PERTINENT DATA

General information, such as moduli of elasticity of various layers of the test sections, time of loading (t_o), wheel load, width and length of tire imprint, average wheel speed, tire pressure, etc., for both fully loaded and unarmed F-15, were listed in Table 35. Penetration Index and Ring & Ball Softening Point of Asphalt Cement used in the test sections are -0.082 and 128°F, respectively. Those data were furnished by the Air Force.

D. CALCULATIONS OF RUT DEPTH PREDICTIONS

The predicted rut depths were calculated based on the Shell Method outlined in Section III of this report. A numerical sample calculations of rut depth predictions for the fully loaded F-15, Section 3, Station A 2+12 based on drilled cores static creep data is illustrated as follows. The mean pavement temperature of Tyndall test sections was 40°C.

$$Rut\ Depth = \frac{C_m \times H \times Z \times \sigma_o}{S_{mix}} \qquad (5)$$

where: C_m = 1.0 (from Table 2)
H = 6.39 inch
Z = 0.62 (from Figure 6)
σ_o = Wheel load/area of tire imprint

$$= \frac{29,500}{7.75 \times 14.5} = 262.5 \ psi$$

$$= 1.81 \times 10^6 \ N/m^2$$

$$S_{bit.visc} = \frac{3}{\sum \frac{Wt_o}{VISC}} \qquad (2)$$

W = 1000 passes
t_o = 0.075 sec (from Table 35)
VISC = 3.5×10^4 N-s/m^2 (from Figure 5) with $T-T_{800}$ = -13.3°C and Penetration Index = -0.082

$$S_{bit.visc} = \frac{3}{(1000)(0.075)/3.5 \times 10^4} = 1400 \frac{N}{m^2}$$

S_{mix} = 1.18×10^7 N/m^2 (from Figure 7 with $S_{bit.visc}$ = 1400 N/m^2)
Rut Depth = $(1)(6.39)(0.62)(1.81 \times 10^6)/1.18 \times 10^7$
= 0.608 inch

Rut depth predictions at various number of wheel passes for the fully loaded F-15, Sections 3 and 4, using pavement temperature of 40°C are listed in Tables 36 and 37, respectively. Rut depth predictions at various number of wheel passes for the unarmed F-15, Sections 9 and 10, also using pavement temperature of 40°C, are listed in Tables 38 and 39, respectively. The rut depth predictions were based on static creep data from both drilled cores and plant mix compacted specimens, as well as dynamic creep data from drilled cores. In Tables 36 and 37, field measurements for actual rut depth at various number of wheel passes over peak rut location are also included. The field measurements were furnished by the U.S. Air Force.

Comparison of rut depth predictions and field measurements for stations A 2+12, A 2+60, A 3+00, A 3+86, A 4+10 and A 4+40 were illustrated in Figure 47 through Figure 52. Due to lack of rut depth field measurement data, only rut depth predictions for the unarmed F-15 stations C 2+13, C 2+57, C 2+85, C 3+25, C 3+69 and C 4+15 were plotted on Figures 53 through 58.

SECTION V

CONCLUSIONS

It is clear that rutting predictions based on dynamic creep curves tended to underestimate the rut depths actually developed in both gyratory and Marshall mixtures. Furthermore, it appears that for this particularly unstable Marshall mix the rut depth predictions based on static creep curves seem to over-predict rutting for less than 1000 passes and under-predict rutting for more than 1000 passes. On the other hand, for the gyratory mix, rut depth predictions based on static creep curves tended to overestimate the rut depths actually developed in the field at all traffic levels.

Field rut depth measurements for the fully loaded F-15 Marshall mix (Section 3) and gyratory mix (Section 4) were plotted in Figures 59 and 60 respectively.

REFERENCES

1. "An Evaluation of the Shell Creep Test Procedure to Predict Rutting in Asphalt Pavements," Final Report on Phase I. Materials and Research Division North Dakota State HighwayDepartment, June, 1980.

2. Yoder and Witczak, Principles of Pavement Design, Second Edition, John Wiley & Sons, Inc., p. 271, 1975.

3. "The Creep Test," SCW Record 5, Study Centre for Road Construction, 6811 AB Arnhem, The Netherlands, February 1981.

4. "The Shell Pavement Design Manual," Koninklijke/Shell-Laboratorium, Amsterdam, 1977. Shell International Petroleum Co.

5. S.F. Brown and C.A. Bell, "Development of a New Procedure for Bituminous Mix Design," Eurobitume Symposium, Madrid, Spain, October, 1989.

6. Van de Loo, P.J., "The Creep Test: A Key Tool in Asphalt Mix Design and in the Prediction of Pavement Rutting," Proceedings Asphalt Paving Technology, February, 1978.

7. J. F. Hills, D. Brien and P. J. Van de Loo, "The Correlation of Rutting and Creep Tests on Asphalt Mixes," Institute of Petroleum, January, 1974.

APPENDIX A

STATIC CREEP TEST

A. APPARATUS AND SUPPLIES (1)

1. Creep Test Machine:

The testing machine itself should consist of two flat, horizontal stainless steel floating platens, one connected to the machine frame and the other to the loading system. Since friction between the platens and end faces of the specimens will prevent free lateral movement and will produce barrelling of the specimen as it is being compressed, the platens should be polished so that with a surface treatment to the specimen, frictional forces may be kept as low as possible. The testing machine itself should be equipped with a water bath capable of maintaining a constant specimen temperature of 40° ±0.5°C. The testing machine also should be capable of applying appropriate vertical load to the specimen (see Figure A-1).

2. Core-Cutting Saw:

The saw should be a self-feed 41 cm (16 inches) diamond blade slab saw. The self-feed is regulated by a friction clutch which feeds the specimen into the blade at a rate governed by the hardness of the material being cut (see Figure A-2).

3. Thin Section Grinder:

The grinder should be equipped with a 15 micrometers, a 30 micrometers a 45 micrometers and a 220 mesh diamond lap. The grinder also should be equipped with a variable speed control (see Figure A-3).

4. Deflection Dial: Accurate to 0.001 inch

5. Silicone Grease

6. Graphite Flakes

7. Thermometer

8. Timer

9. Coolant for core cutting saw

B. DIMENSIONS OF TEST SPECIMEN (3)

1. Mixes with a maximum particle dimension less than 16 mm: diameter of specimen 100 mm (4 inches), height 60± 5 mm (2.5 inches).

2. Mixes with a maximum particle dimension between 16 and 40 mm: diameter of specimen 150 mm (6.0 inches), height 100± 5 mm (4.0 inches).

In order to obtain the required height, it is permissible to place several (but not more than three) polished drilled cores loosely one upon another. If it is desired to employ a gluing or bonding agent, plaster of paris may be used for the purpose. If the height of a drilled core is more than the required dimension, the core may be cut by a slab saw and the end faces should be polished by a grinder.

C. TEST CONDITIONS (3)

To obtain good agreement between creep and rutting tests, it is necessary to perform the creep test in the linear range.

1. Temperature of specimen (T): 40°C or 104°F

2. Stress applied (σ): 0.1 MN/m^2 or 14.5 psi

3. Duration of test: load to act for 60 minutes

4. Preload

   Duration: 2 minutes
   Magnitude: 0.01 MN/m^2 (or 1.45 psi)

D. PREPARATION OF TEST SPECIMEN (1) (4)

The first step before performing the creep test is the preparation of test samples. Cores must be brought to the appropriate length with the specimen ends cut and polished. The saw self-feeds the specimen into the blade at a rate governed by the hardness of the material being cut (see Figure A-2). This produces a smooth cut, although it takes about 20 minutes to cut one specimen end. The 4-inch diameter cores were cut at both ends to produce test specimens of 2 1/2 inches high.

To ensure that the samples would have complete point-to-point contact with the platens in the creep testing apparatus, the specimen ends were polished by a Hillquist thin section grinder (See Figure A-3). If point-to-point contact is not achieved, the load distribution will be unequal and the final results will be questionable. The specimen end faces were first polished by a 220 mesh, then a 45 micrometers lap. Finally a 30 micrometers lap was used to bring the specimen to a highly polished state. This was the "mirror finish" that was required by the Shell Procedures. Care must be taken to ensure that the polished end faces are accurately perpendicular to the axis of the cylinder.

The frictional forces between the platens and end faces of the specimens must be kept to a minimum. The results will be open to question if friction prevents free lateral movement of the specimen as it is being compressed, resulting in barrelling of the specimen.

Since the ideal uniaxial stress distribution is not present when friction occurs, the results obtained may not be accurate. To eliminate the frictional forces between the end faces of the specimens and the platens in the testing device, a thin coating of silicone grease was applied on both end faces of the specimen and the platens were sprinkled with an excess of graphite flakes (see Figure A-4). This coating of silicone grease and graphite flakes effectively prevents the specimen from sticking to the platens and, prevents barreling of the specimen during creep testing. The coating of silicone grease on the platens can last through several tests.

E. TEST PROCEDURE (1) (4)

The length of time required for bringing the specimens to the desired test temperature (in a water bath) is 30-35 minutes for specimens with a diameter of 100 mm (4 inches) and is 50-60 minutes for specimens with a diameter of 150 mm (6 inches).

The carefully prepared specimens are now placed on the lower platen in the water bath of the testing apparatus. The 4-inch diameter specimens from Tyndall AFB test sections are left in the constant temperature bath at test temperature (40° $\pm$ 0.5°C) to be cured for 30-35 minutes. After that point a 2 minute preload of 10^4 N/m^2 (or 1.45 psi) is applied to the specimen.

At the end of 2-minute preload, an initial dial reading was observed and recorded, and then the loading weight was engaged, subjecting the specimen to a stress of 10^5 N/m^2 (or 14.5 psi). The deformation in the axial direction is measured with the aid of a mechanical dial gauge. Additional deformation dial readings (other than the 2-minute reading) are required and taken at elapsed times of 2, 5, 10, 15, 30, 45, and 60 minutes. During the entire process of testing, the temperature of water bath in the testing machine is maintained at 40°$\pm$ 0.5°C.

APPENDIX B

DYNAMIC CREEP TEST (5)

A. APPARATUS AND SUPPLIES

1. MTS Machine: Capable of loading the test specimens with 1/2 Hz square wave pulse at the maximum axial stress of 100 kPa (i.e. 14.5 psi) (see Figure B-1).

2. MTS Machine Control Panel (see Figure B-2).

3. Environmental Chamber: Capable of maintaining 40°C (i.e. 104°F) for at least 2 hours (see Figure B-3).

4. Capping Equipment: Including capping plates, alignment devices and melting pots for sulfur mortar.

5. Sulfur Mortar

6. Oven: Capable of maintaining 40°C or 104°F.

B. DIMENSIONS OF TEST SPECIMEN

1. The length of the specimen shall be as nearly as practicable twice its diameter. The length of drilled cores tested was 6 inches and the diameter was 3 inches.

2. The ends of core specimens to be tested shall be smooth, perpendicular to the logitudinal axis, and of the same diameter as the body of the specimen.

C. TEST CONDITIONS

1. Temperature of specimen: 40°C or 104°F

2. Stress applied: 100 kPa or 14.5 psi

3. Duration of test: 1/2 Hz square wave for 2 hours

D. PREPARATION OF TEST SPECIMENS

1. Capping: Before performing the test, cap the ends of the specimens with sulfur mortar.

2. Measurement: Before testing, measure the length as well as the diameter of the core specimens.

E. TEST PROCEDURE (5)

1. Place the prepared test specimens in an oven at 40°C or 104°F to bring the core specimens to the desired test temperature.

2. The carefully prepared specimens are now placed on the lower platen of the environmental chamber which is also maintained at the desired temperature of 40°C or 104°F.

3. The sample is loaded uniaxially (under unconfined conditions) with a 1/2 Hz square wave pulse. The maximum axial stress shall be 100 kpa, (i.e. 14.5 psi).

4. The permanent strain of the test specimens shall be recorded at 10, 50, 100, 500, 1000, and 3600 load repetitions. The entire test should last 2 hours.

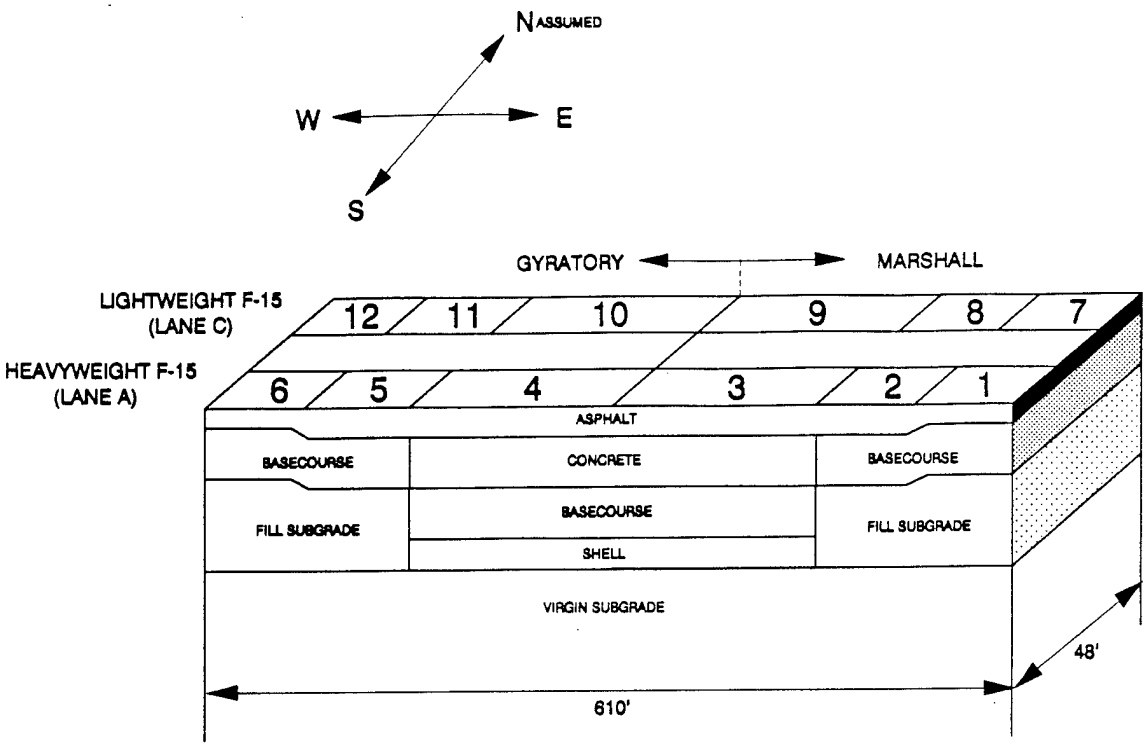

Figure 1. Layout of Test Sections.

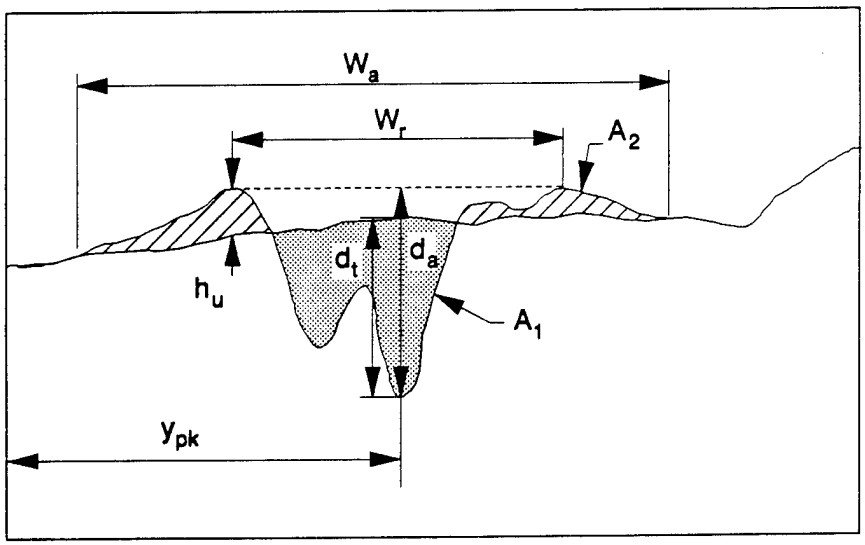

A_1 - AREA OF RUT
A_2 - AREA OF UPHEAVAL
h_u - HEIGHT OF UPHEAVAL
d_t - TRUE RUT DEPTH
W_r - RUT WIDTH
y_{pk} - LATERAL POSITION OF TRUE RUT DEPTH
d_a - APPARENT RUT DEPTH
W_a - AFFECTED WIDTH

Figure 2. Damage Parameters.

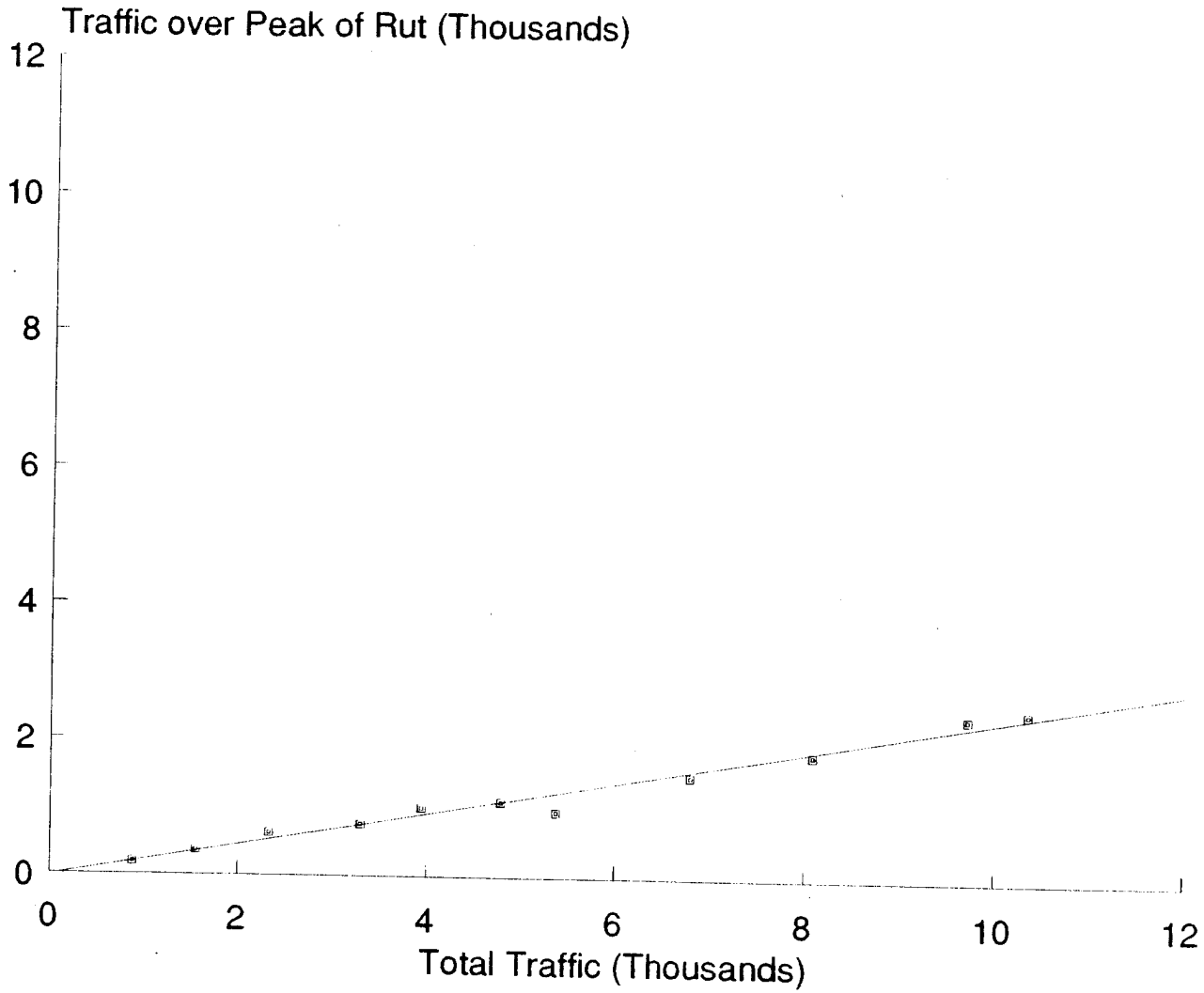

Figure 3. Total vs Actual Traffic on Peak of Rut .

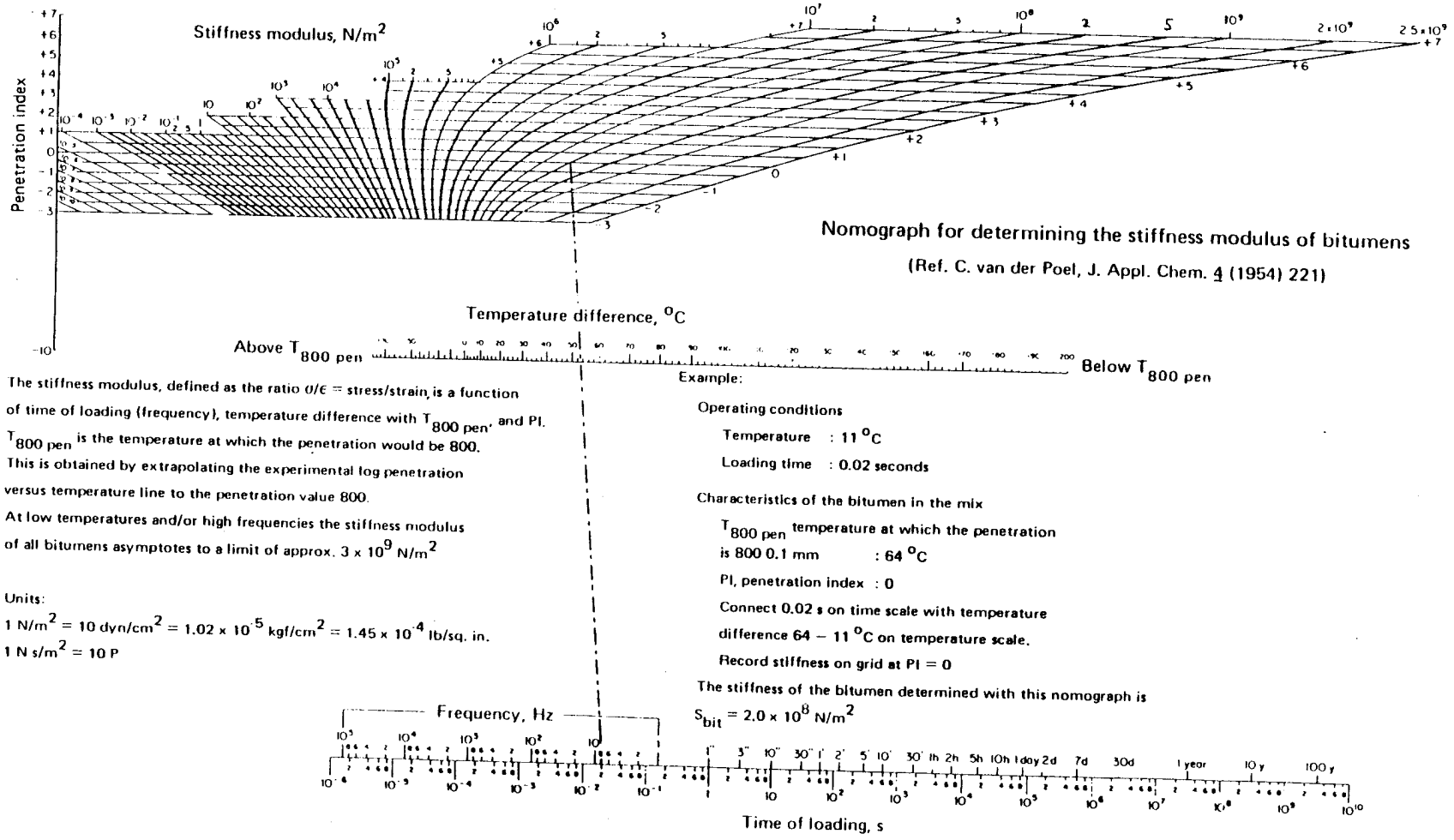

Figure 4. Nomograph for Determining the Stiffness Modulus of Bitumens (2) (4).

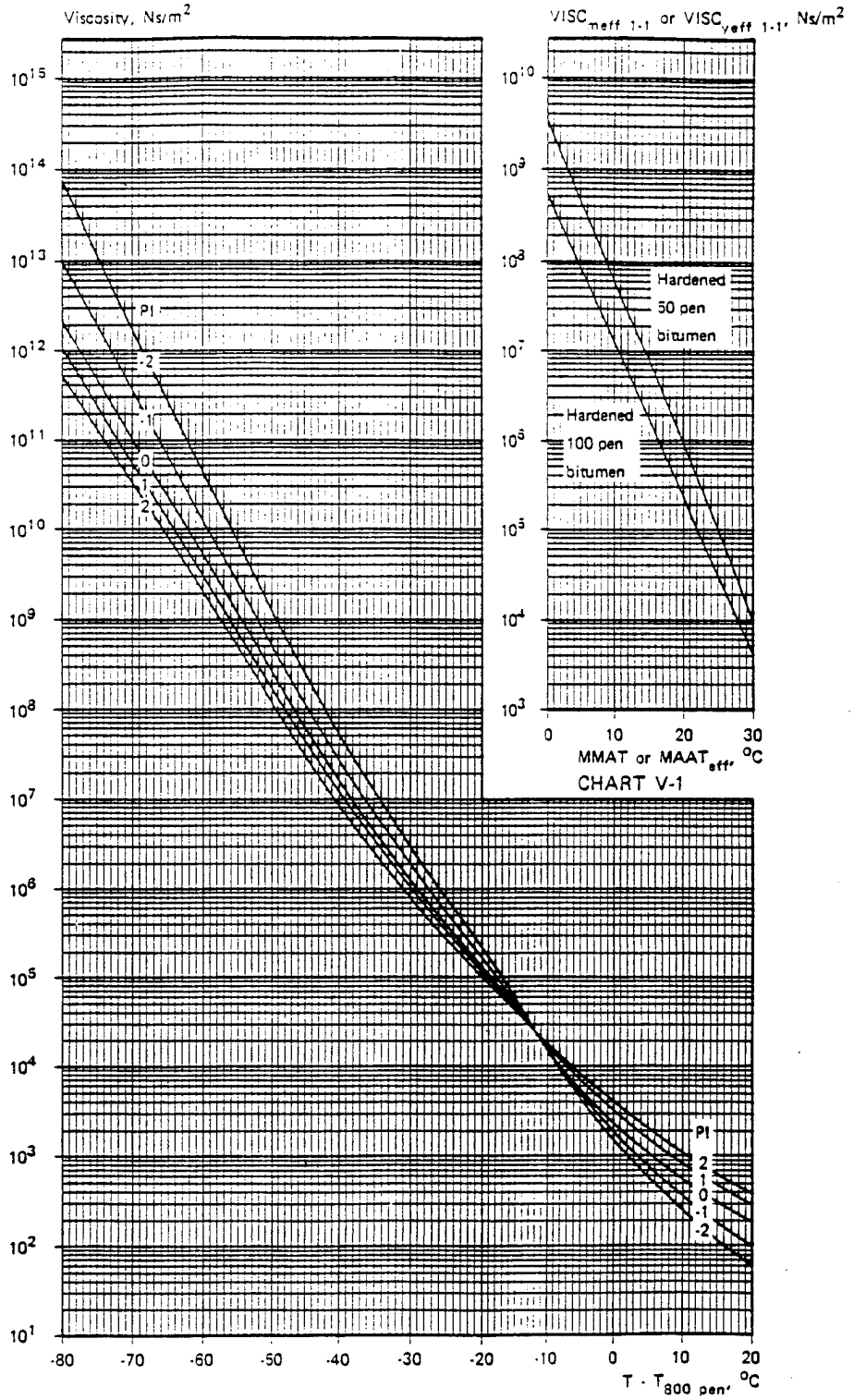

Figure 5. Nomograph for Determining Effective Bituminous Viscosity (4) (6).

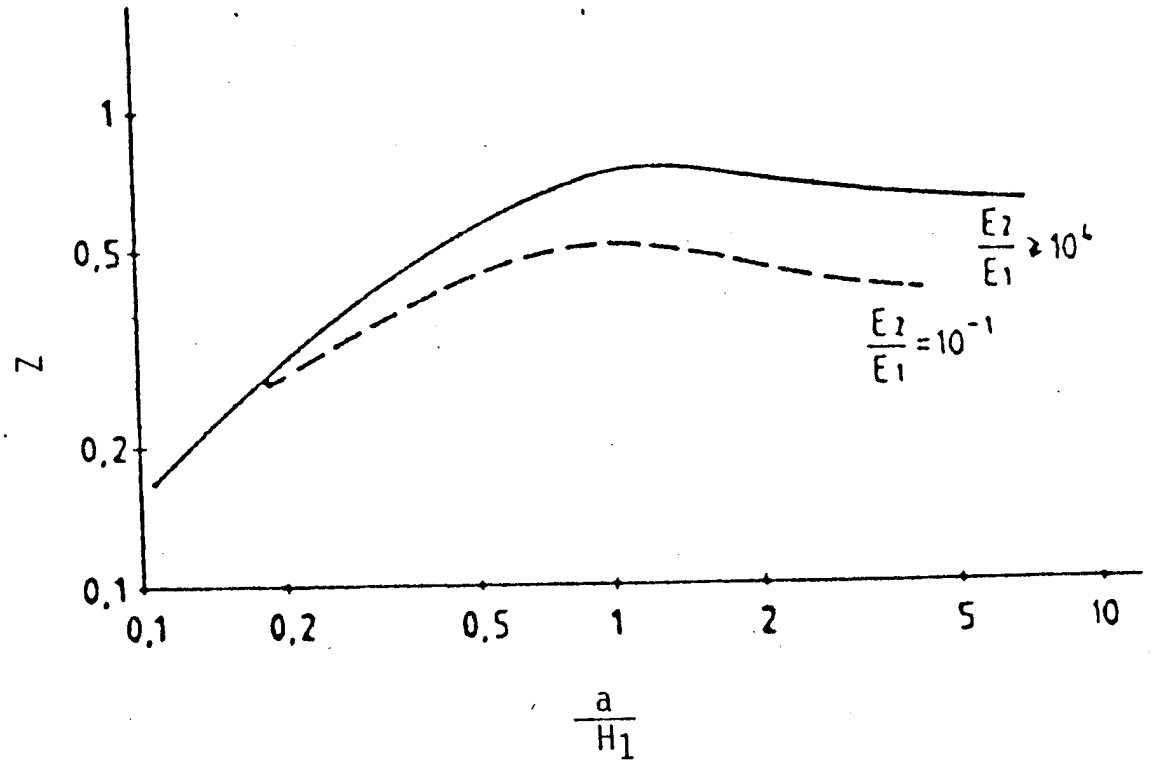

Figure 6. Factor Z Calculated with BISTRO Program (3) (7).

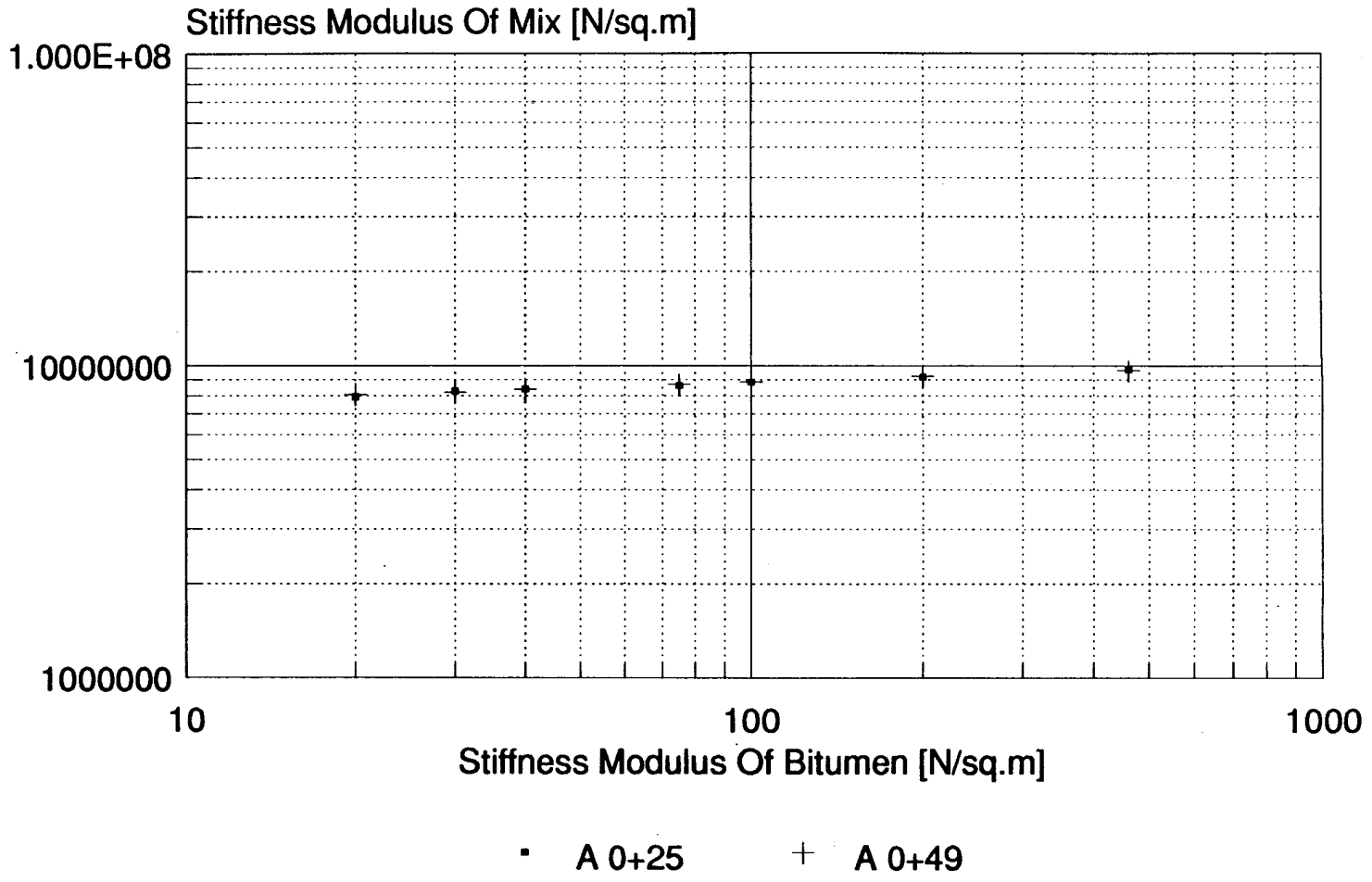

Figure 7. Static Creep Curves - Drilled Cores Fully Loaded F-15 Section 1.

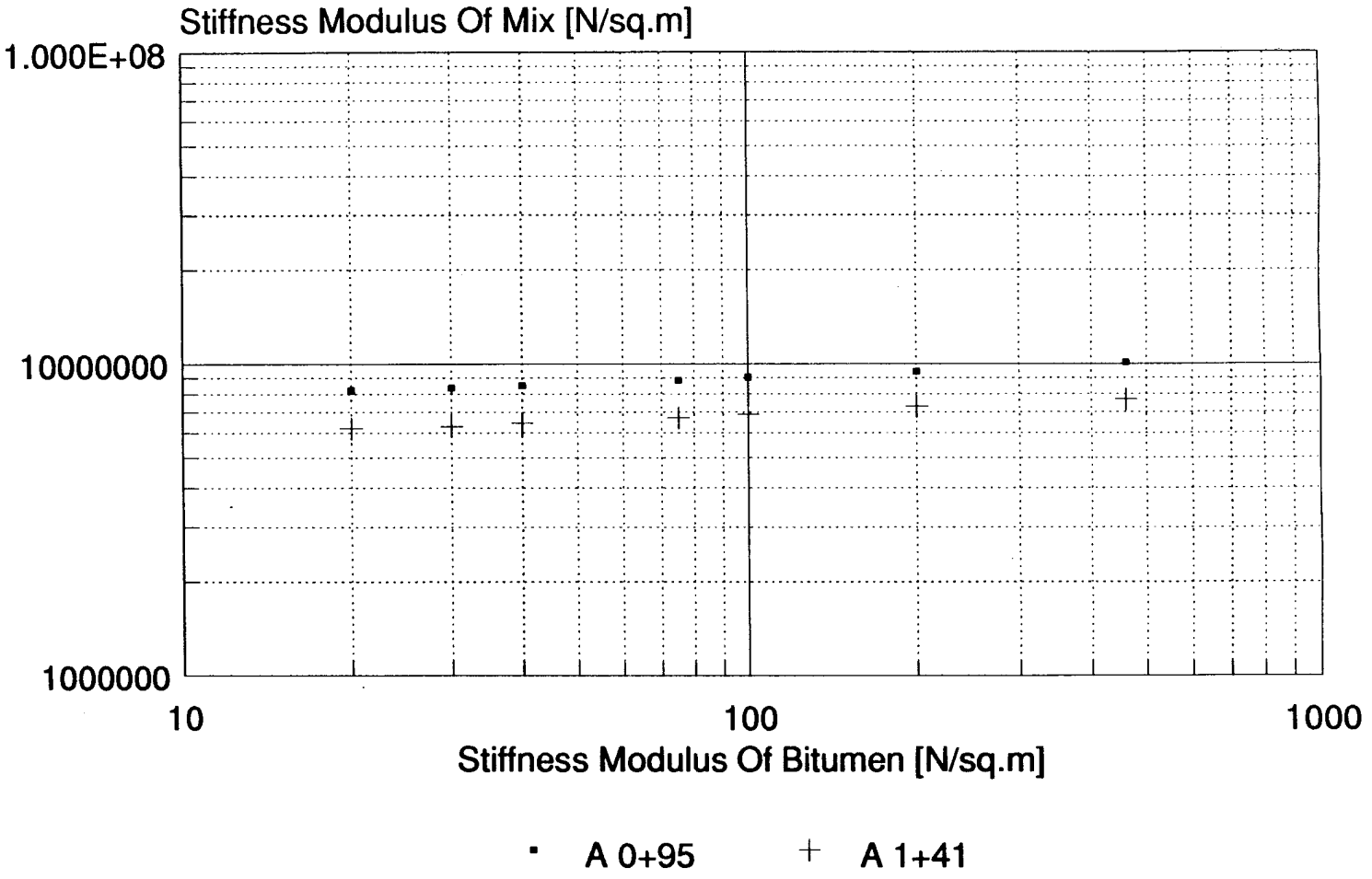

Figure 8. Static Creep Curves-
Drilled Cores
Fully Loaded F-15
Section 2.

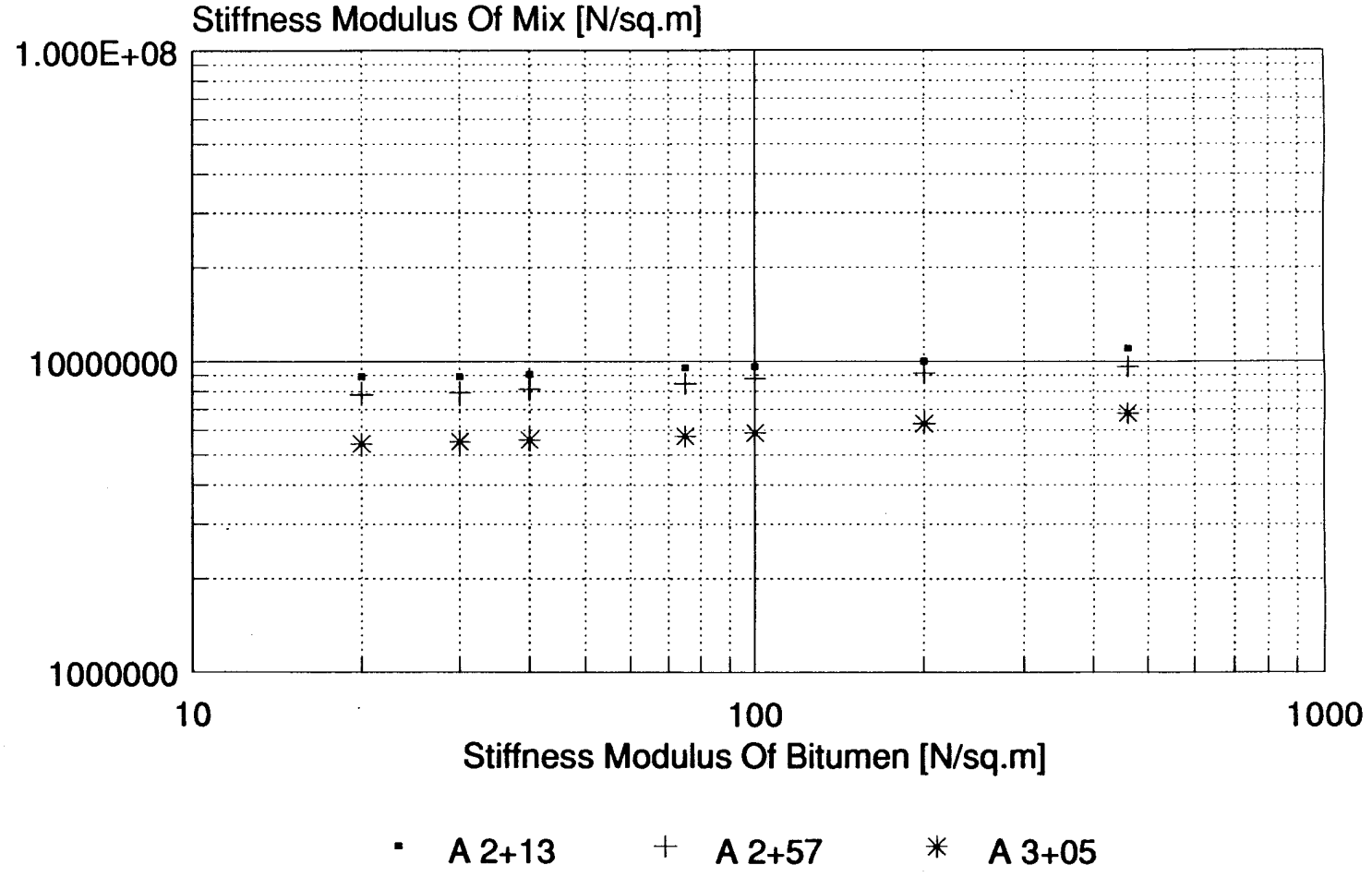

Figure 9. Static Creep Curves-
Drilled Cores
Fully Loaded F-15
Section 3.

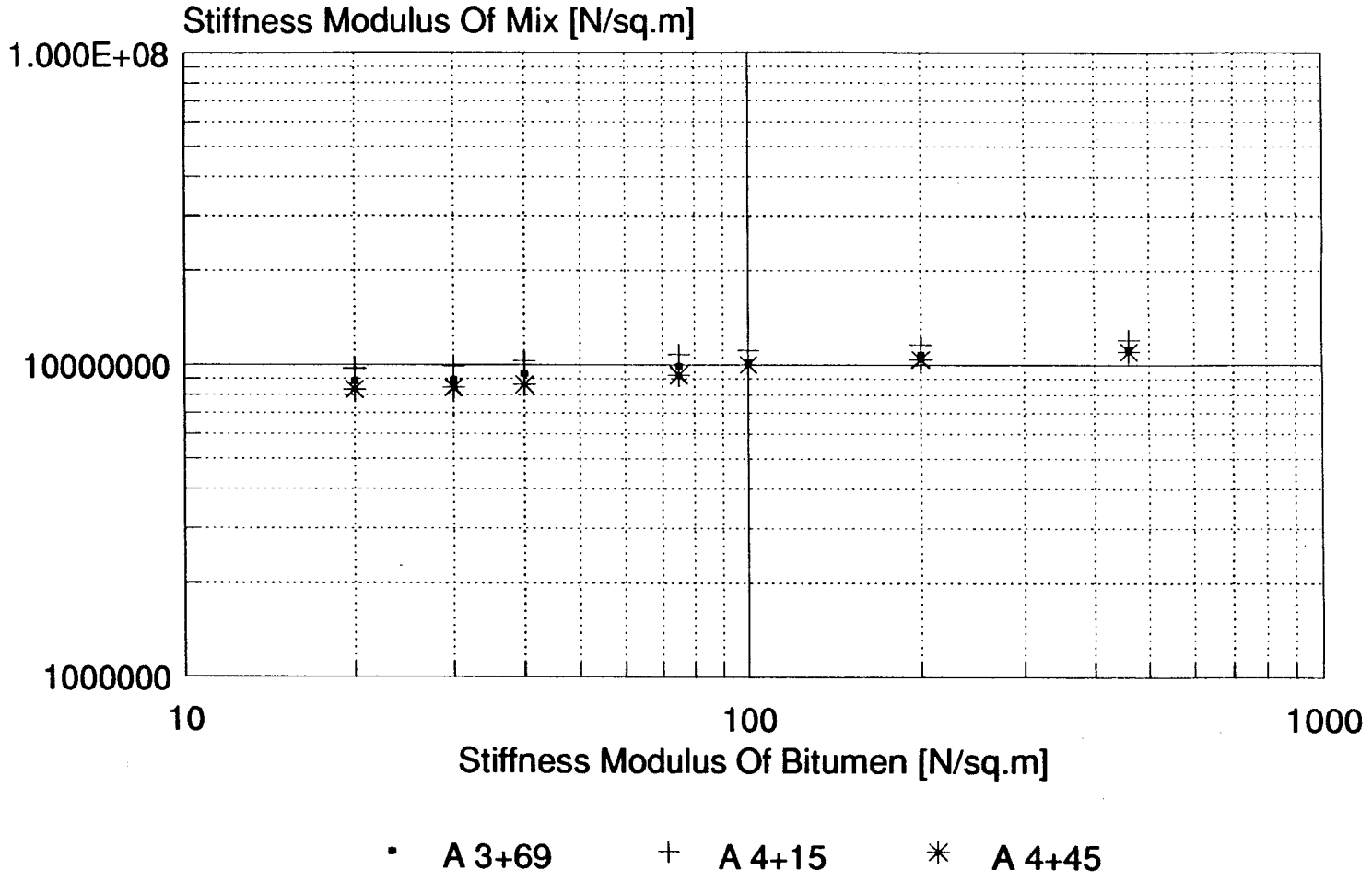

Figure 10. Static Creep Curves-
Drilled Cores
Fully Loaded F-15
Section 4.

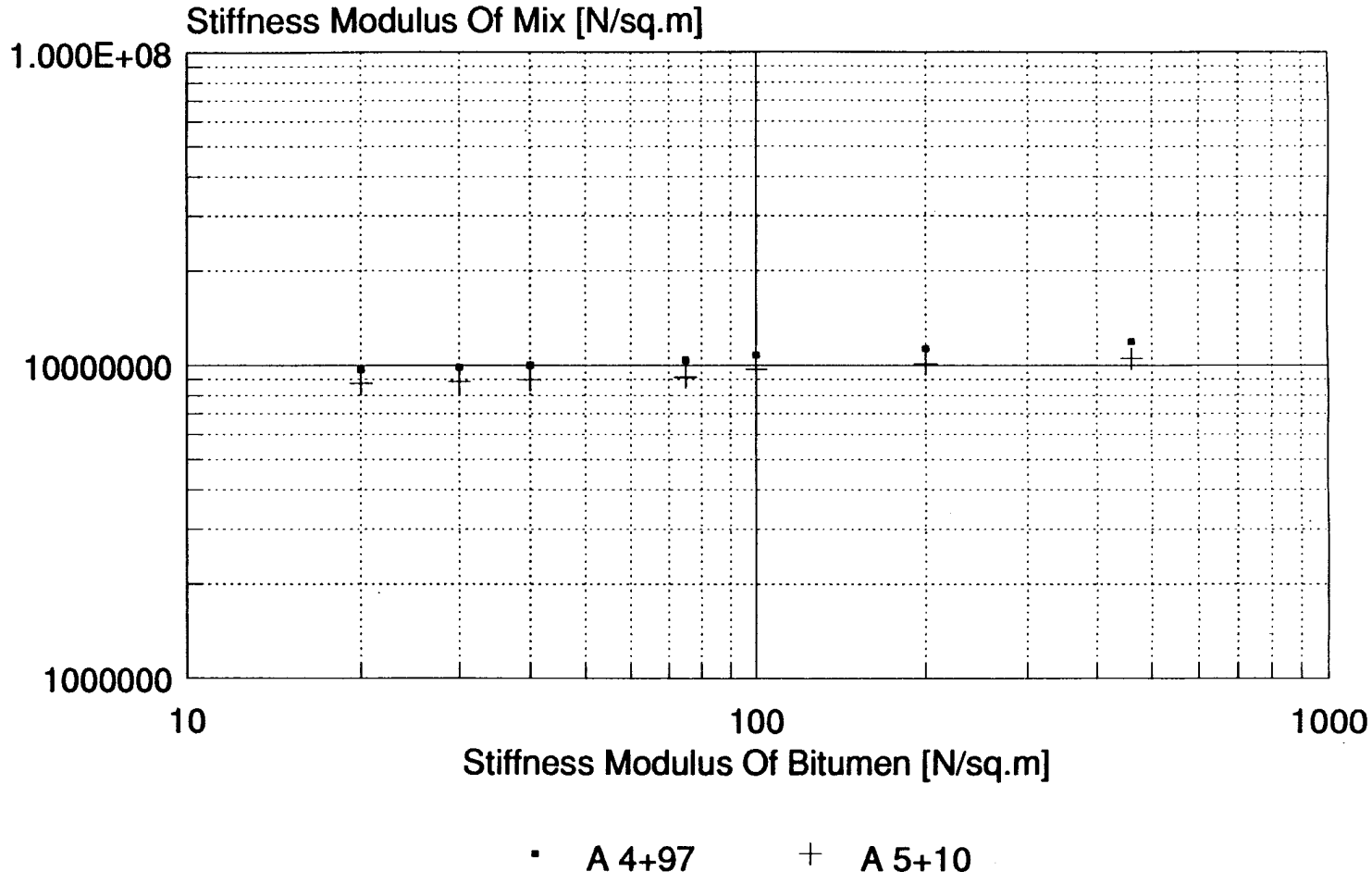

Figure 11. Static Creep Curves-
Drilled Cores
Fully Loaded F-15
Section 5.

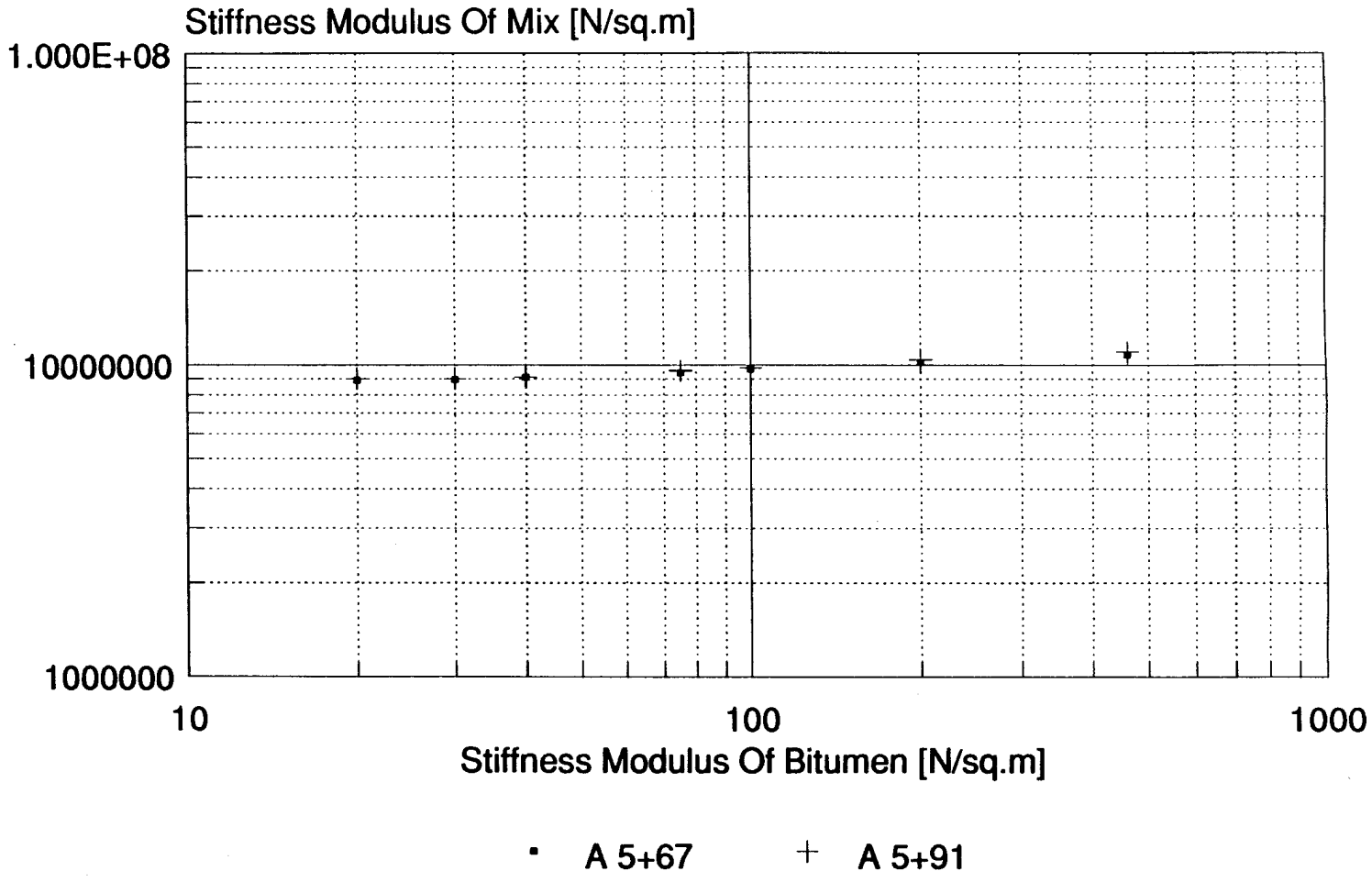

Figure 12. Static Creep Curves-
Drilled Cores
Fully Loaded F-15
Section 6.

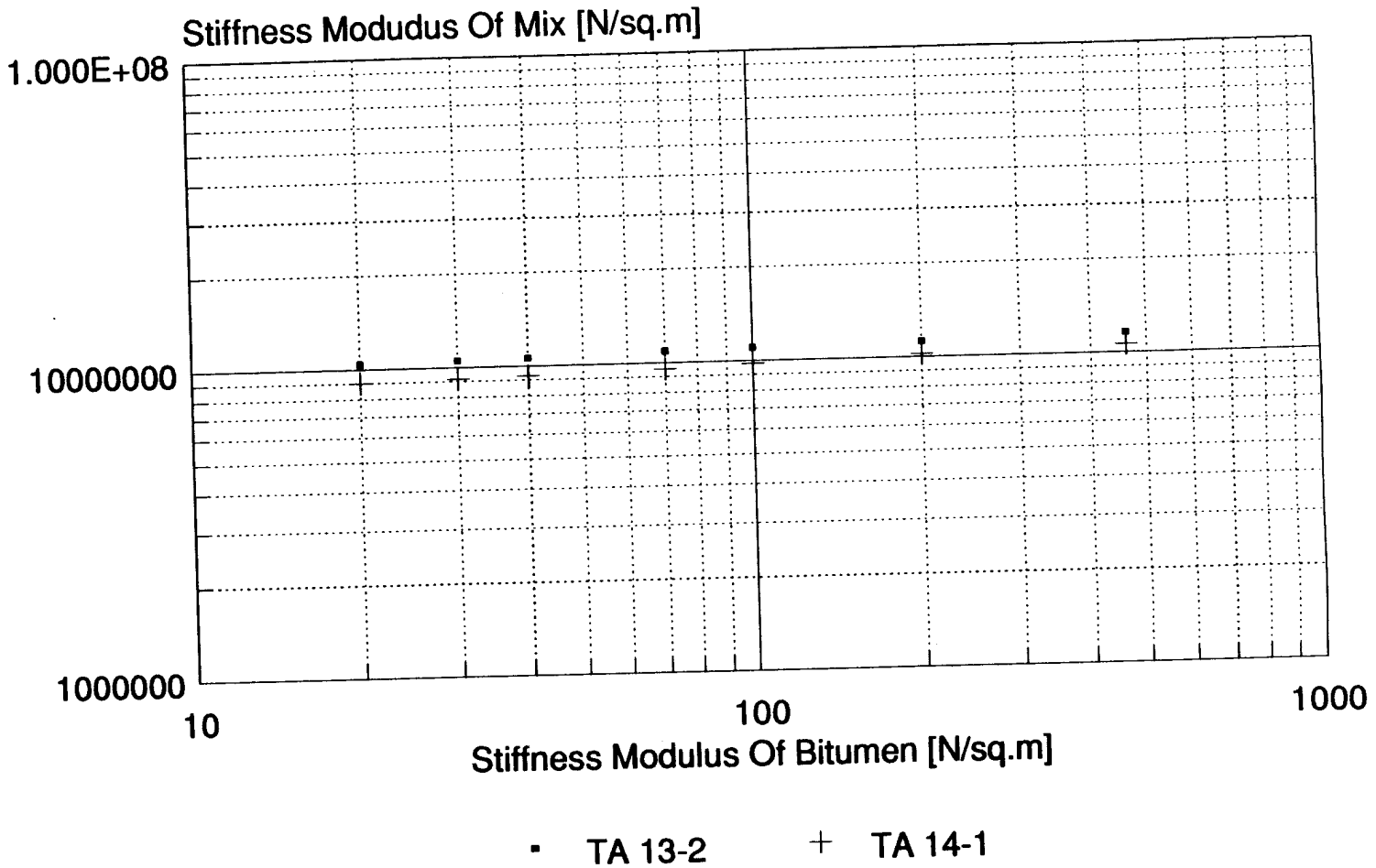

Figure 13. Static Creep Curves-
Compacted Specimens
Fully Loaded F-15
Section 1.

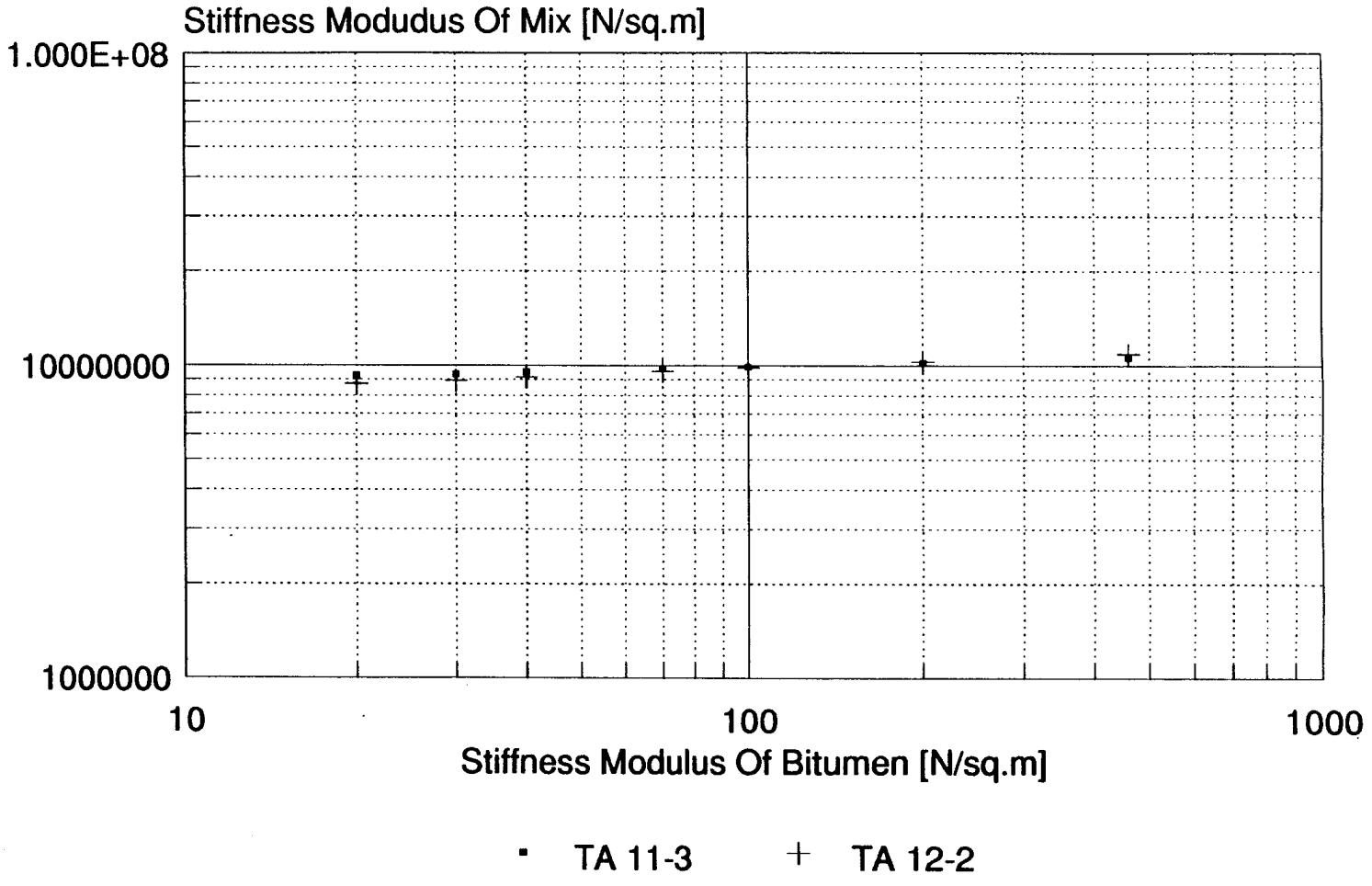

Figure 14. Static Creep Curves-
Compacted Specimens
Fully Loaded F-15
Section 2.

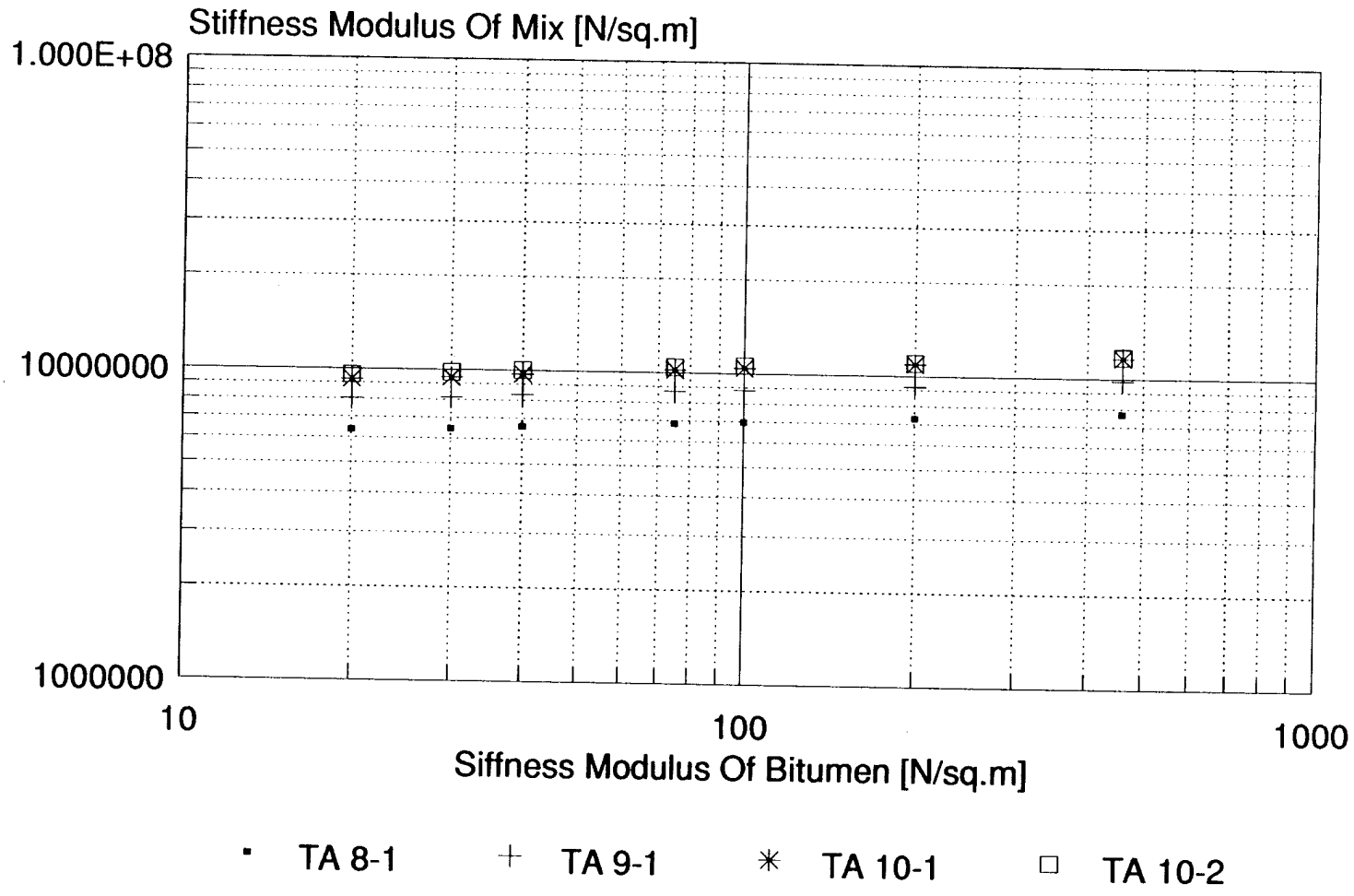

Figure 15. Static Creep Curves-Compacted Specimens Fully Loaded F-15 Section 3.

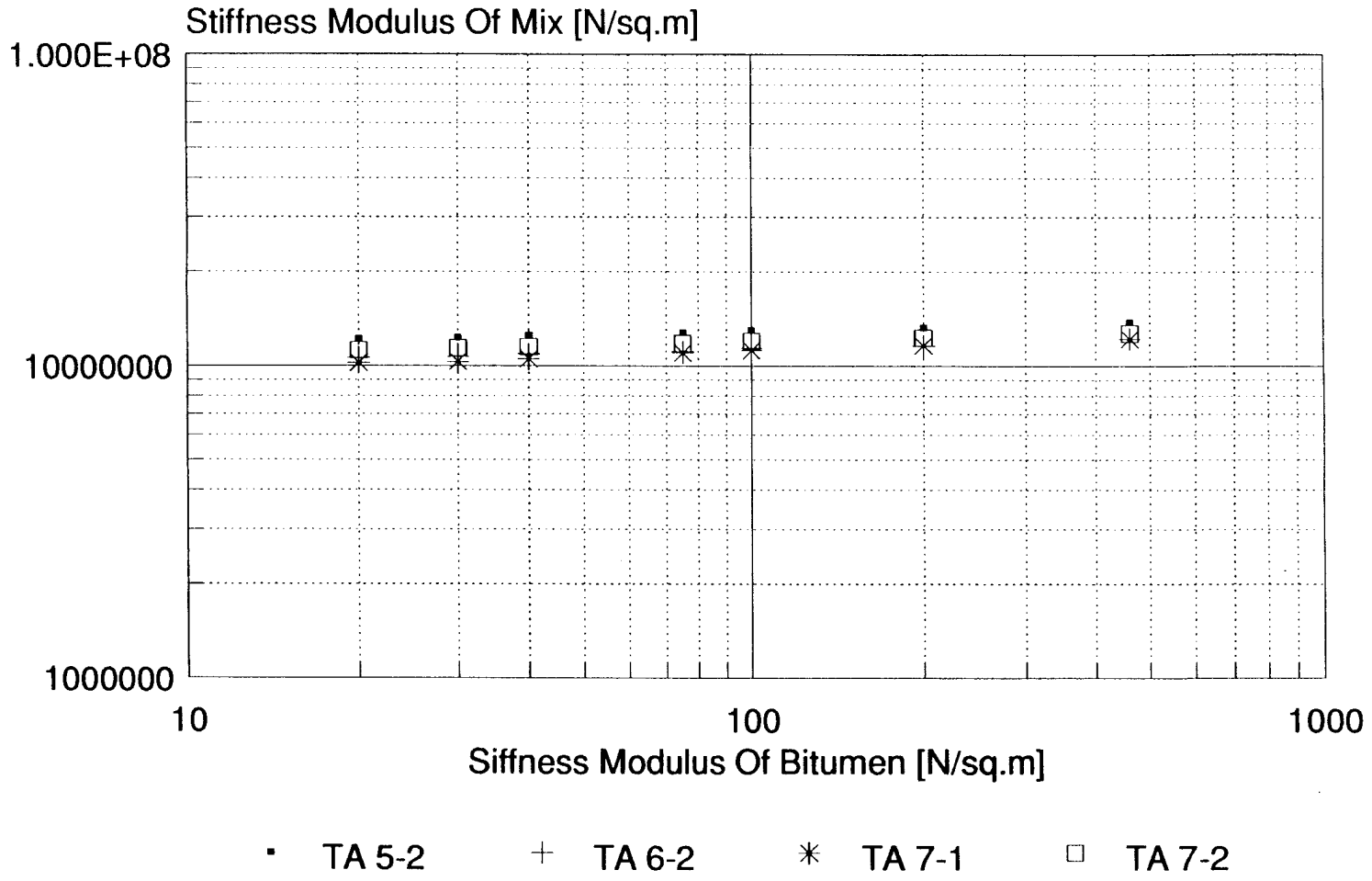

Figure 16. Static Creep Curves-
Compacted Specimens
Fully Loaded F-15
Section 4.

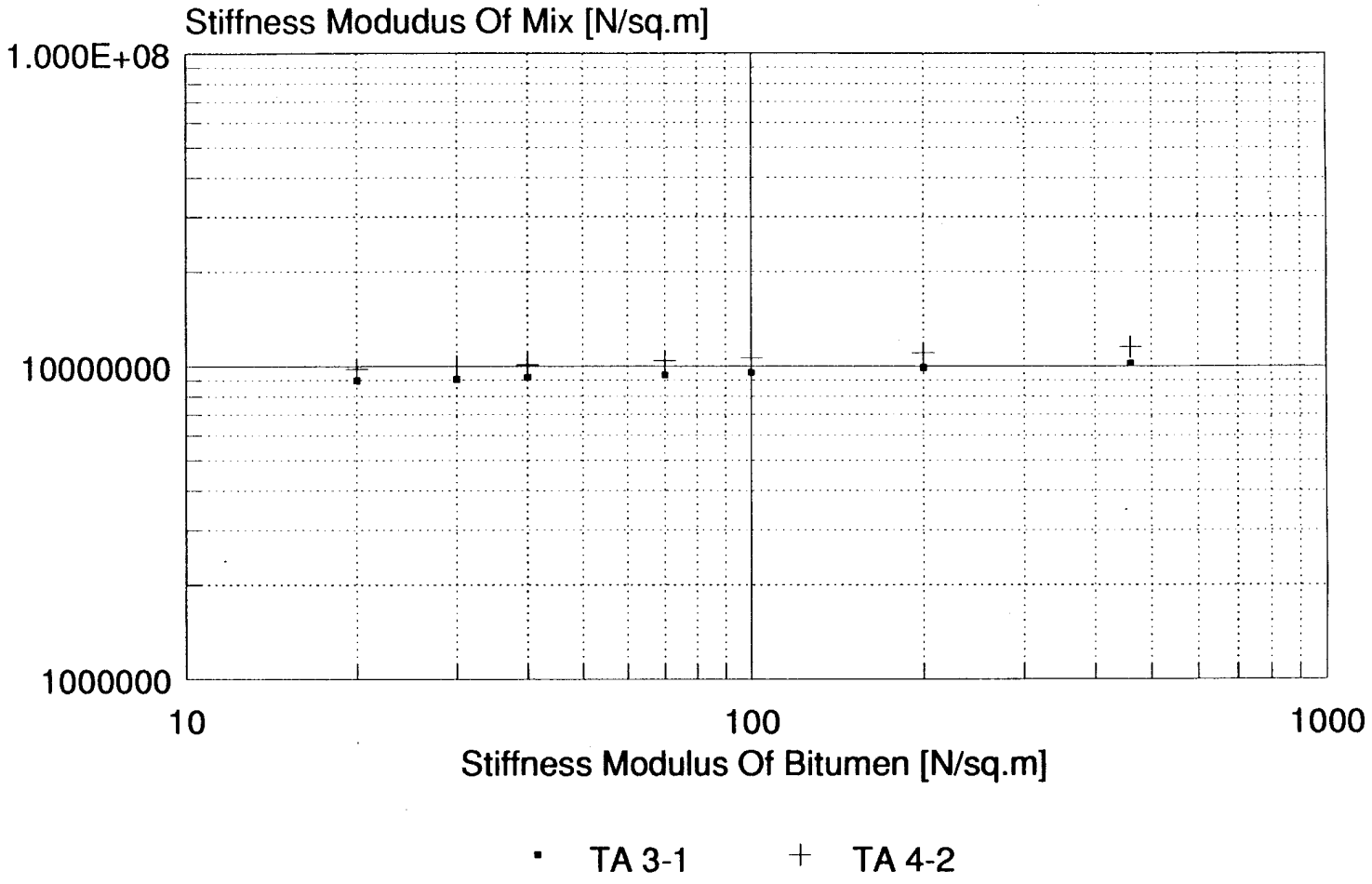

Figure 17. Static Creep Curves Compacted Specimens Fully Loaded F-15 Section 5.

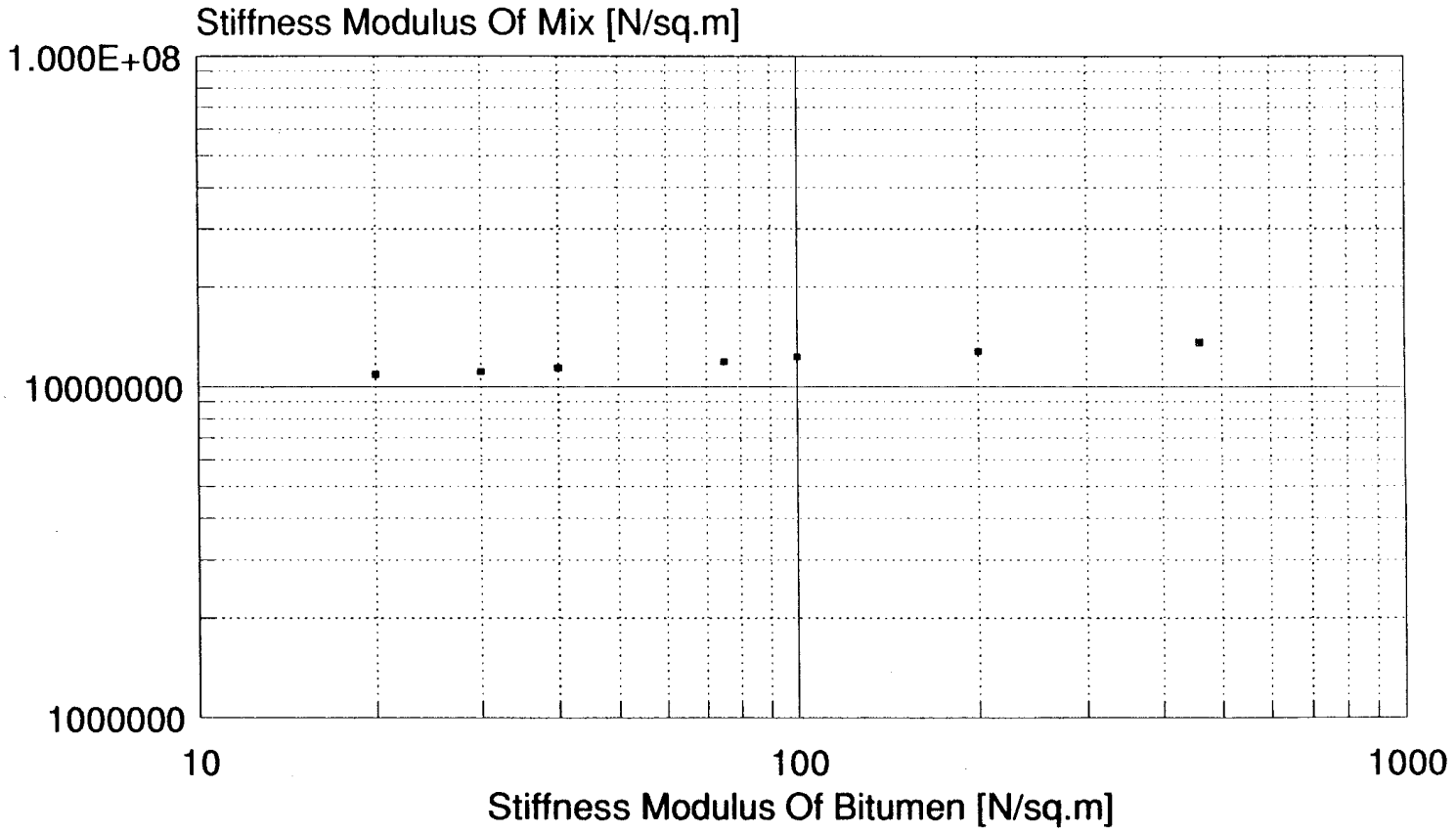

Figure 18. Static Creep Curve - Compacted Specimen Fully Loaded F-15 Section 6.

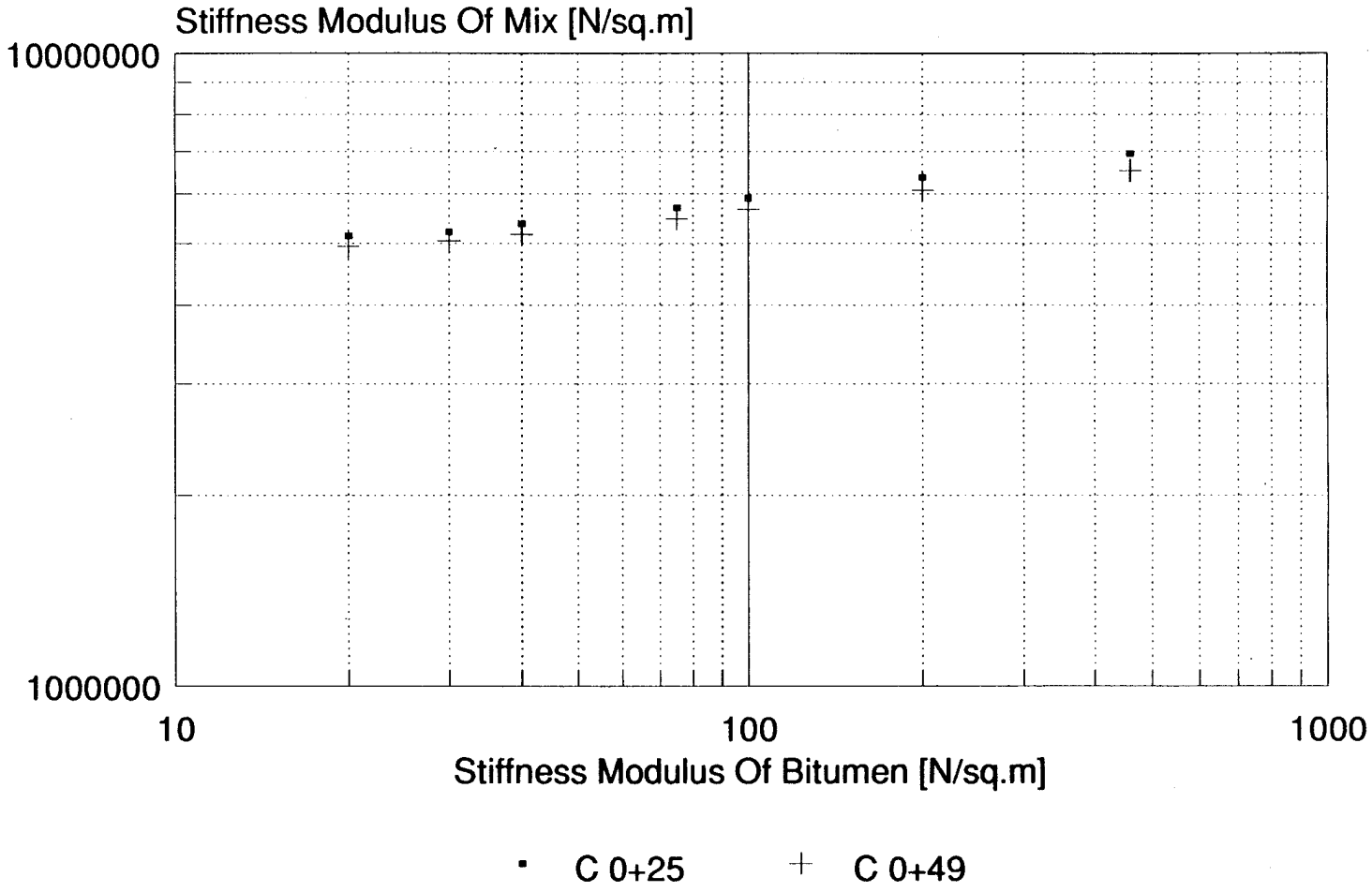

Figure 19. Static Creep Curves-
Drilled Cores
Unarmed F-15
Section 7.

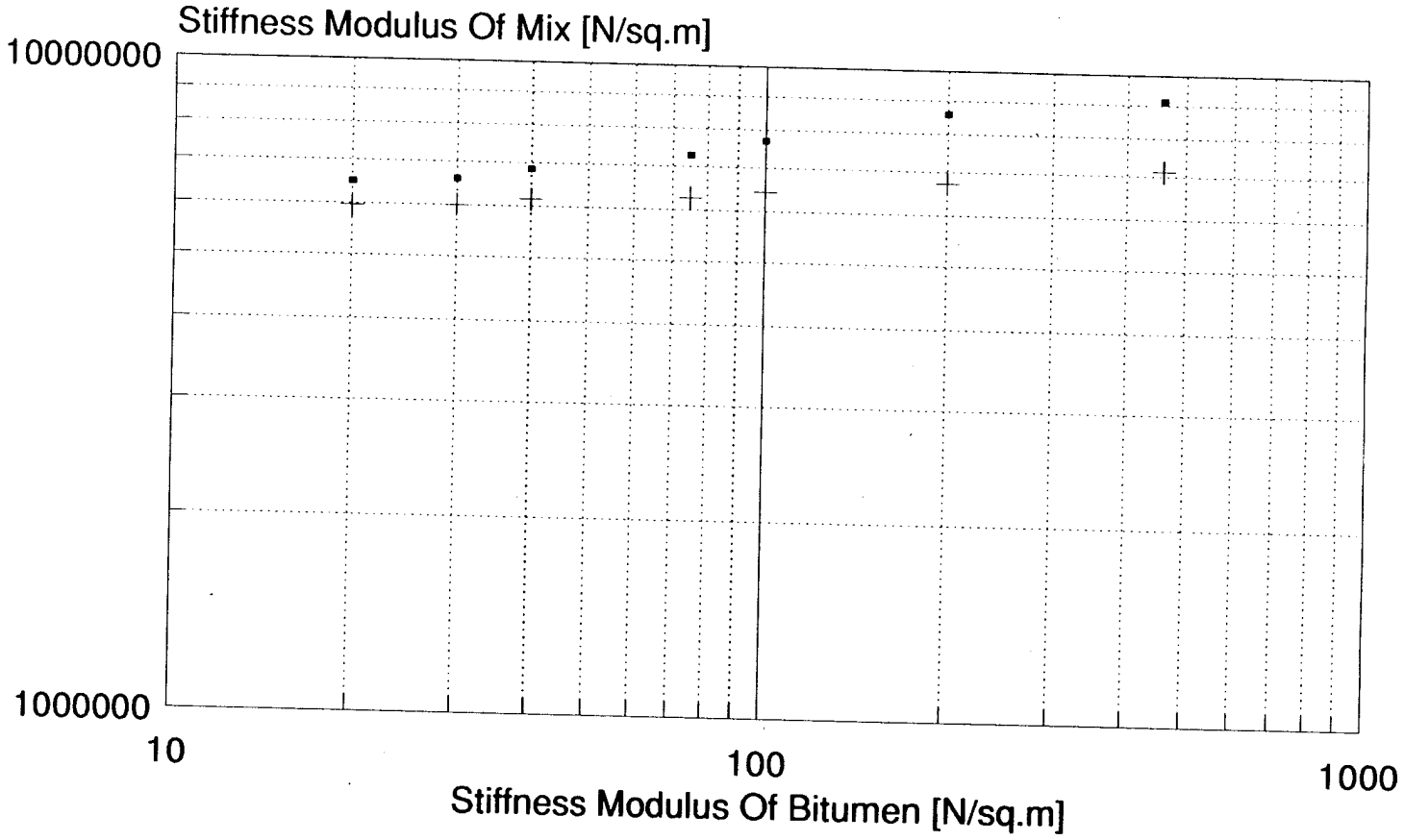

Figure 20. Static Creep Curves-
Drilled Cores
Unarmed F-15
Section 8.

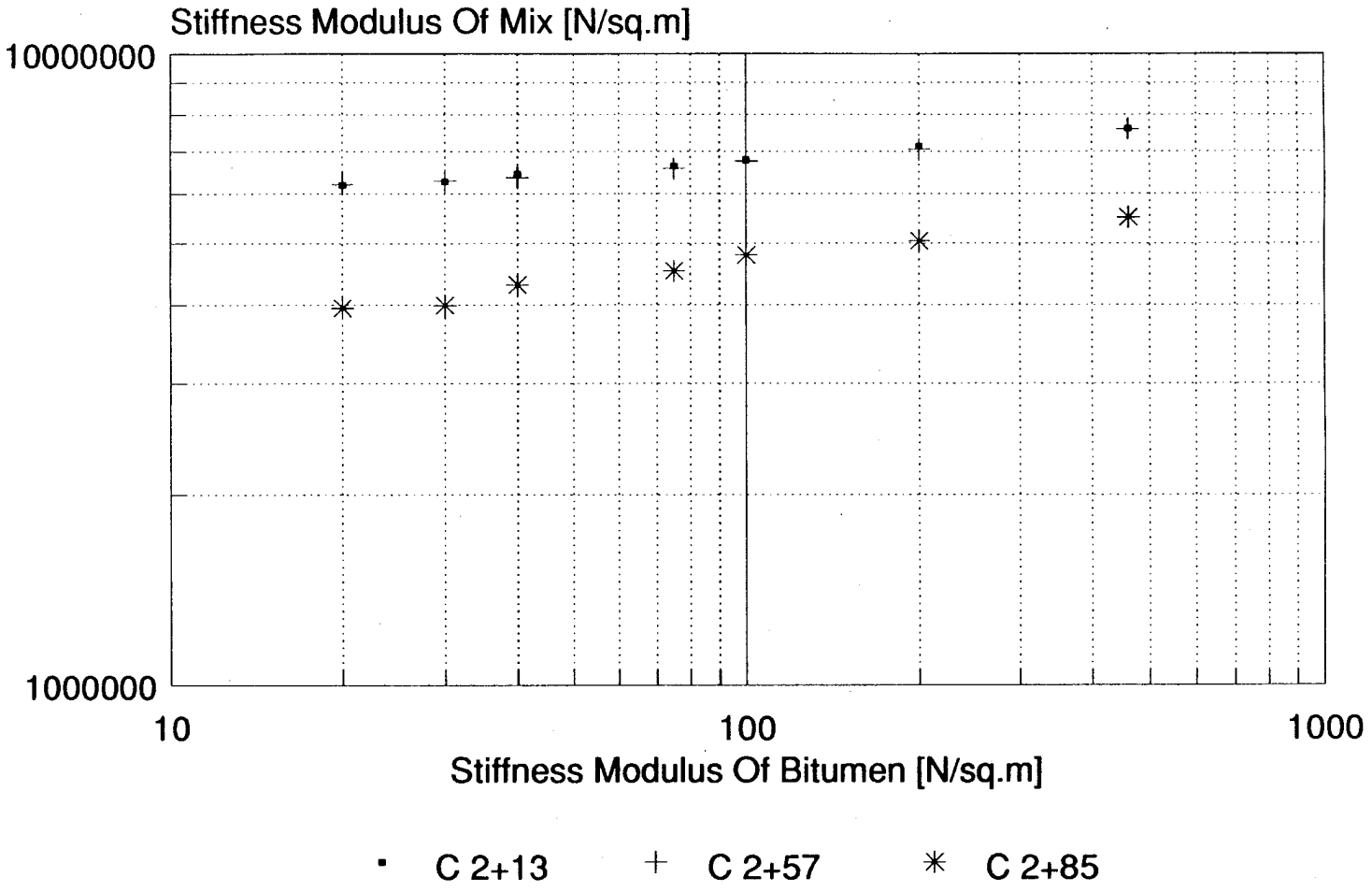

Figure 21. Static Creep Curves-
Drilled Cores
Unarmed F-15
Section 9.

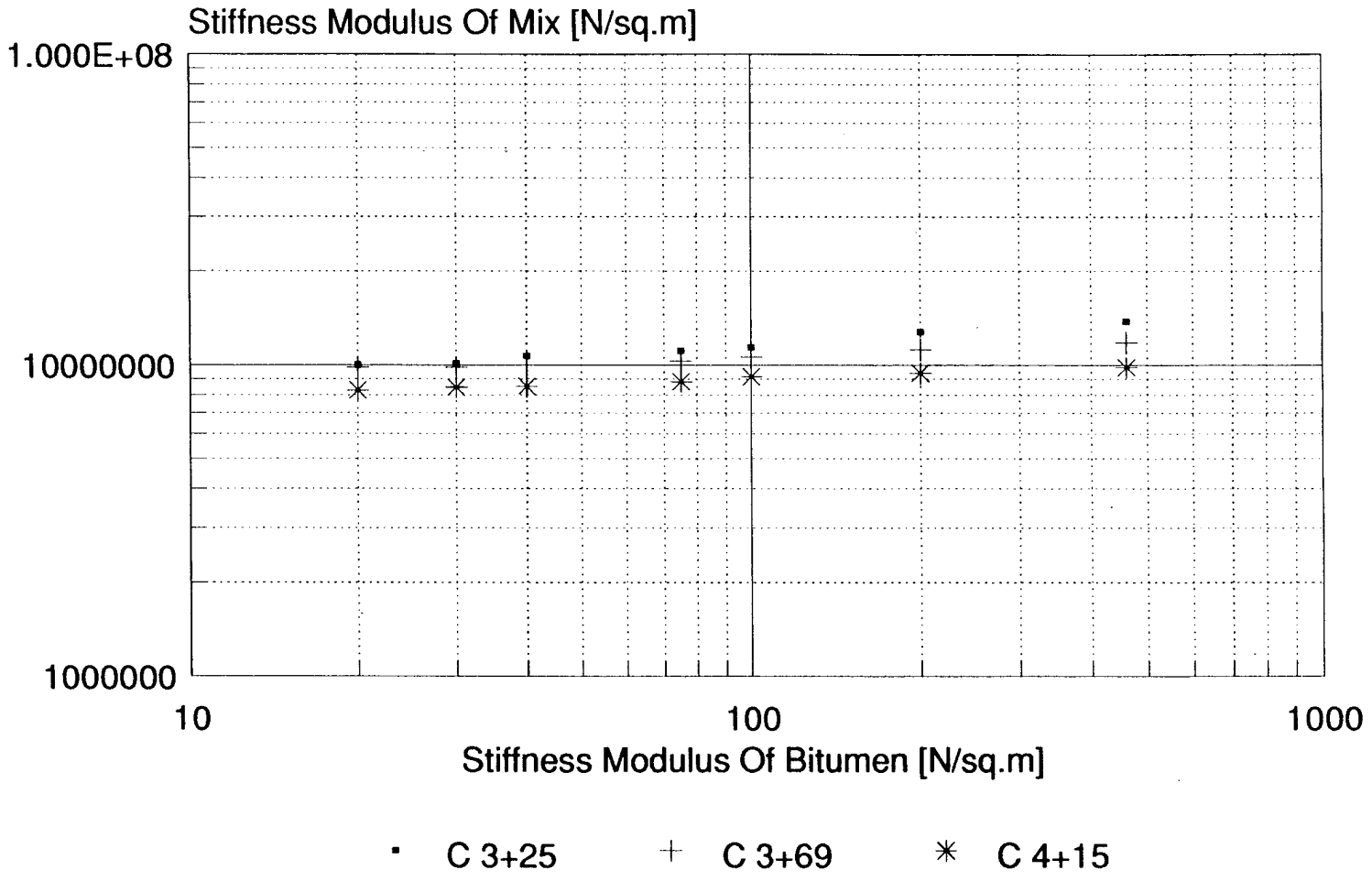

Figure 22. Static Creep Curves-
Drilled Cores
Unarmed F-15
Section 10.

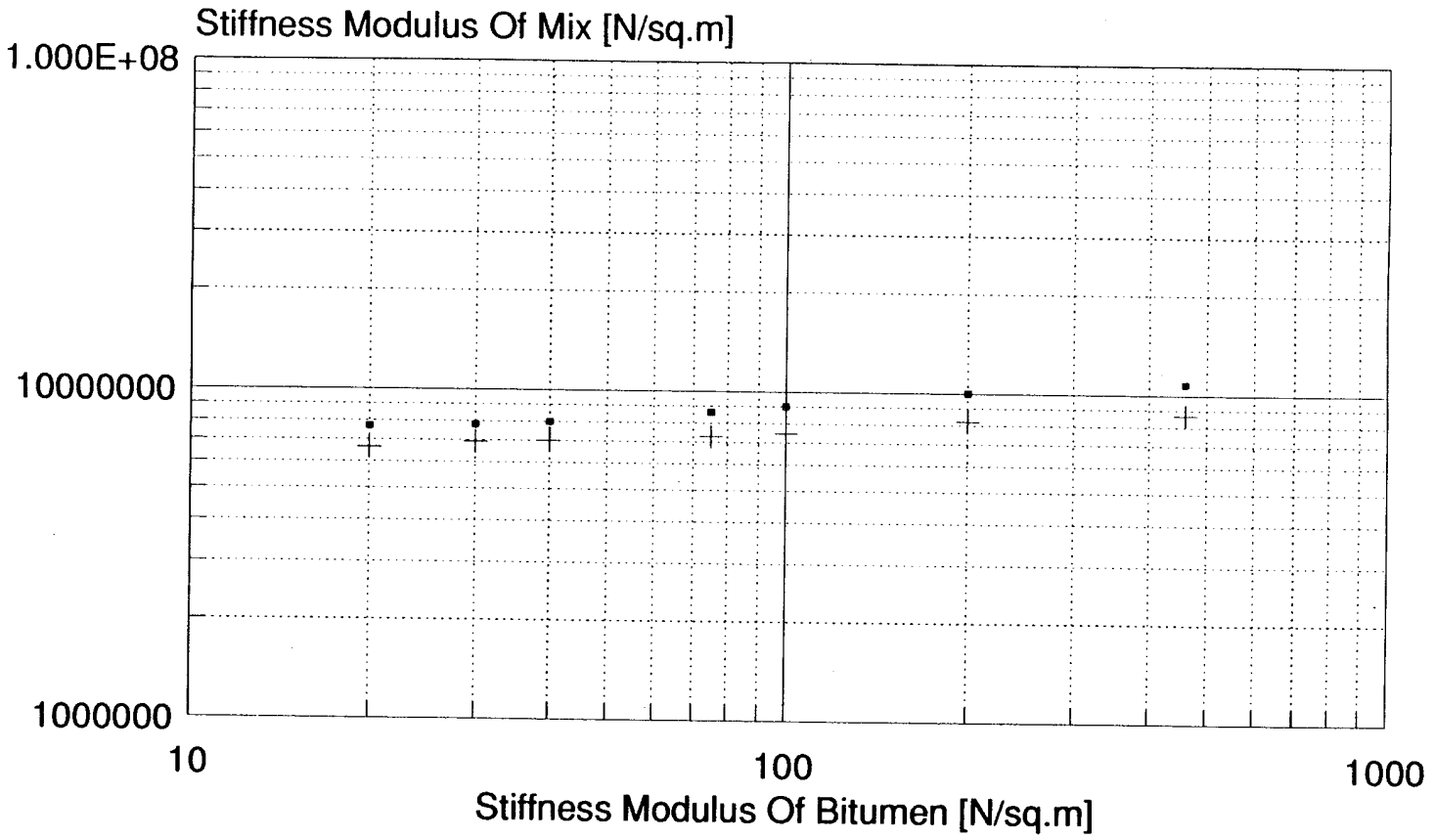

Figure 23. Static Creep Curves-
Drilled Cores
Unarmed F-15
Section 11.

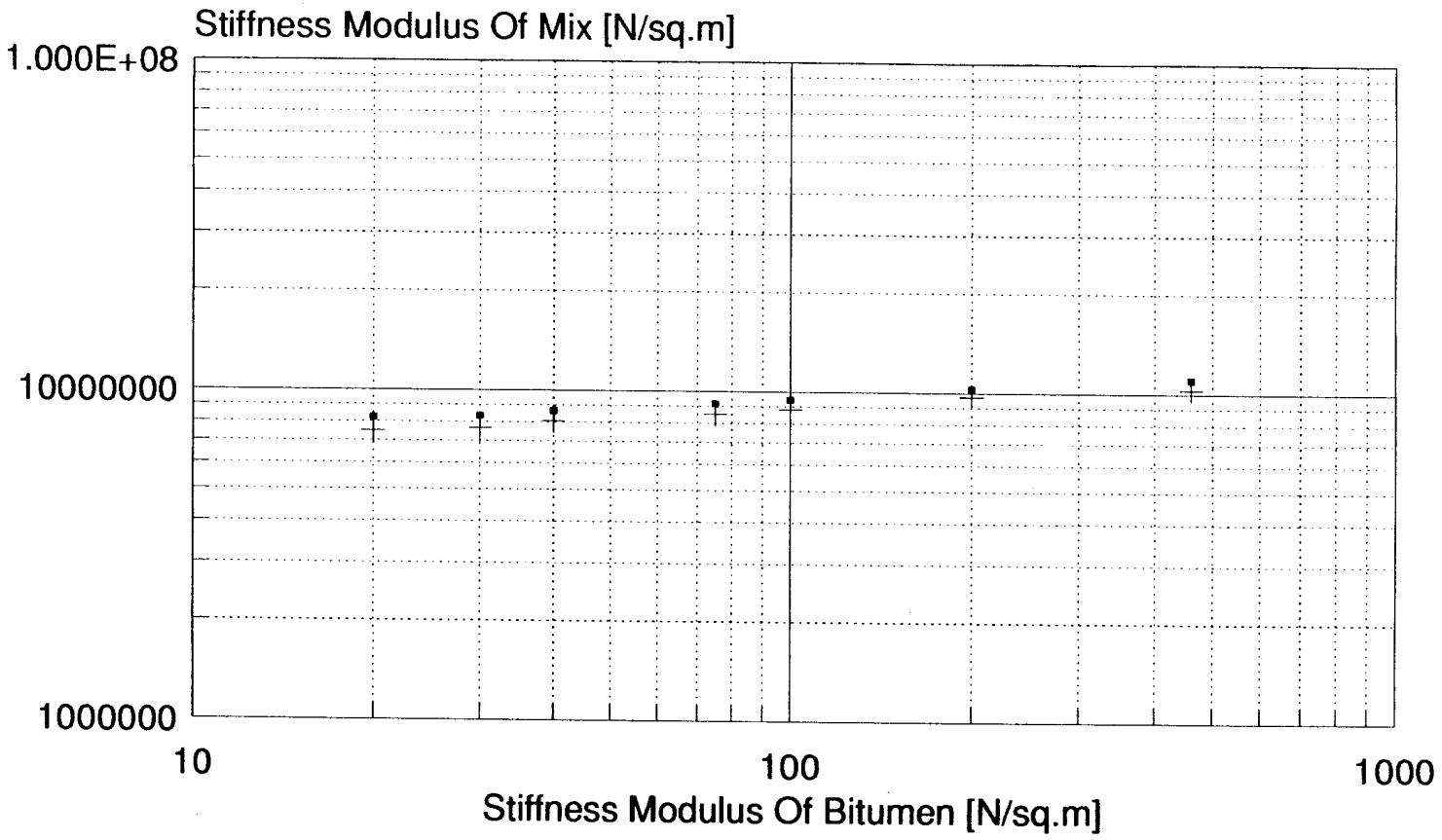

Figure 24. Static Creep Curves-
Drilled Cores
Unarmed F-15
Section 12.

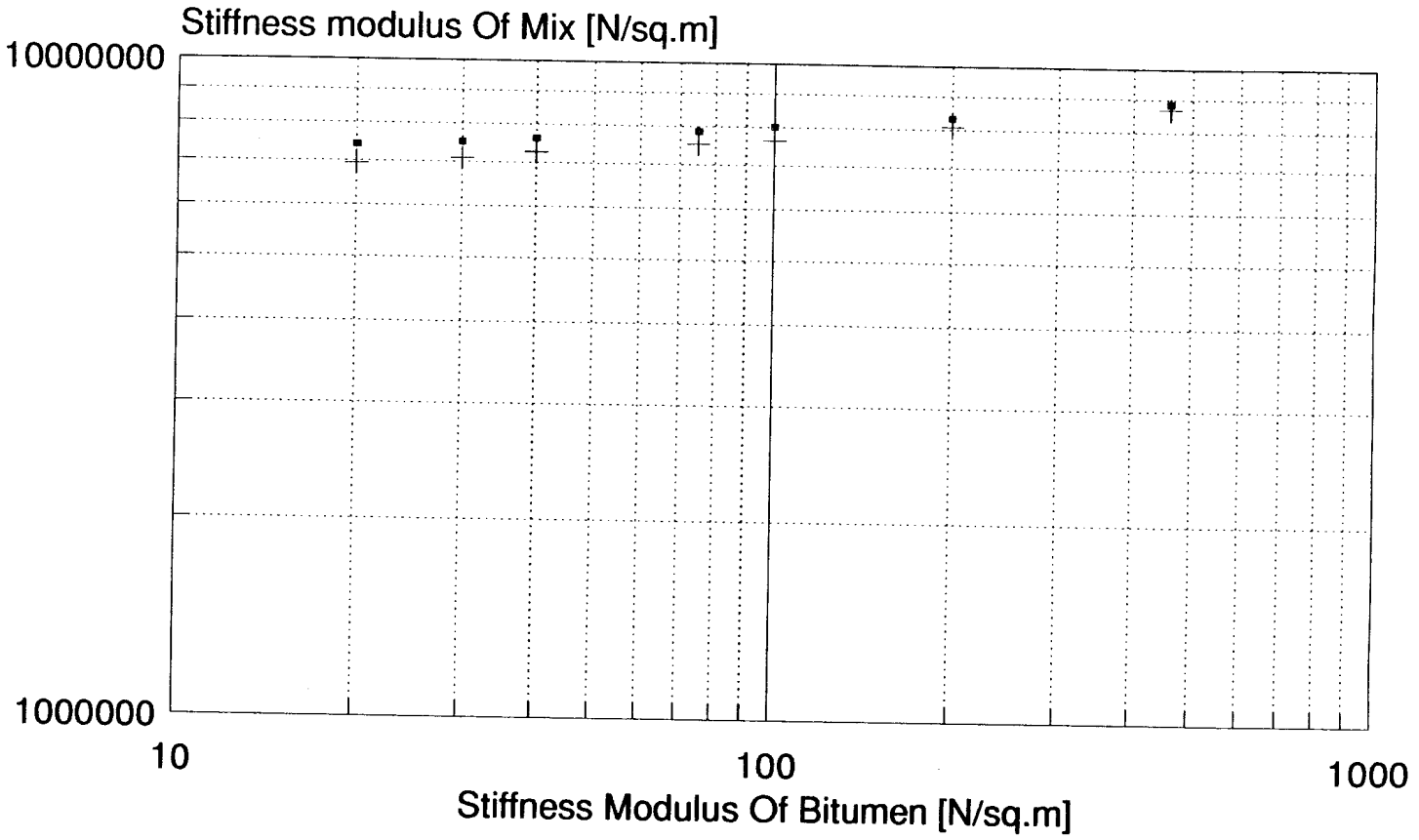

Figure 25. Static Creep Curves-
Compacted Specimens
Unarmed F-15
Section 7.

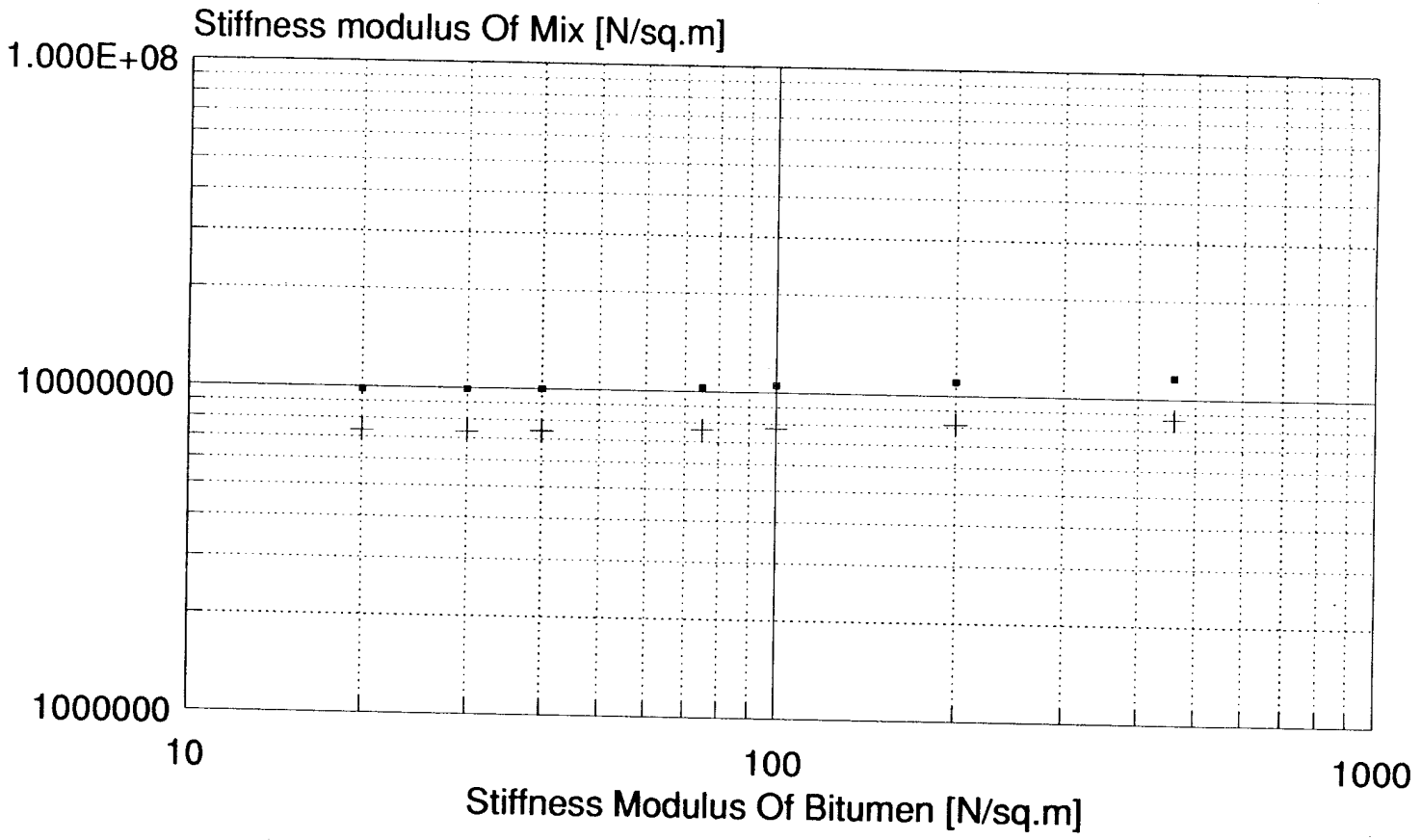

Figure 26. Static Creep Curves-
Compacted Specimens
Unarmed F-15
Section 8.

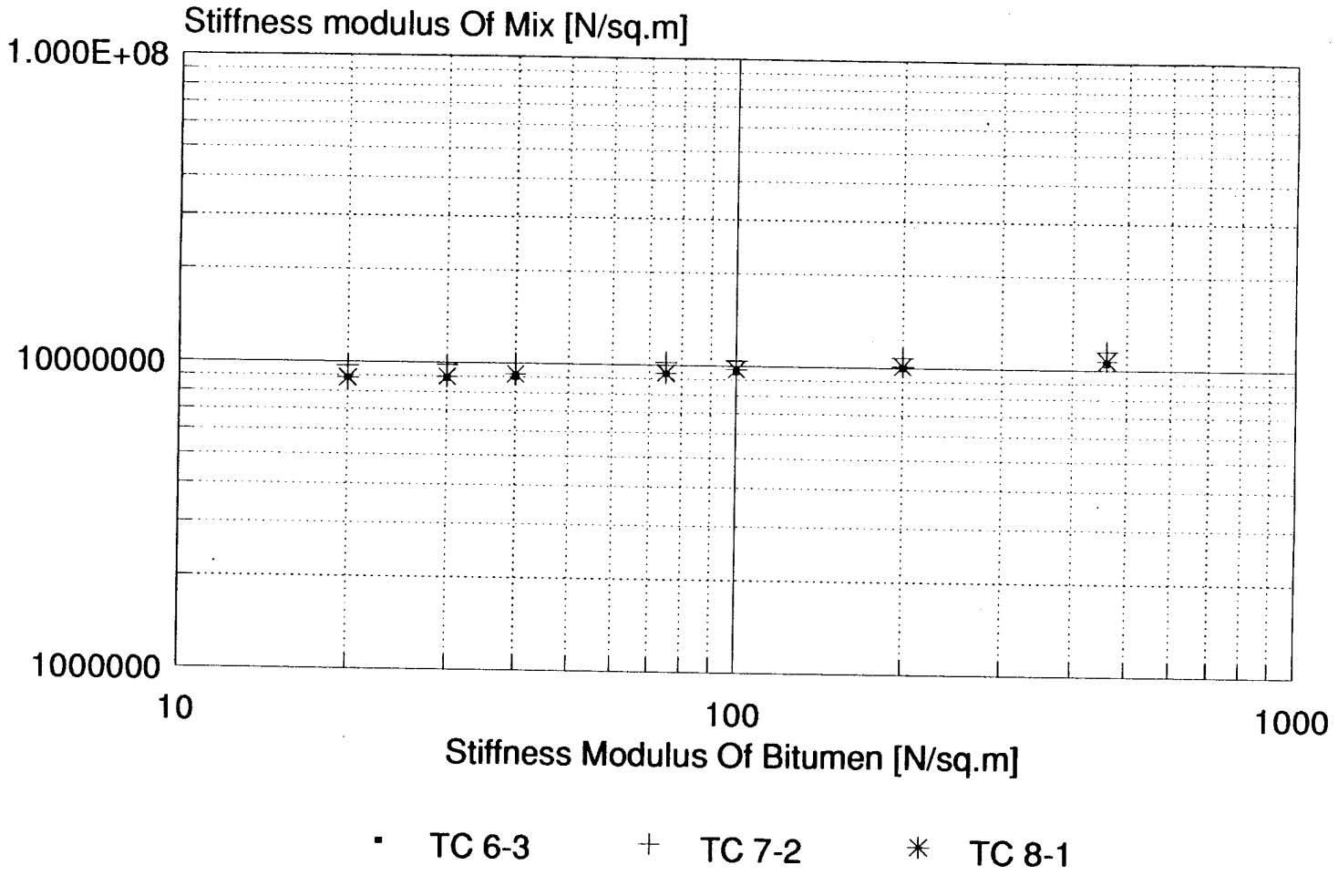

Figure 27. Static Creep Curves-
Compacted Specimens
Unarmed F-15
Section 9.

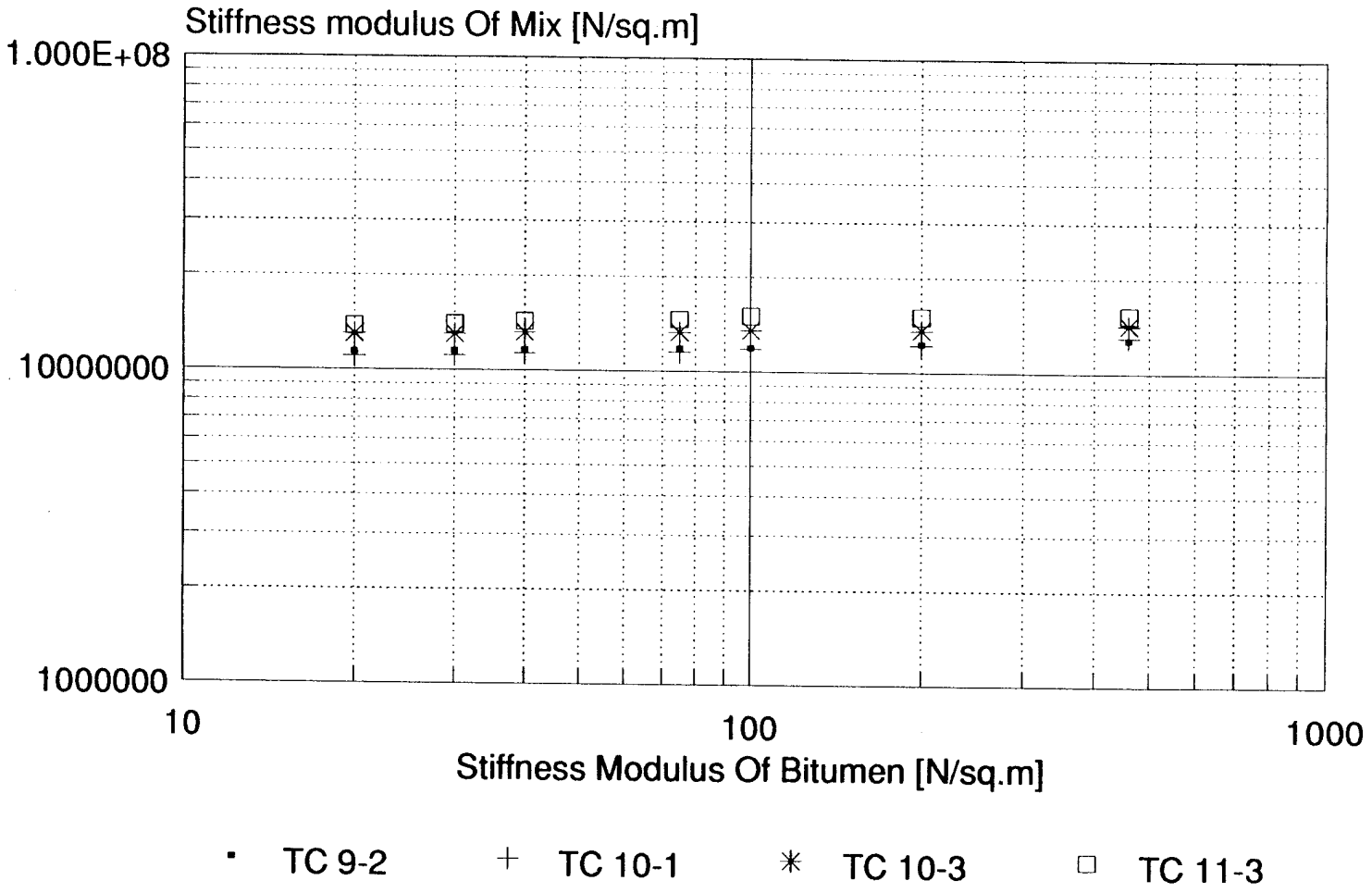

Figure 28. Static Creep Curves-
Compacted Specimens
Unarmed F-15
Section 10.

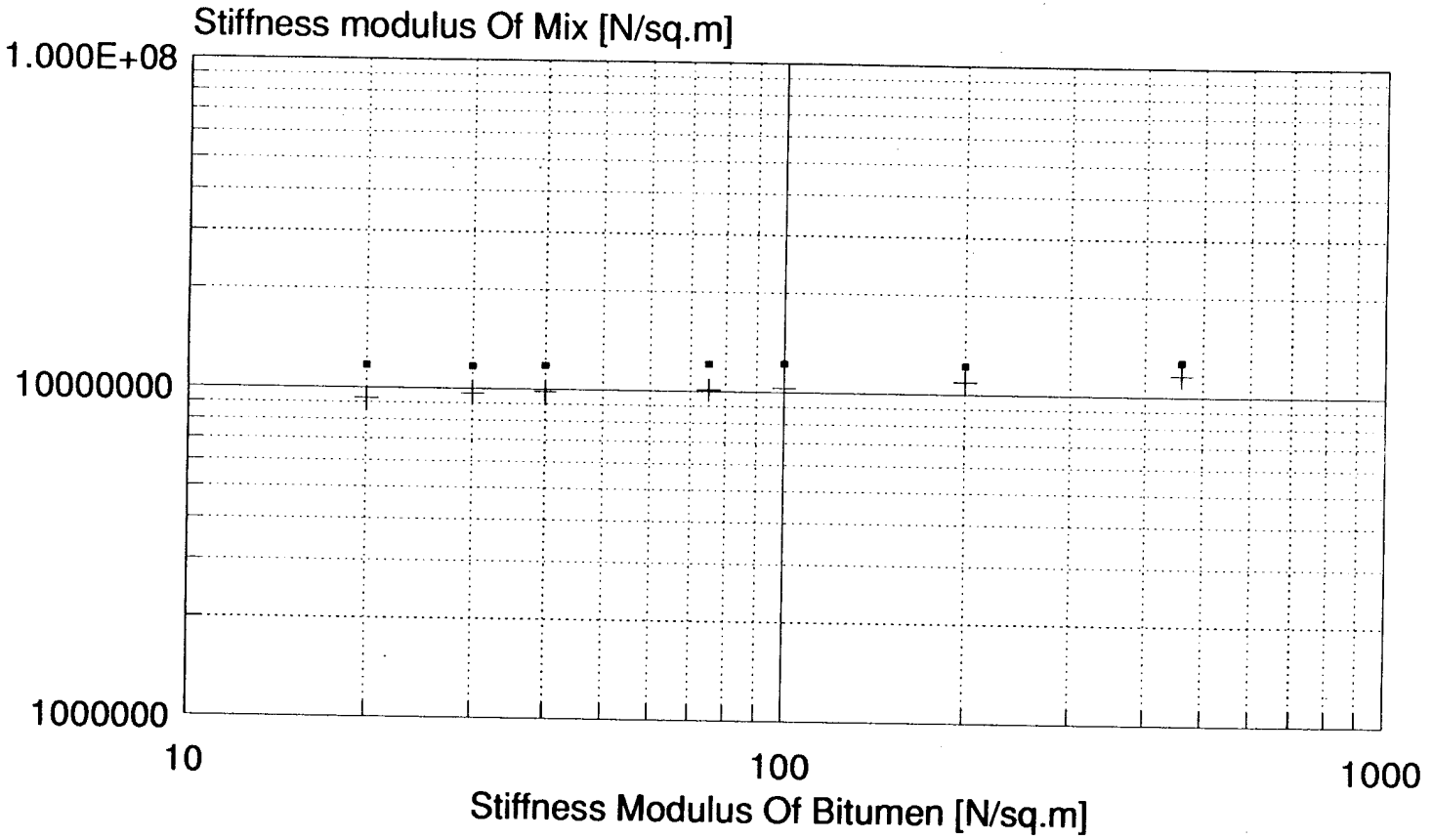

Figure 29. Static Creep Curves-
Compacted Specimens
Unarmed F-15
Section 11.

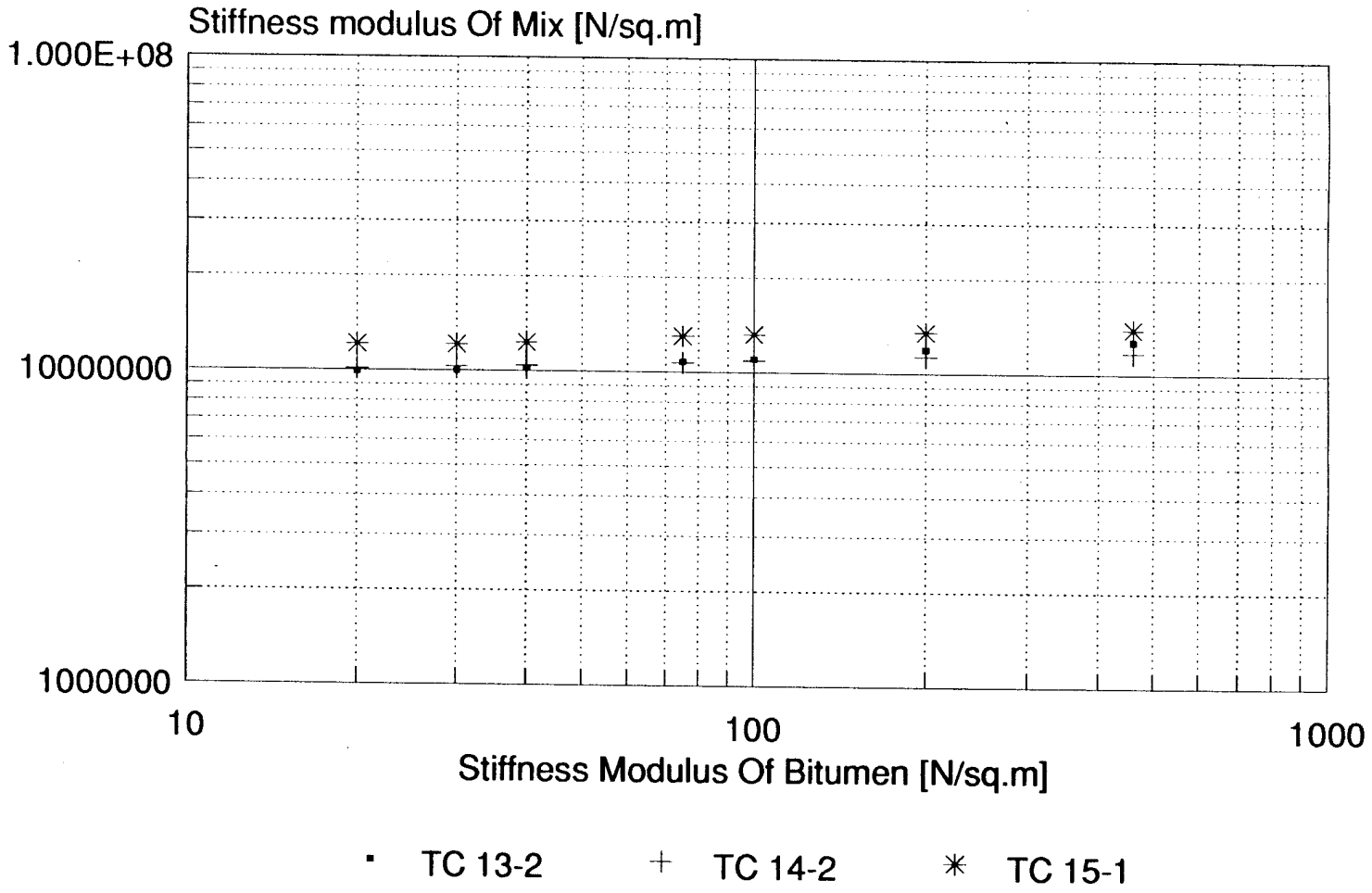

Figure 30. Static Creep Curves-
Compacted Specimens
Unarmed F-15
Section 12.

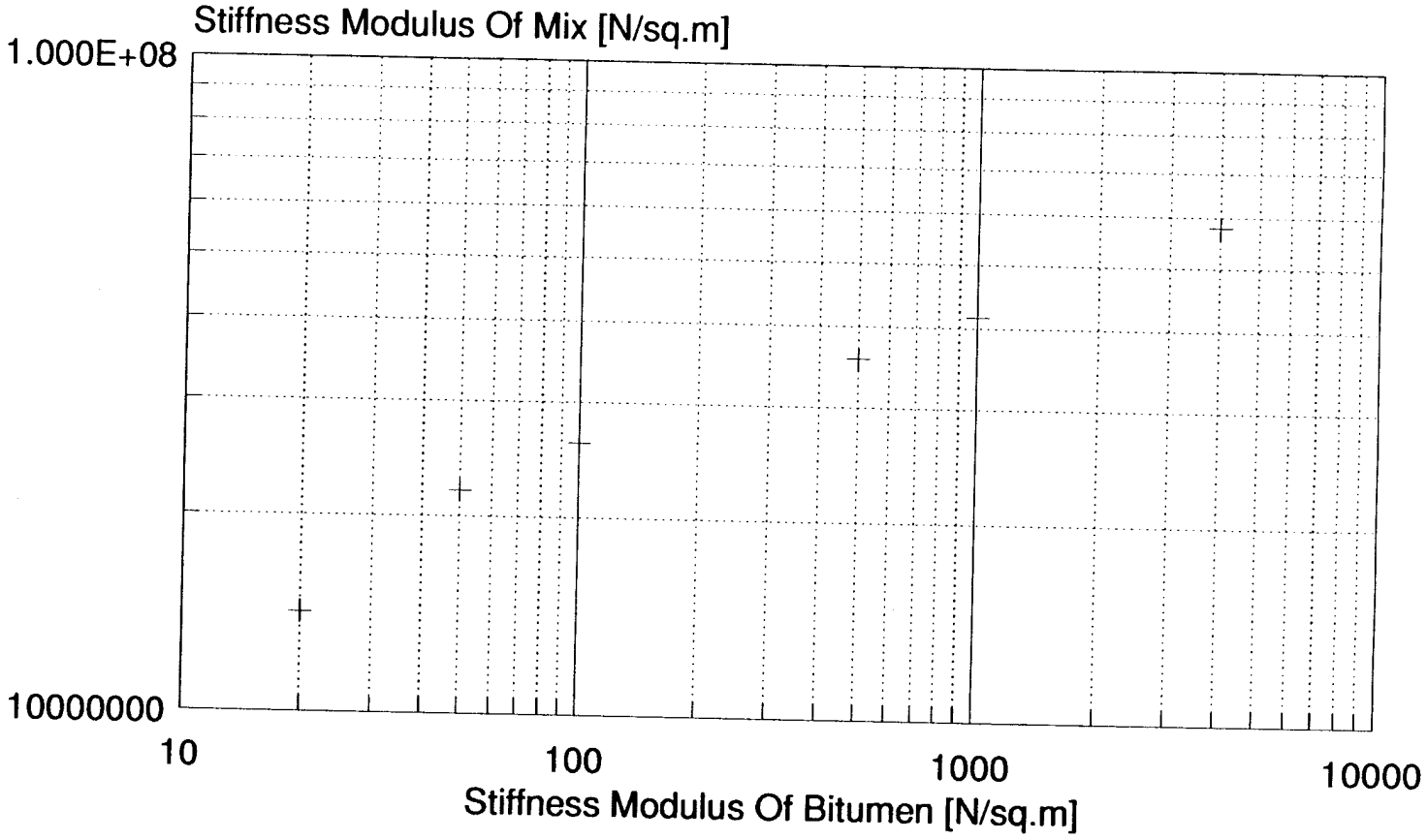

Figure 31. Dynamic Creep Curve - Drilled Core Fully Loaded F-15 Section 2.

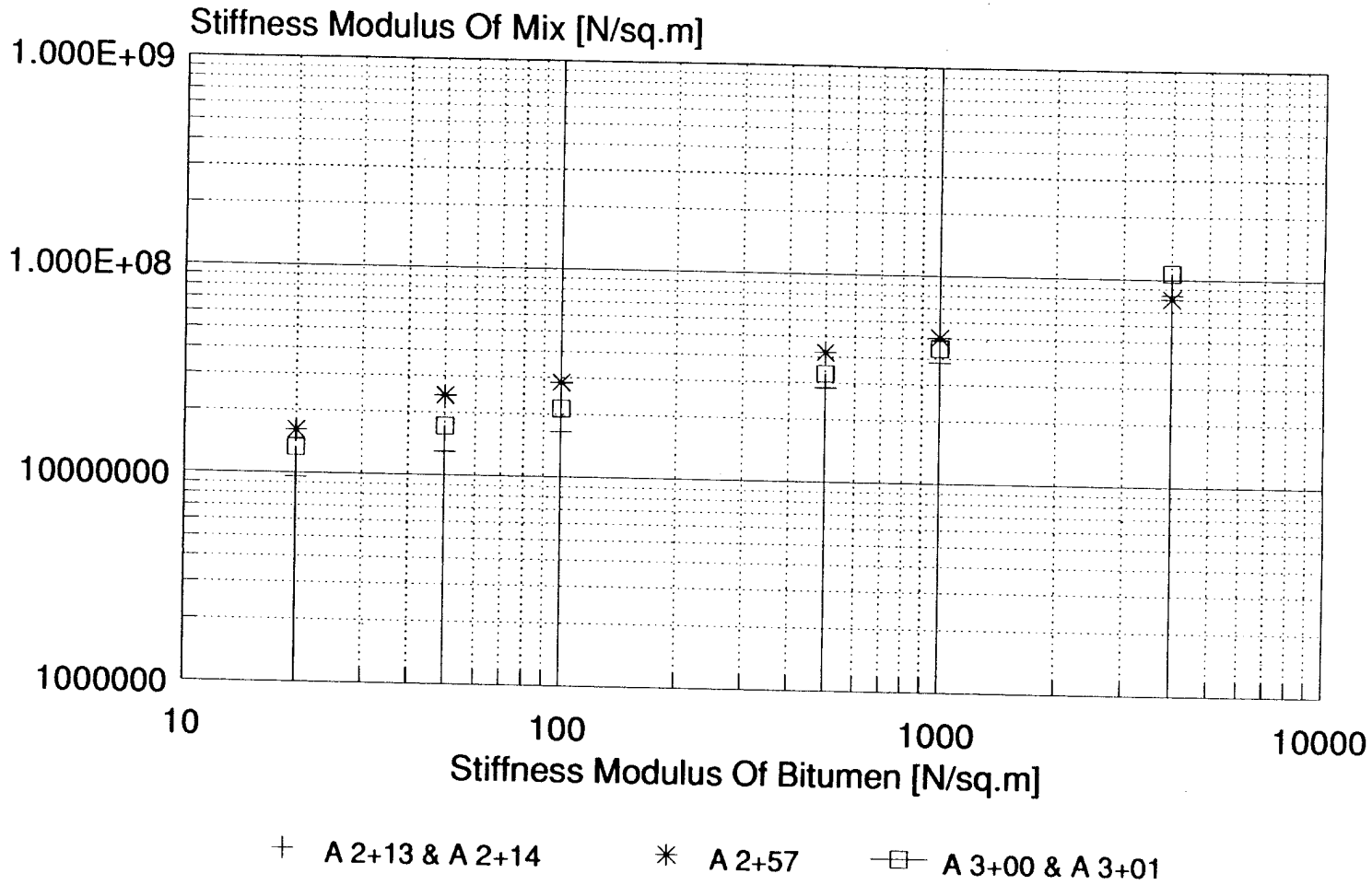

Figure 32. Dynamic Creep Curves-
Drilled Cores
Fully Loaded F-15
Section 3.

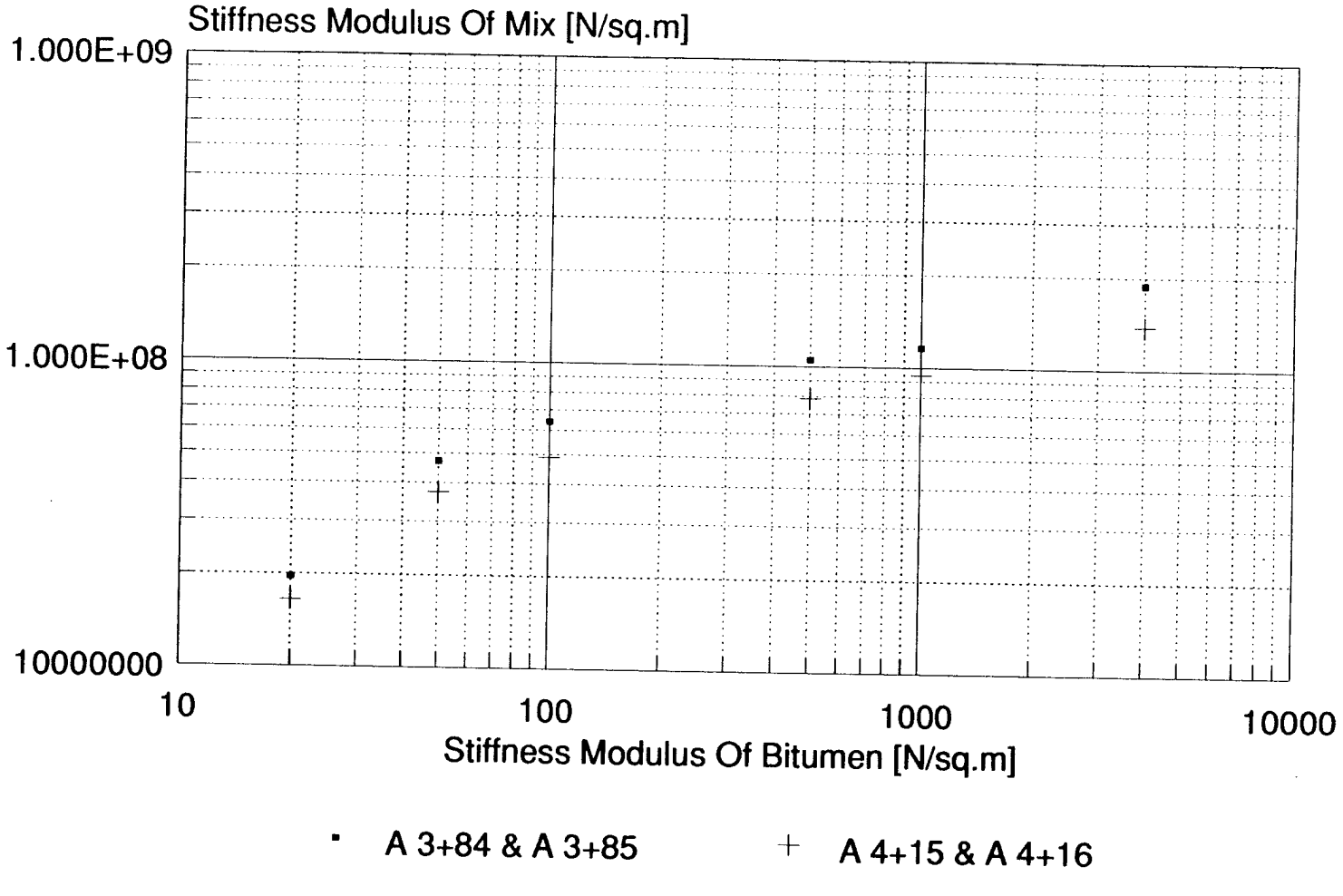

Figure 33. Dynamic Creep Curves-
Drilled Cores
Fully Loaded F-15
Section 4.

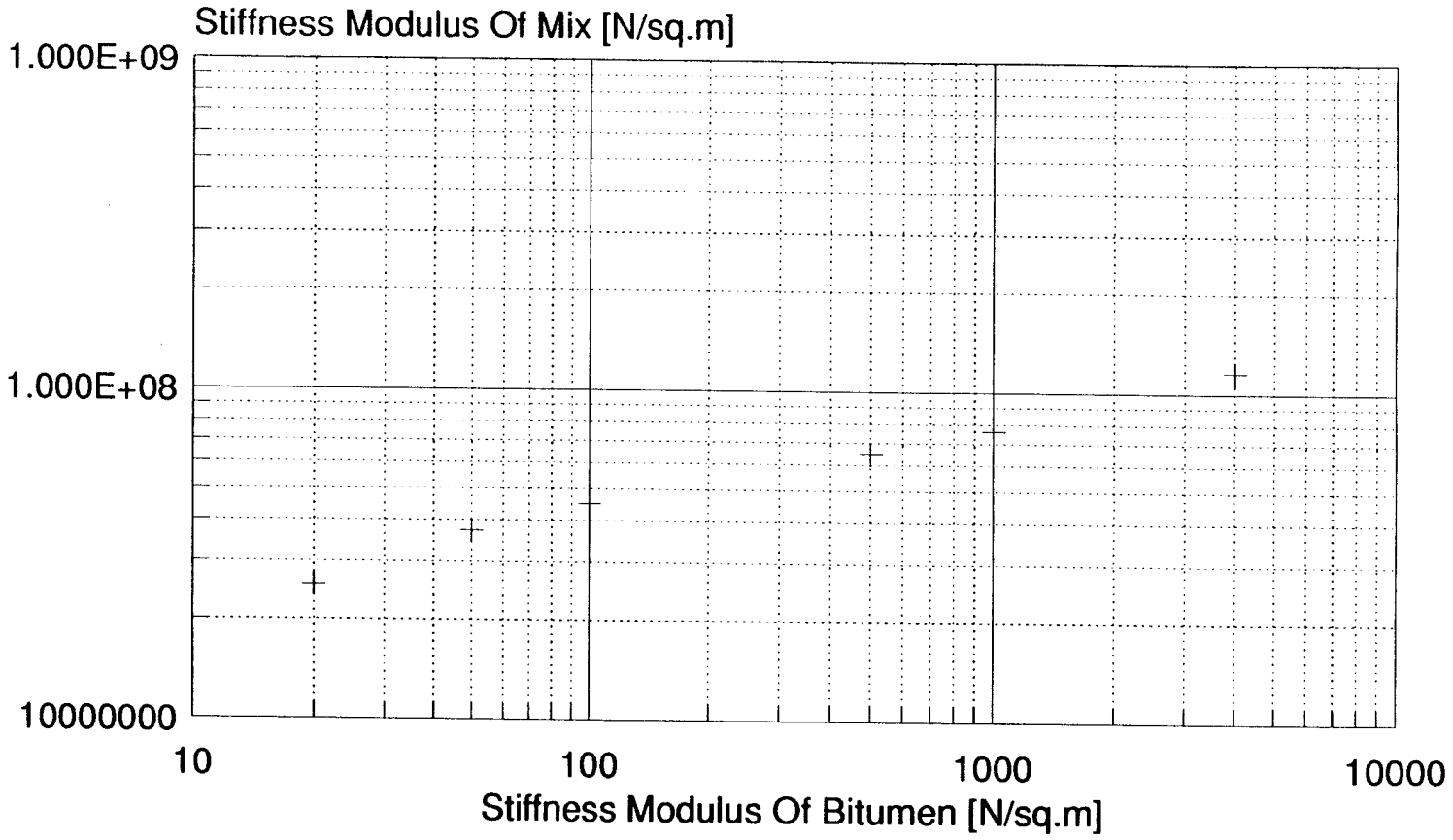

Figure 34. Dynamic Creep Curve - Drilled Core Fully Loaded F-15 Section 5.

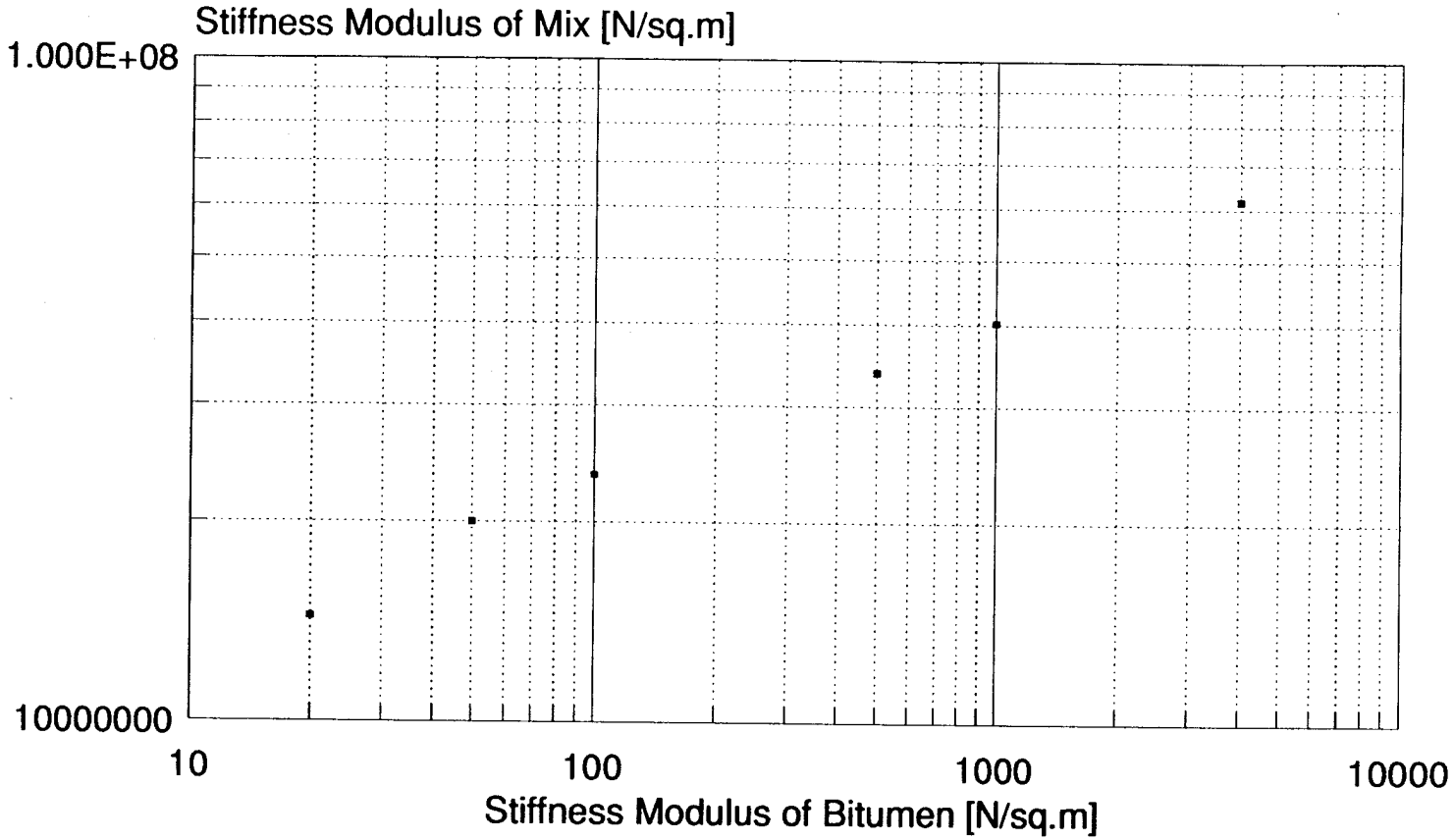

Figure 35. Dynamic Creep Curve - Drilled Core Unarmed F-15 Section 8.

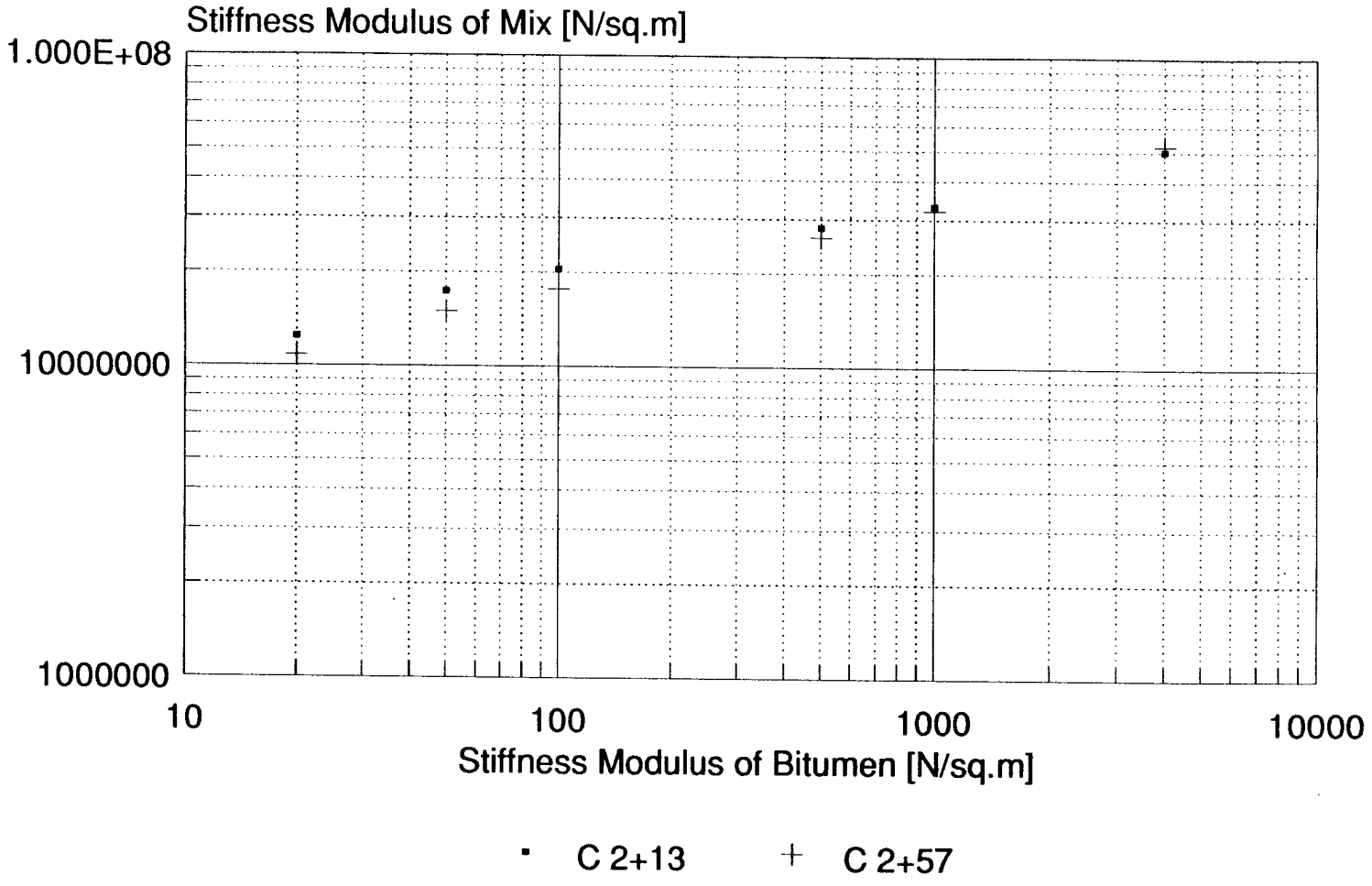

Figure 36. Dynamic Creep Curves-
Drilled Cores
Unarmed F-15
Section 9.

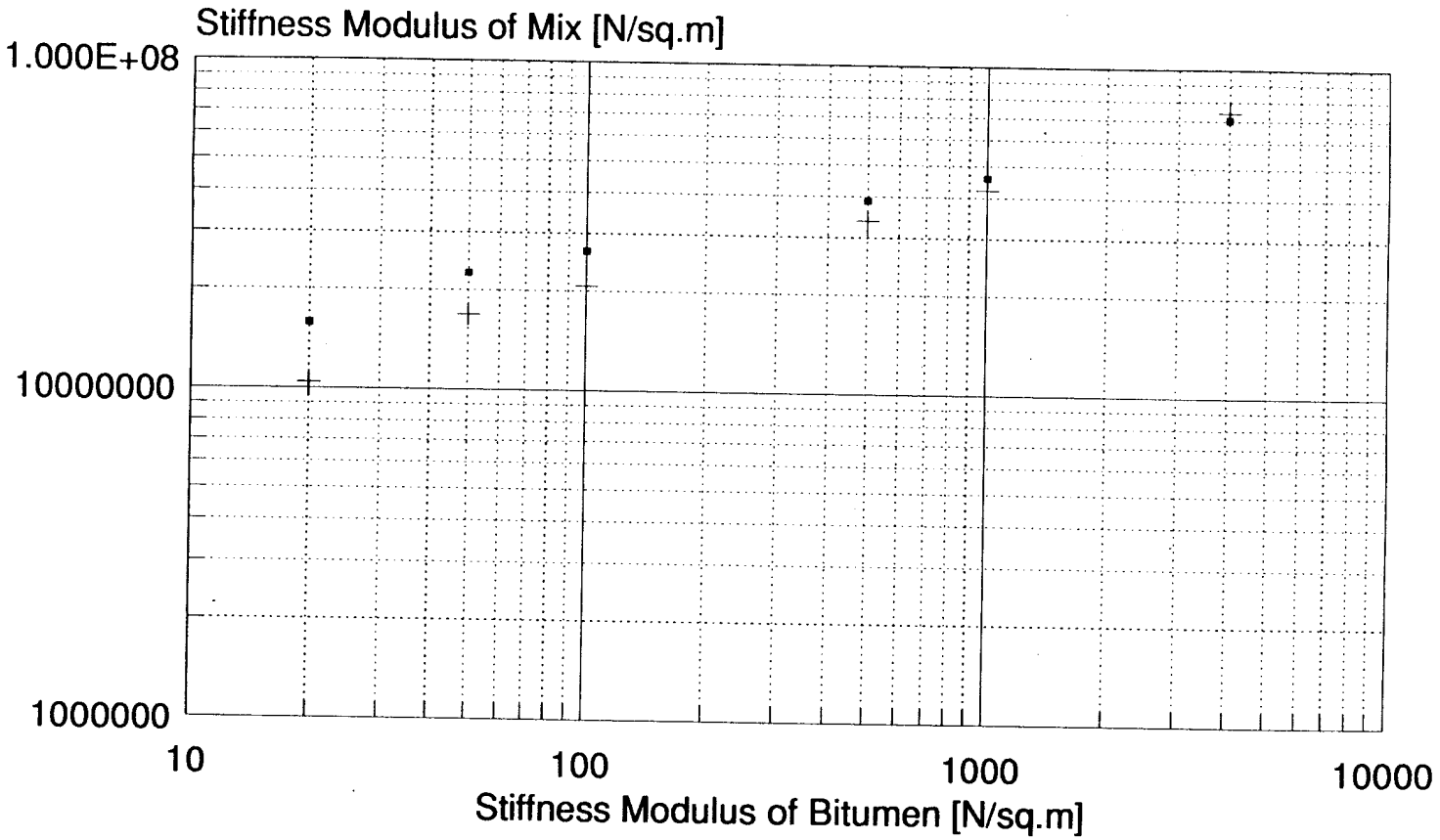

Figure 37. Dynamic Creep Curves-
Drilled Cores
Unarmed F-15
Section 10.

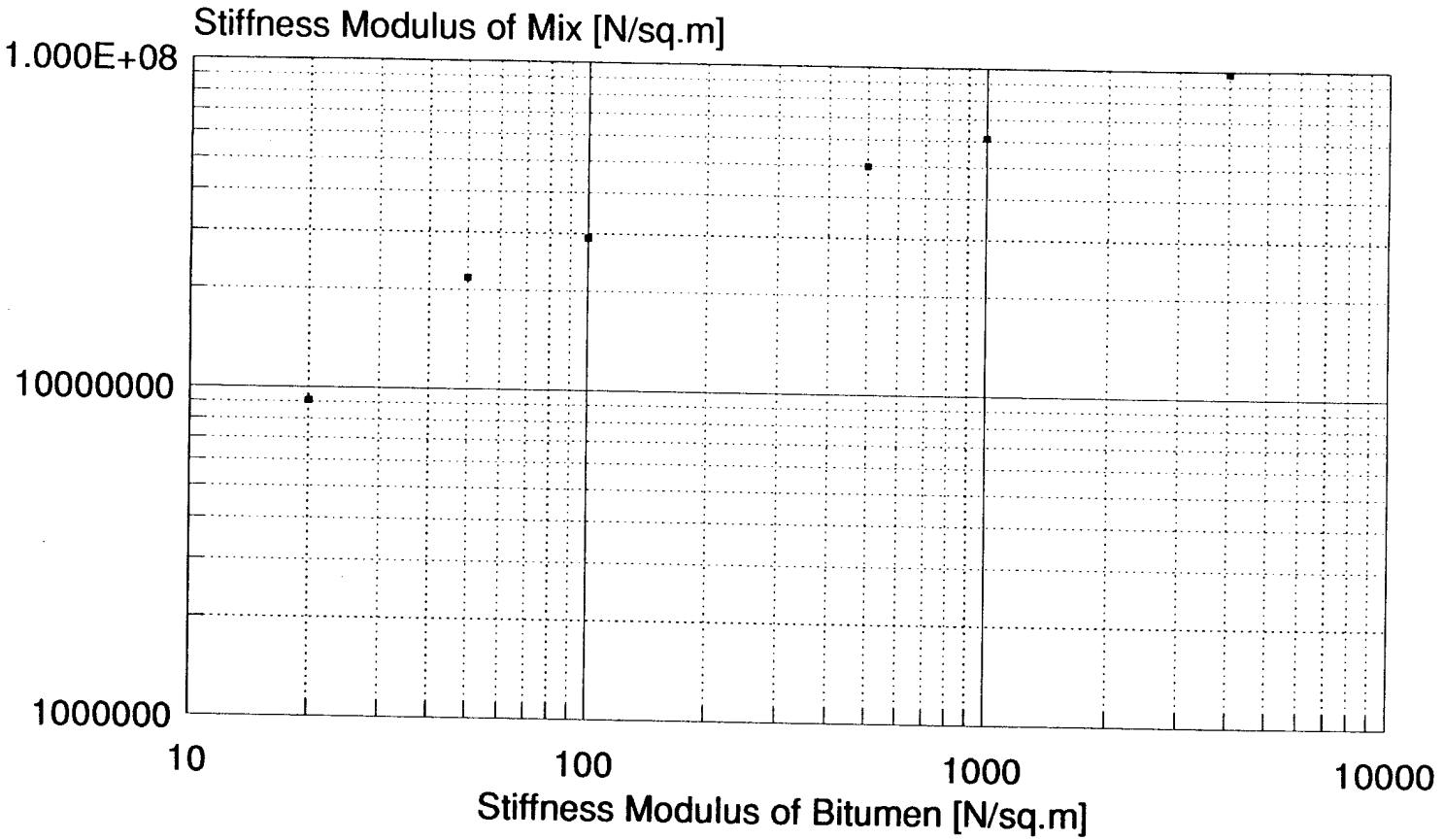

Figure 38. Dynamic Creep Curve - Drilled Core Unarmed F-15 Section 11.

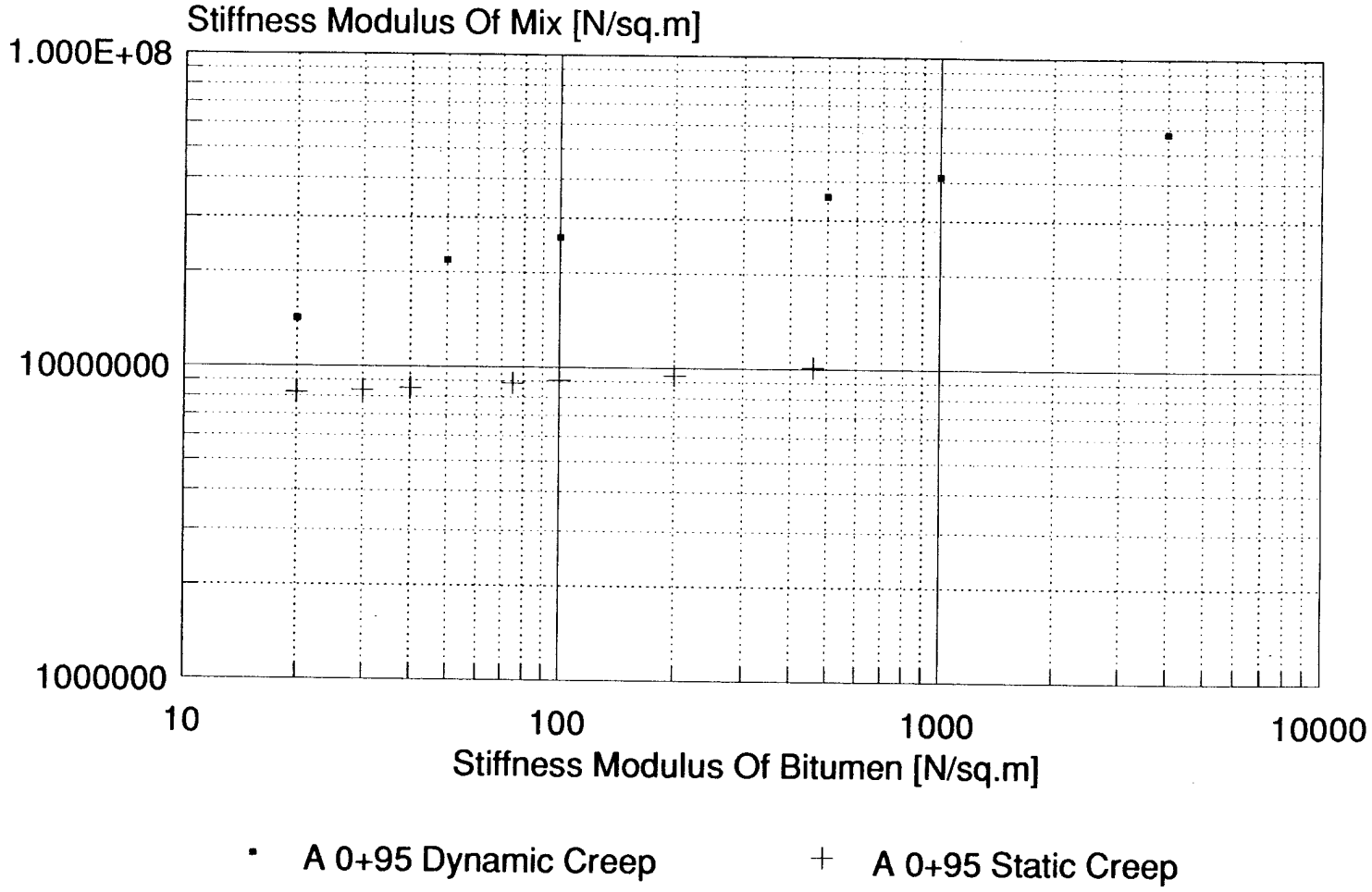

Figure 39. Comparison of Dynamic Creep Curve and Static Creep Curve (Drilled Cores) Section 2 Fully Loaded F-15.

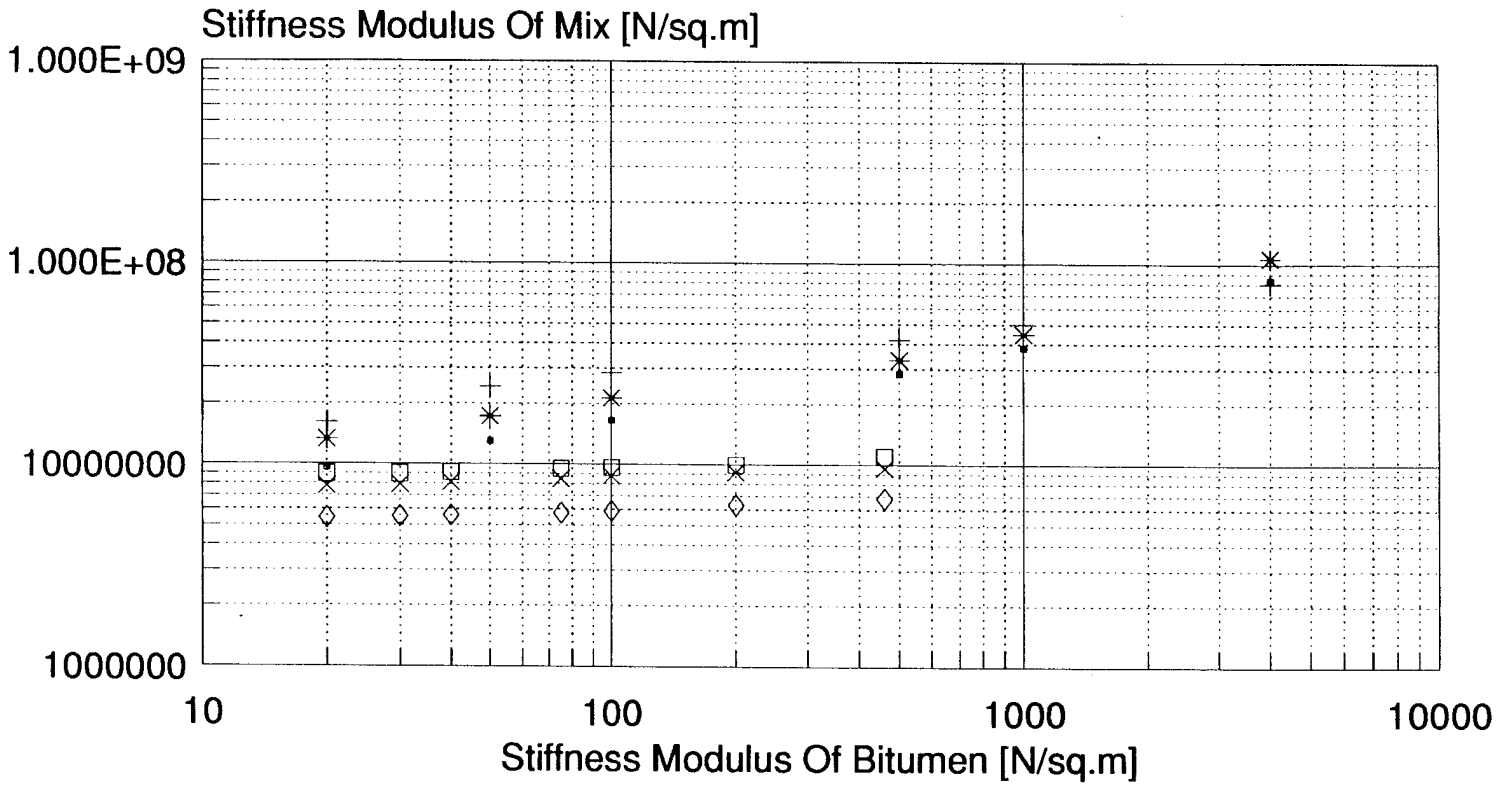

Figure 40. Comparison of Dynamic Creep Curves and Static Creep Curves (Drilled Cores) Section 3 Fully Loaded F-15.

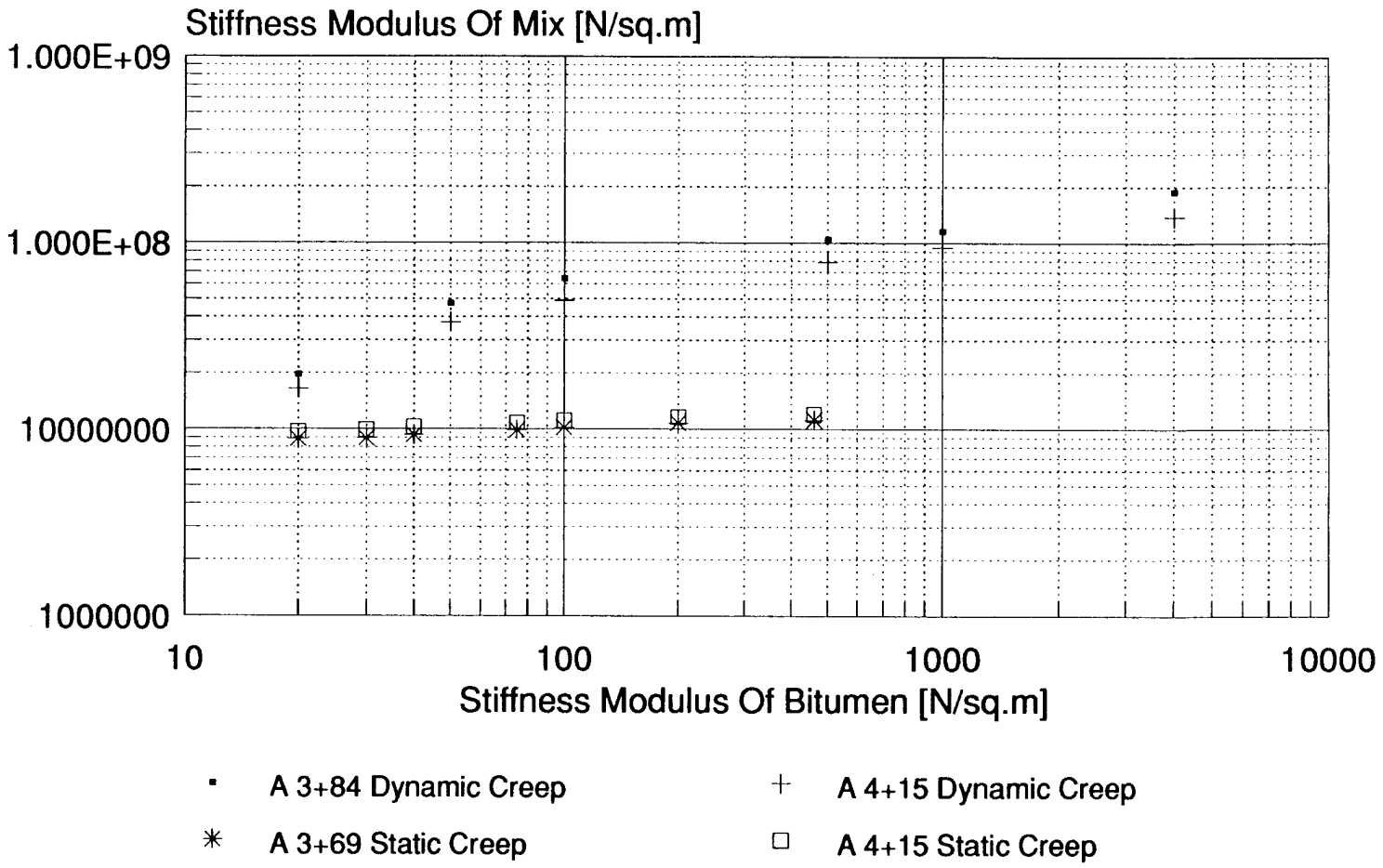

Figure 41. Comparison of Dynamic Creep Curves and Static Creep Curves (Drilled Cores) Section 4 Fully Loaded F-15.

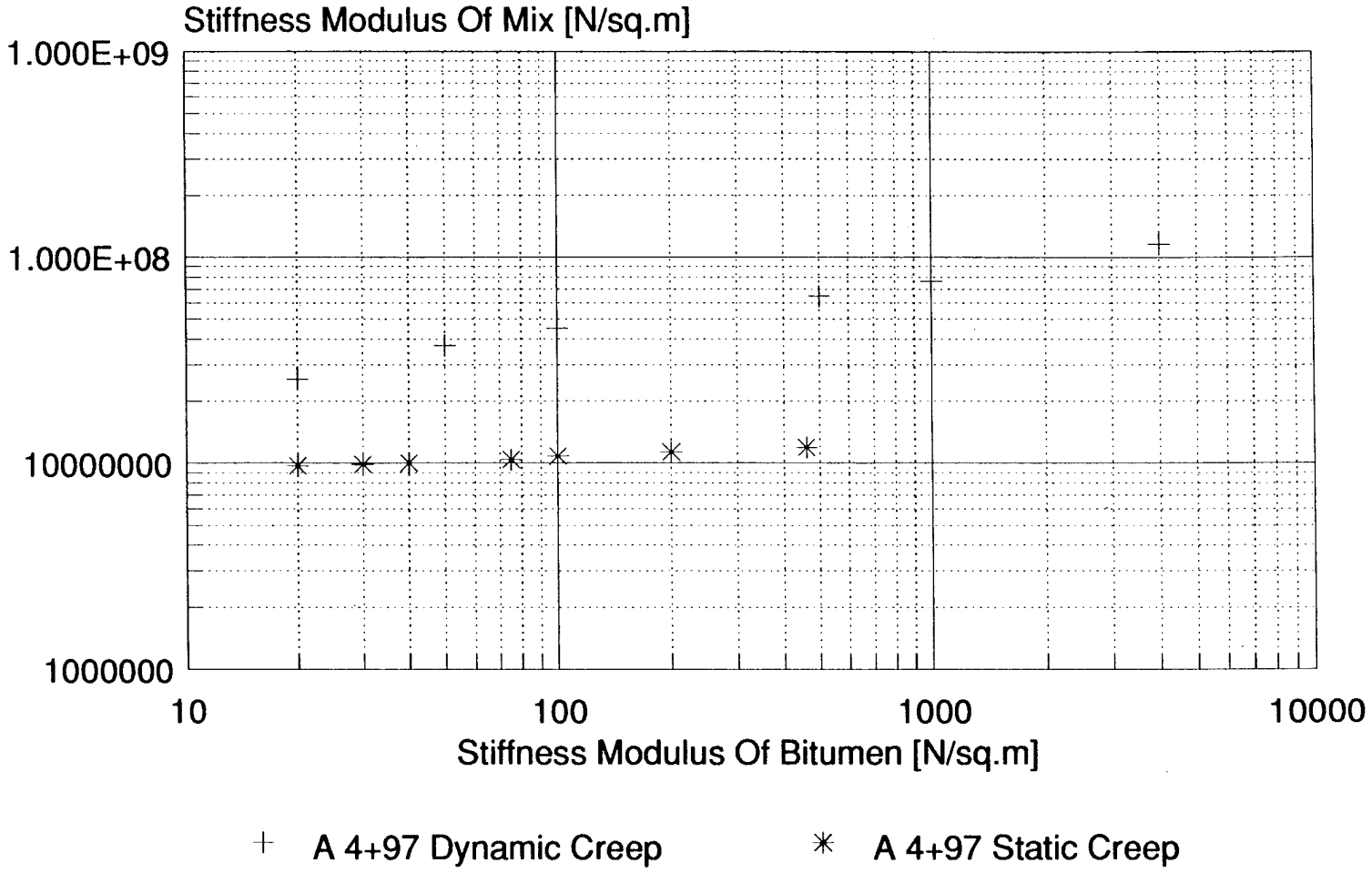

Figure 42. Comparison of Dynamic Creep Curve and Static Creep Curve (Drilled Cores) Section 5 Fully Loaded F-15.

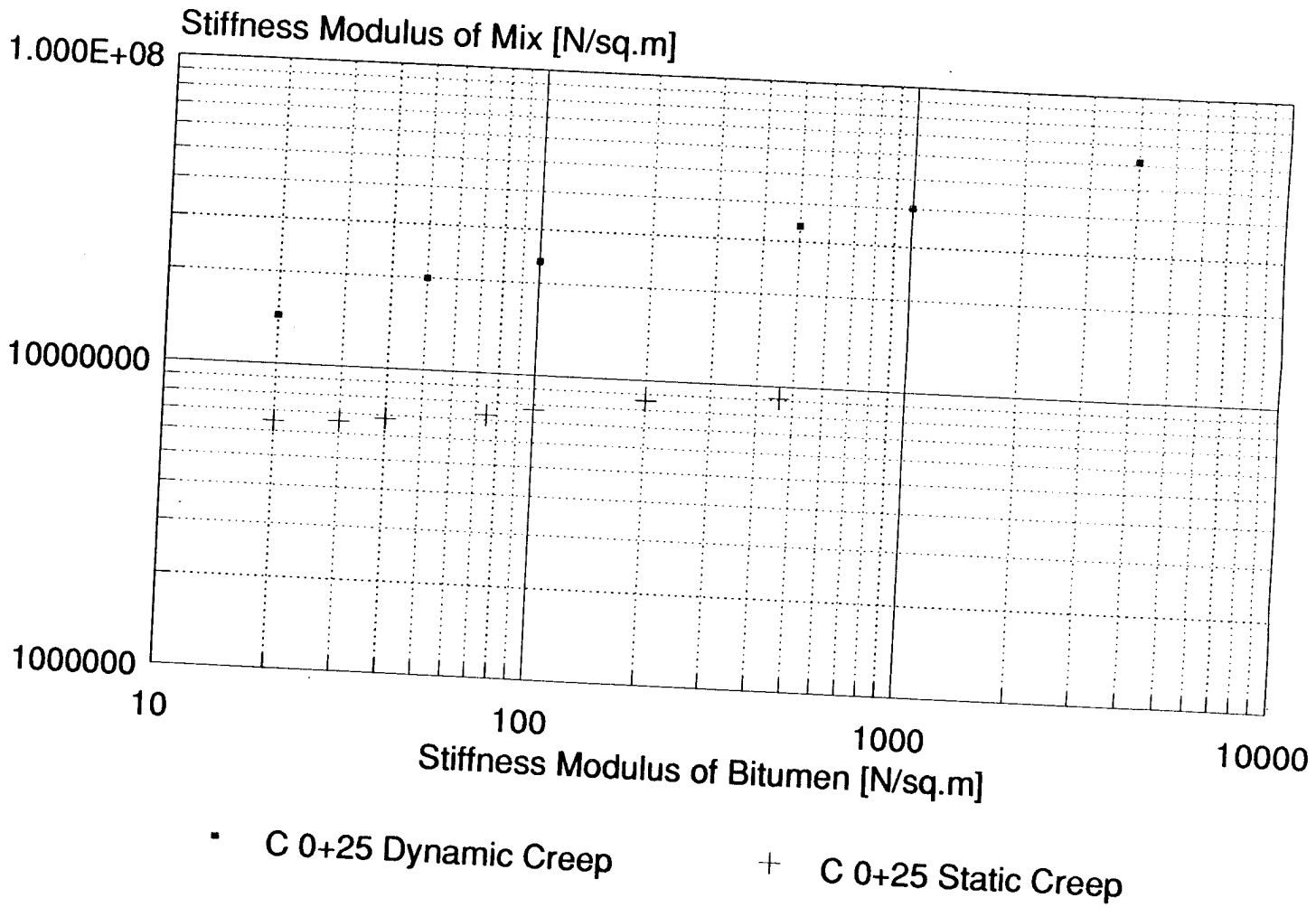

Figure 43. Comparison of Dynamic Creep Curve and Static Creep Curve (Drilled Cores) Section 8 Unarmed F-15.

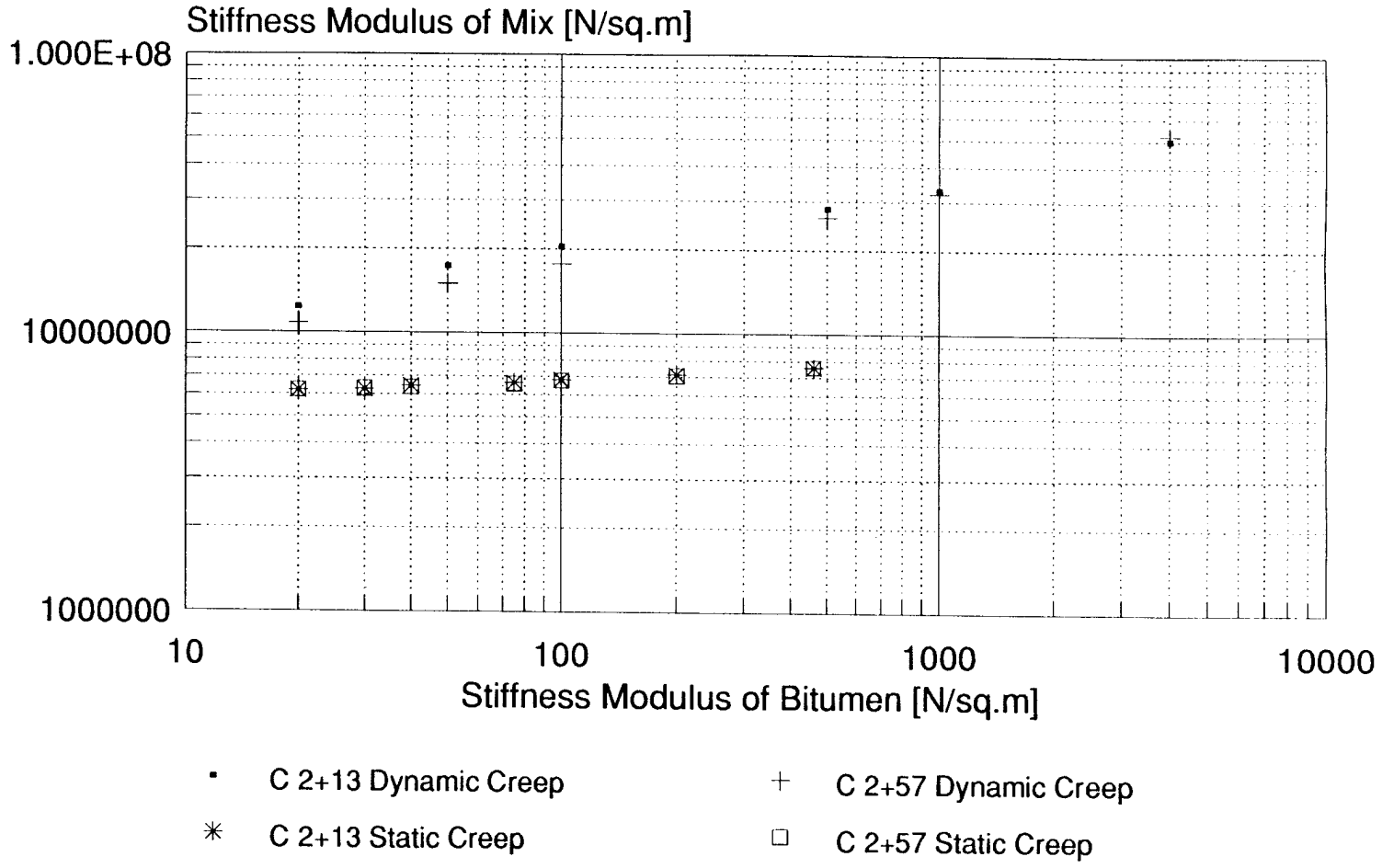

Figure 44. Comparison of Dynamic Creep Curves and Static Creep Curves (Drilled Cores) Section 9 Unarmed F-15.

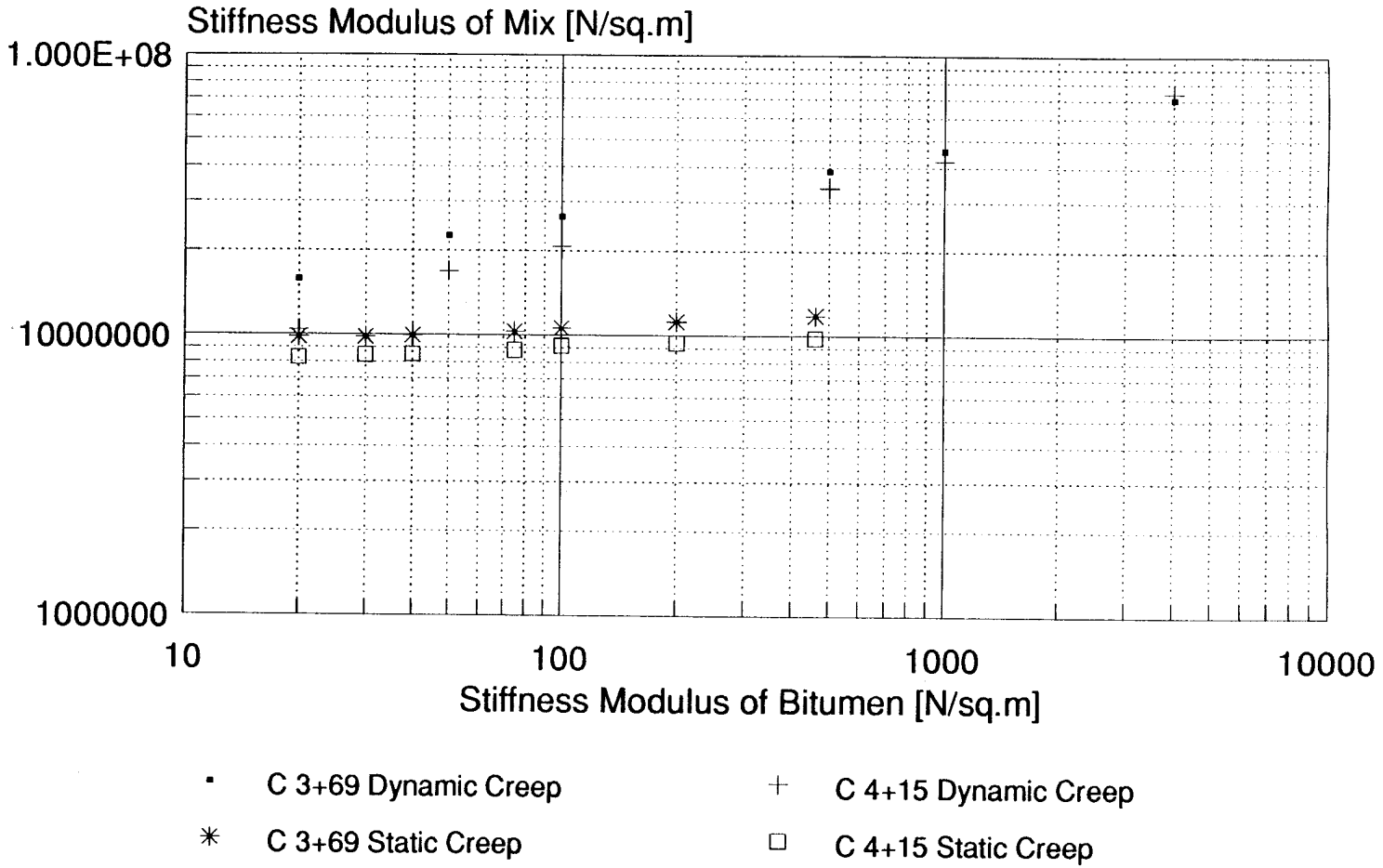

Figure 45. Comparison of Dynamic Creep Curves and Static Creep Curves (Drilled Cores) Section 10 Unarmed F-15.

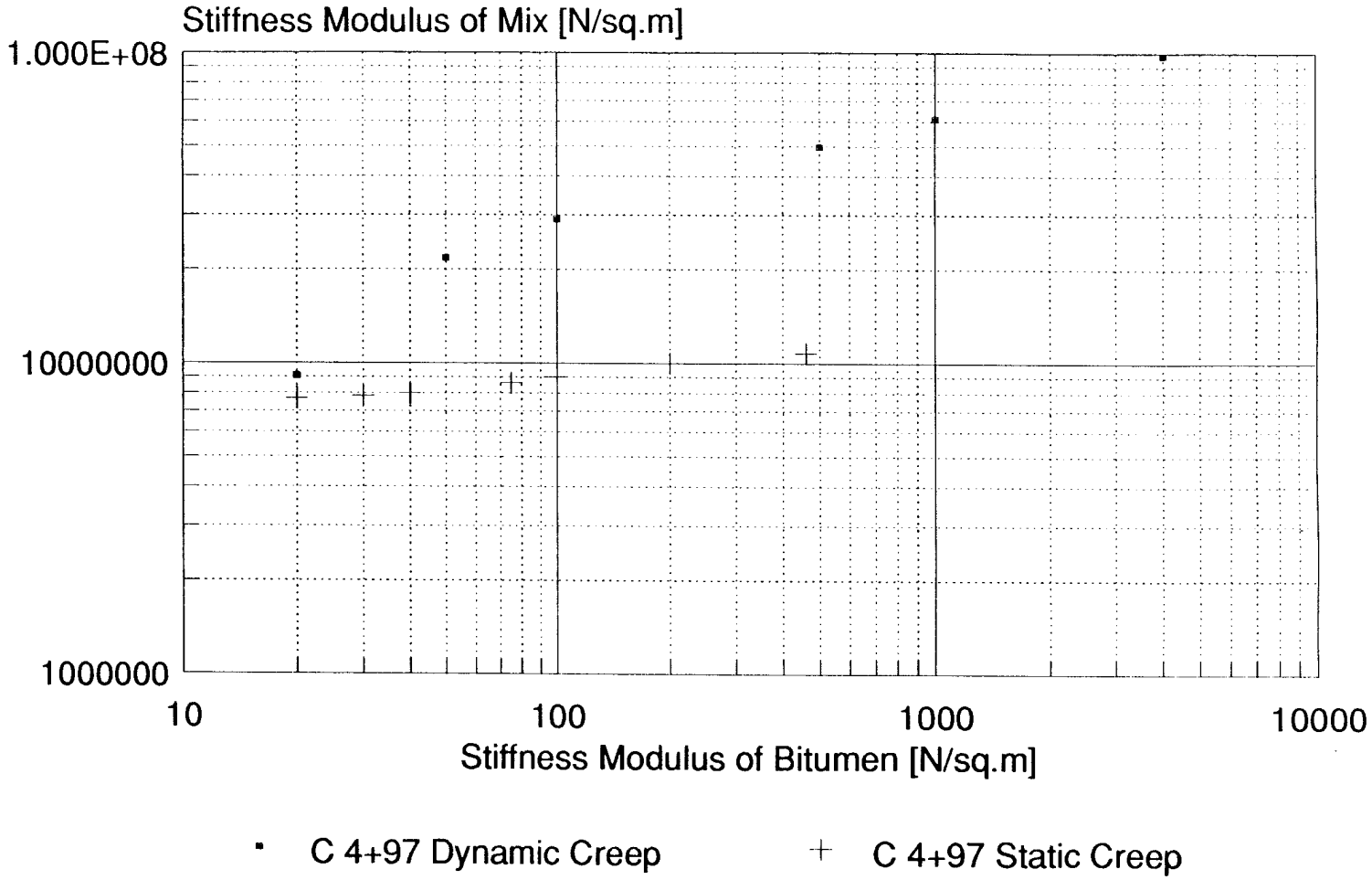

Figure 46. Comparison of Dynamic Creep Curve and Static Creep Curve (Drilled Cores) Section 11 Unarmed F-15.

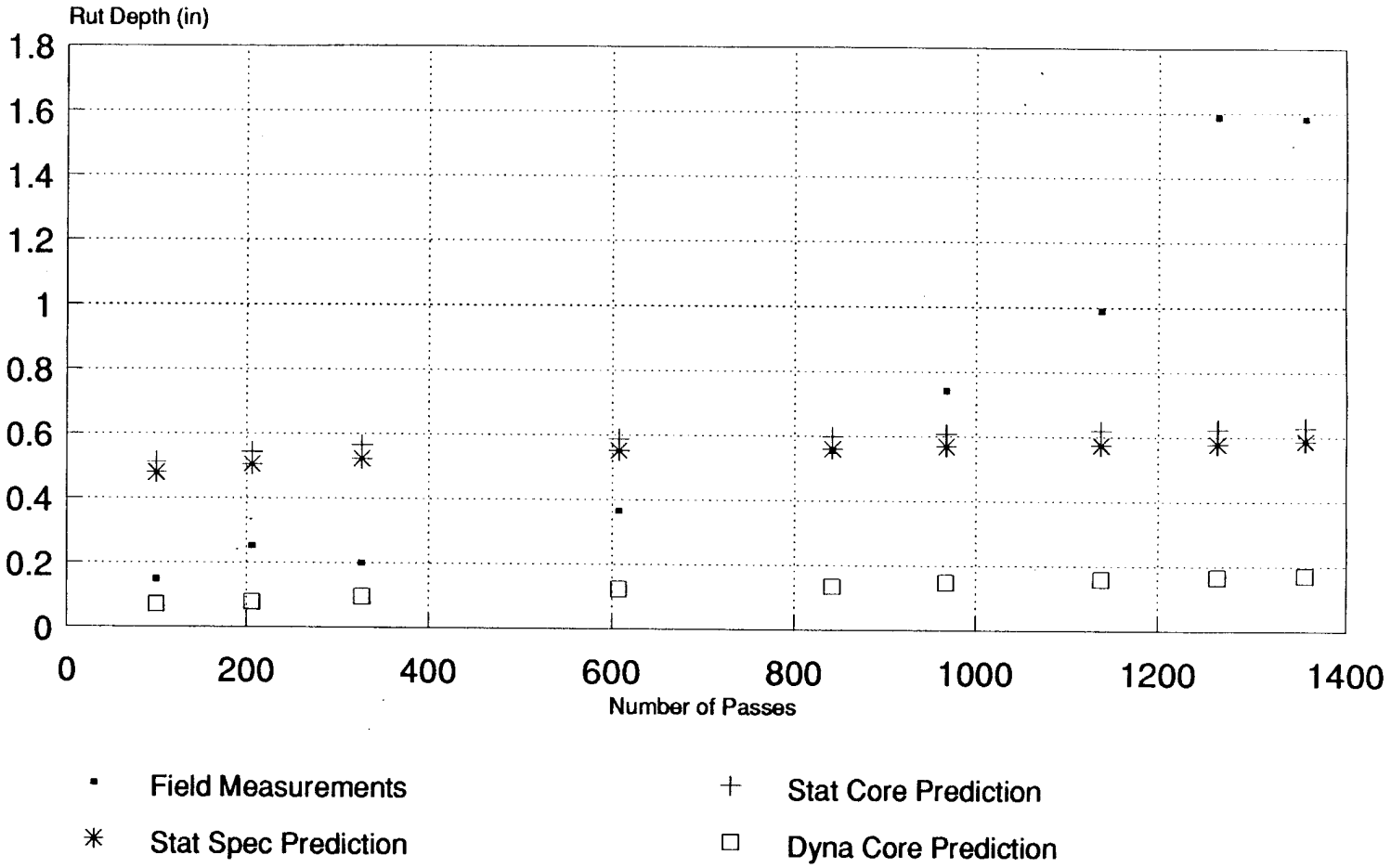

Figure 47. Comparison of Rut Depth Predictions and Field Measurements for Station A 2+12.

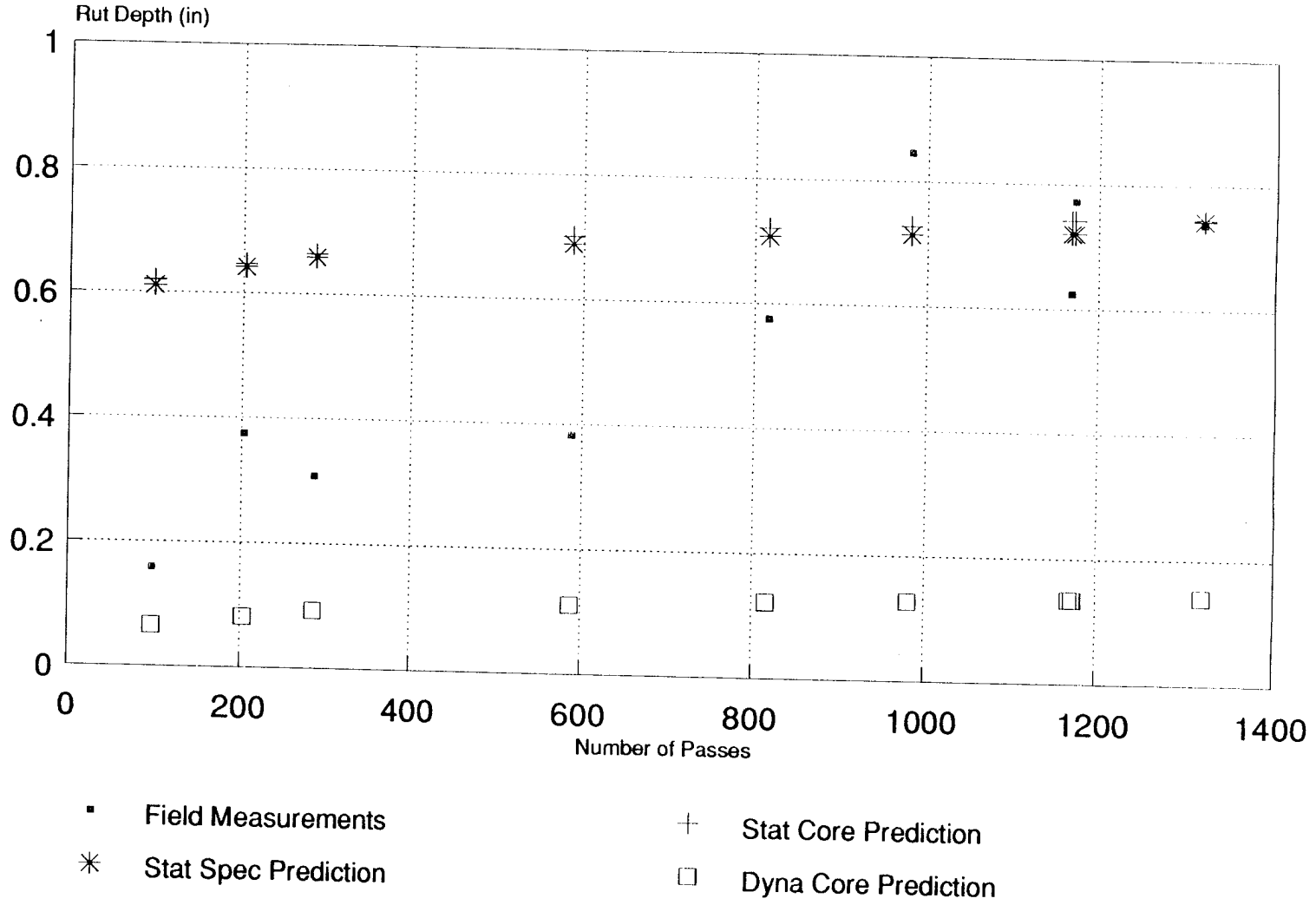

Figure 48. Comparison of Rut Depth Predictions and Field Measurements for Station A 2+60.

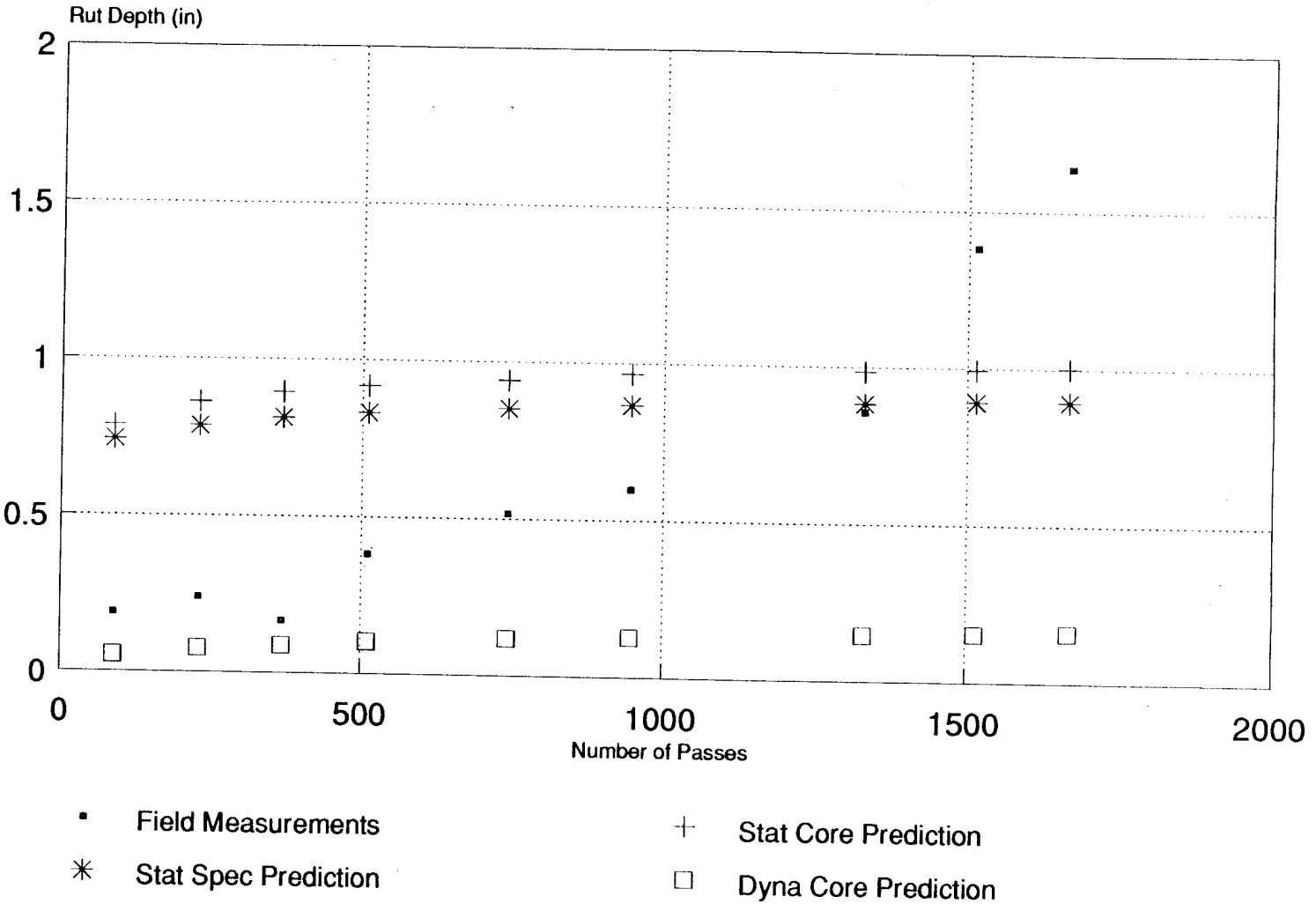

Figure 49. Comparison of Rut Depth Predictions and Field Measurements for Station A 3+00.

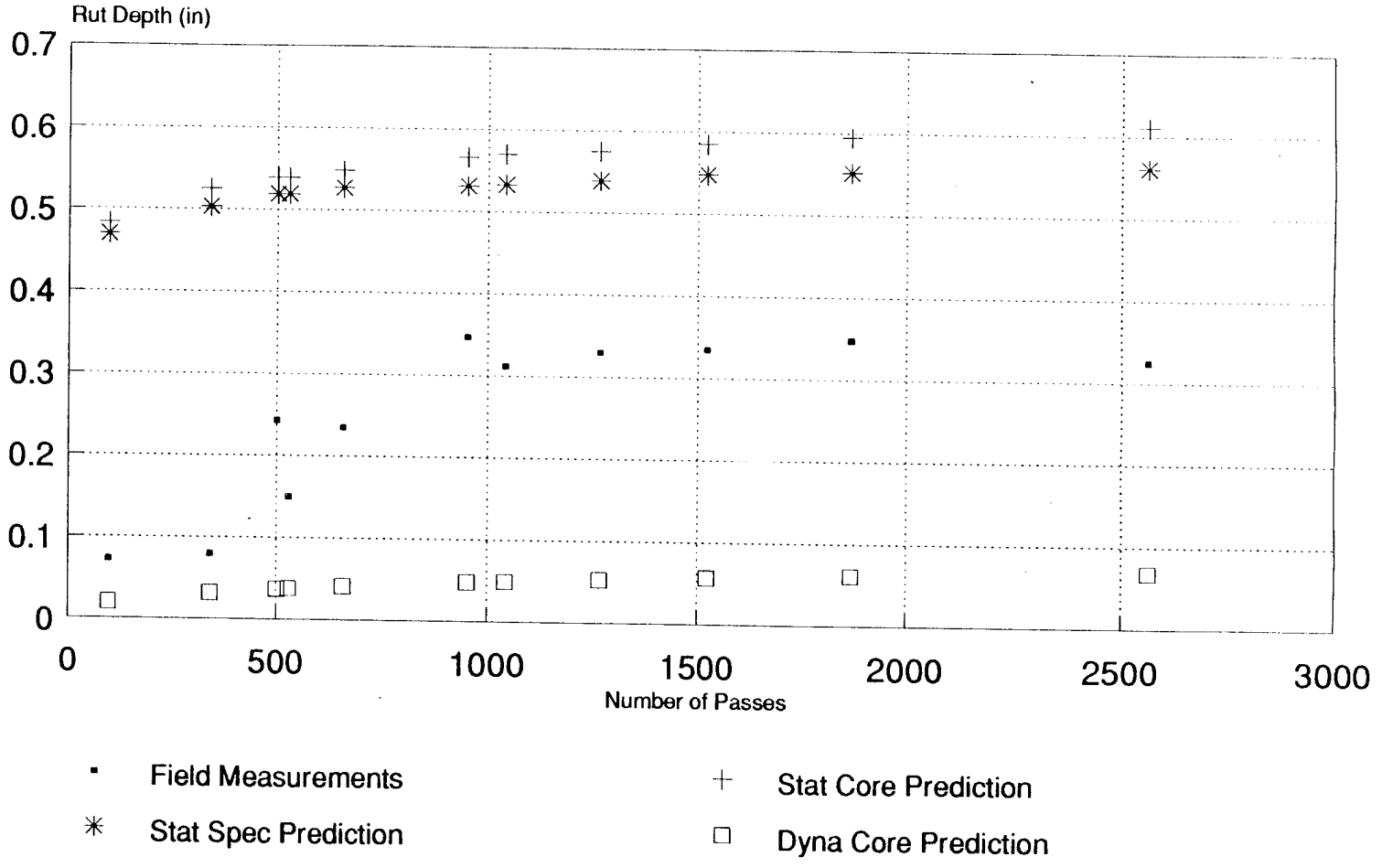

Figure 50. Comparison of Rut Depth Predictions and Field Measurements for Station A 3+86.

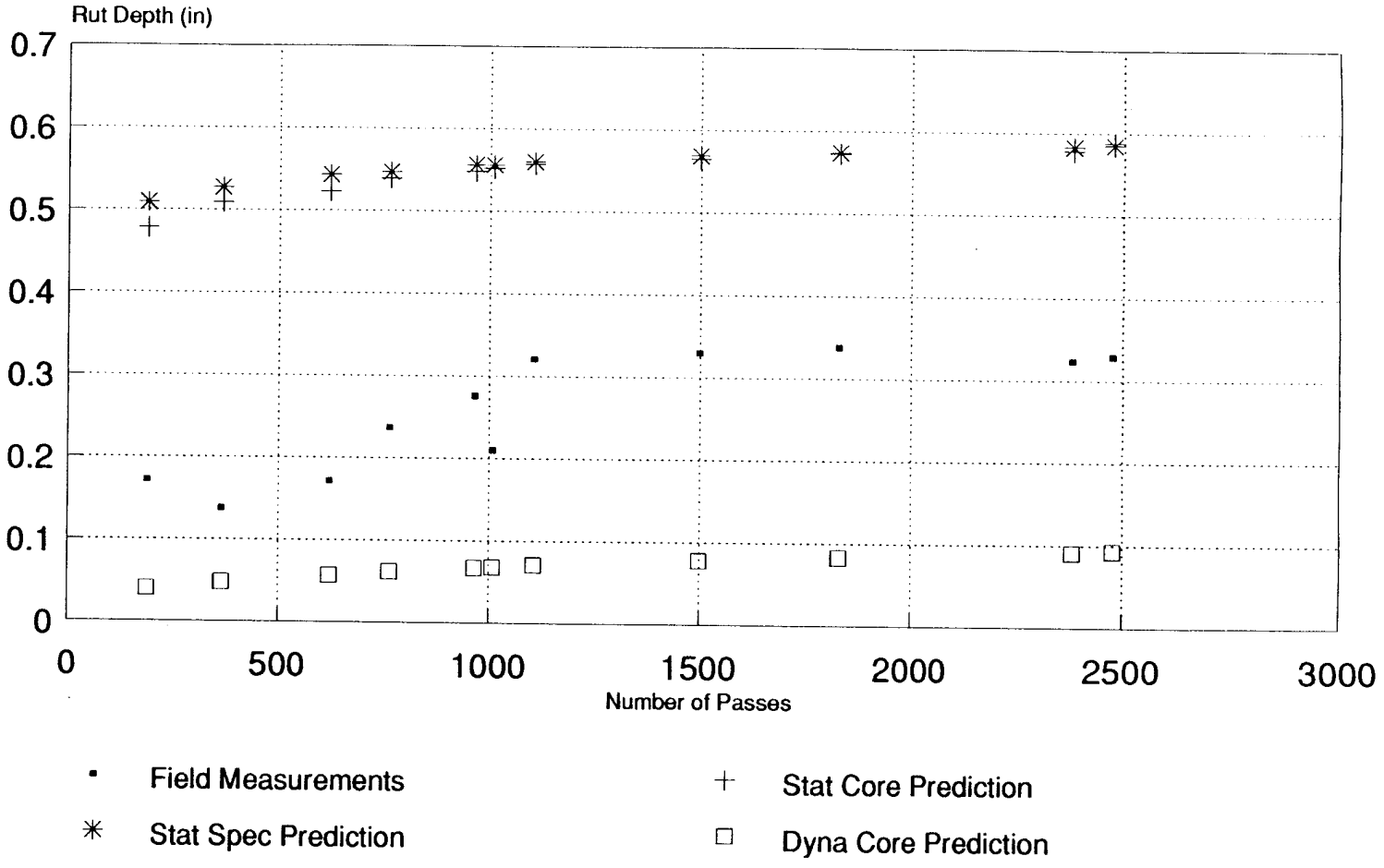

Figure 51. Comparison of Rut Depth Predictions and Field Measurements for Station A 4+10.

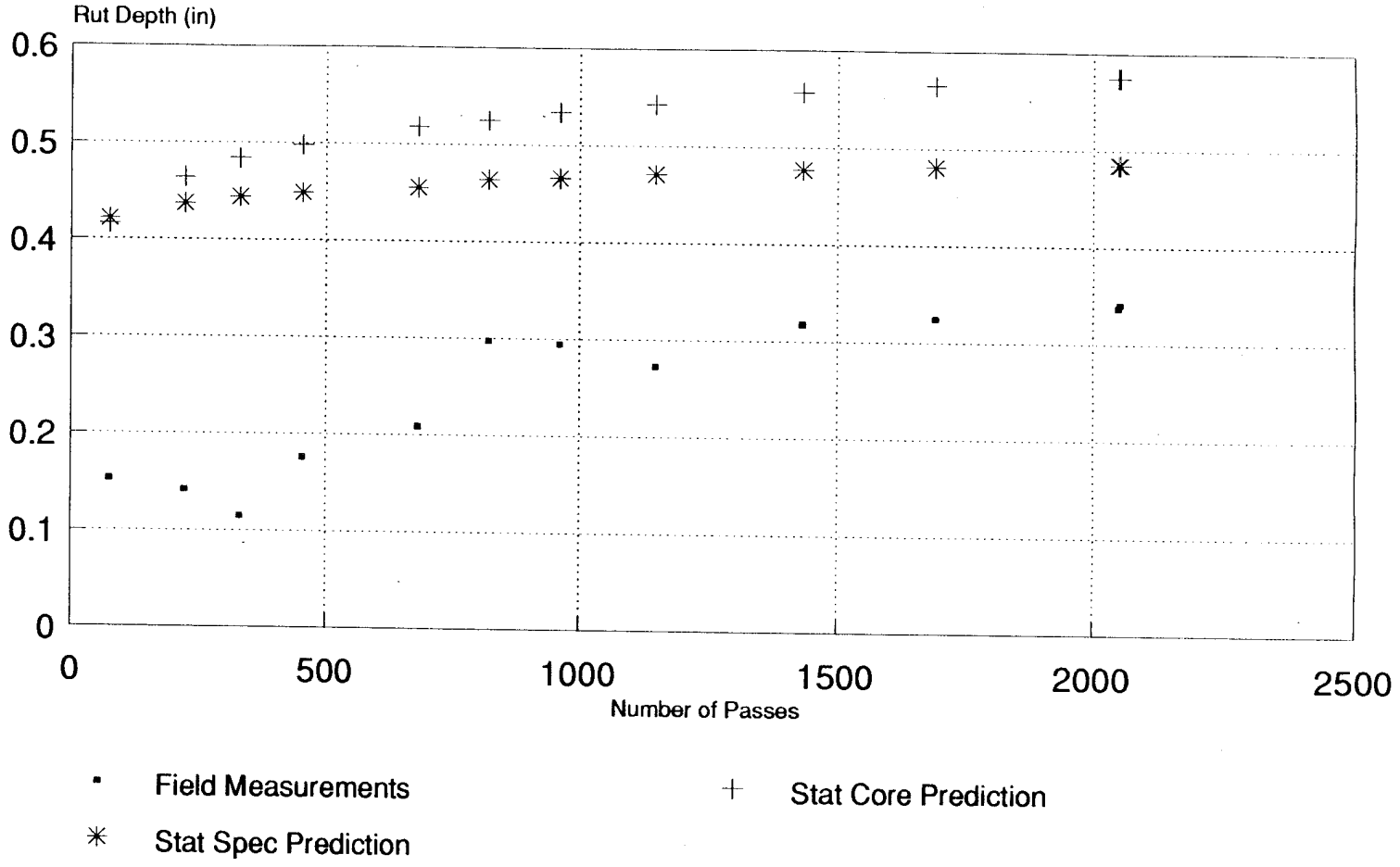

Figure 52. Comparison of Rut Depth Predictions and Field Measurements for Station A 4+40.

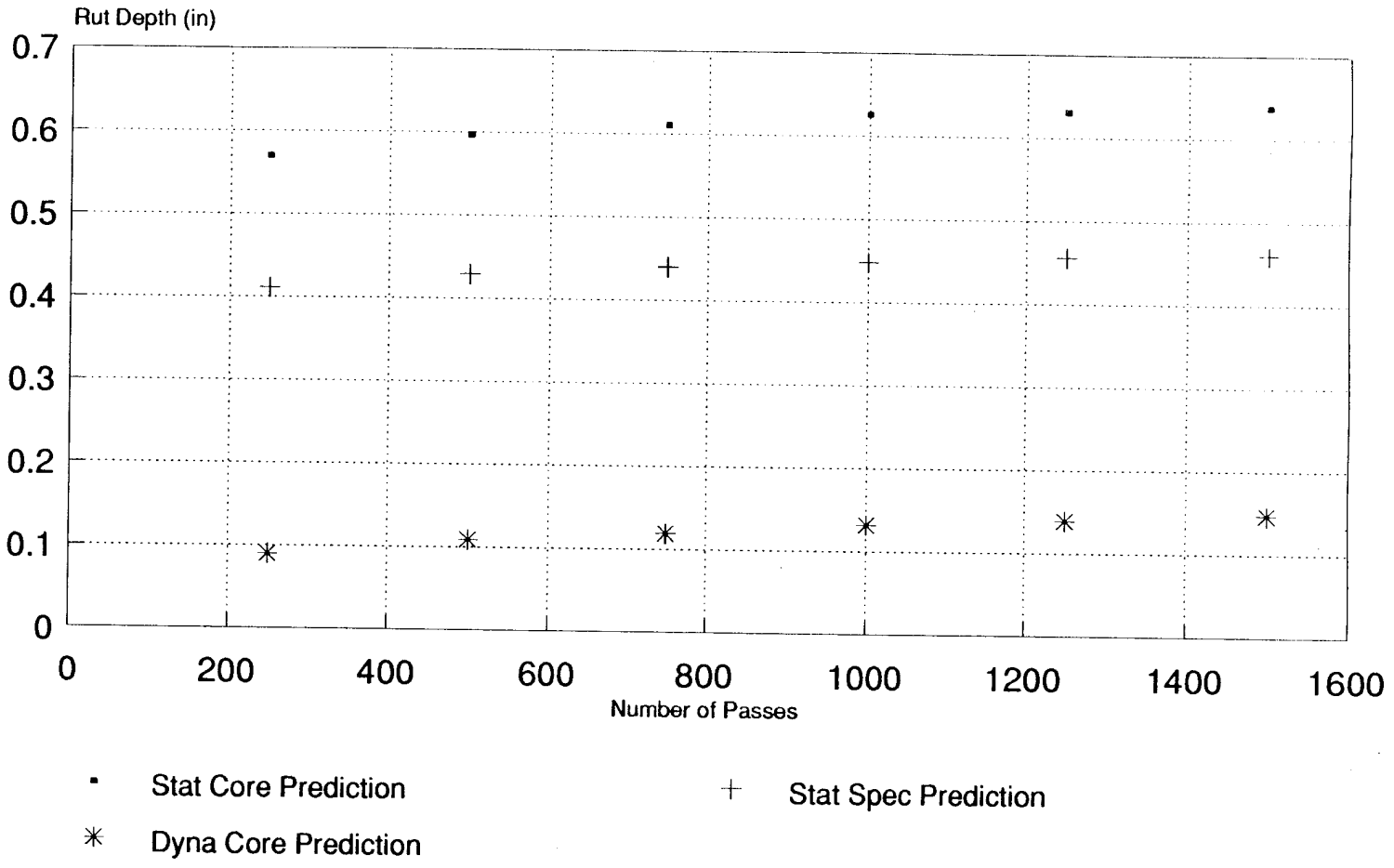

Figure 53. Rut Depth Predictions for Station C 2+13.

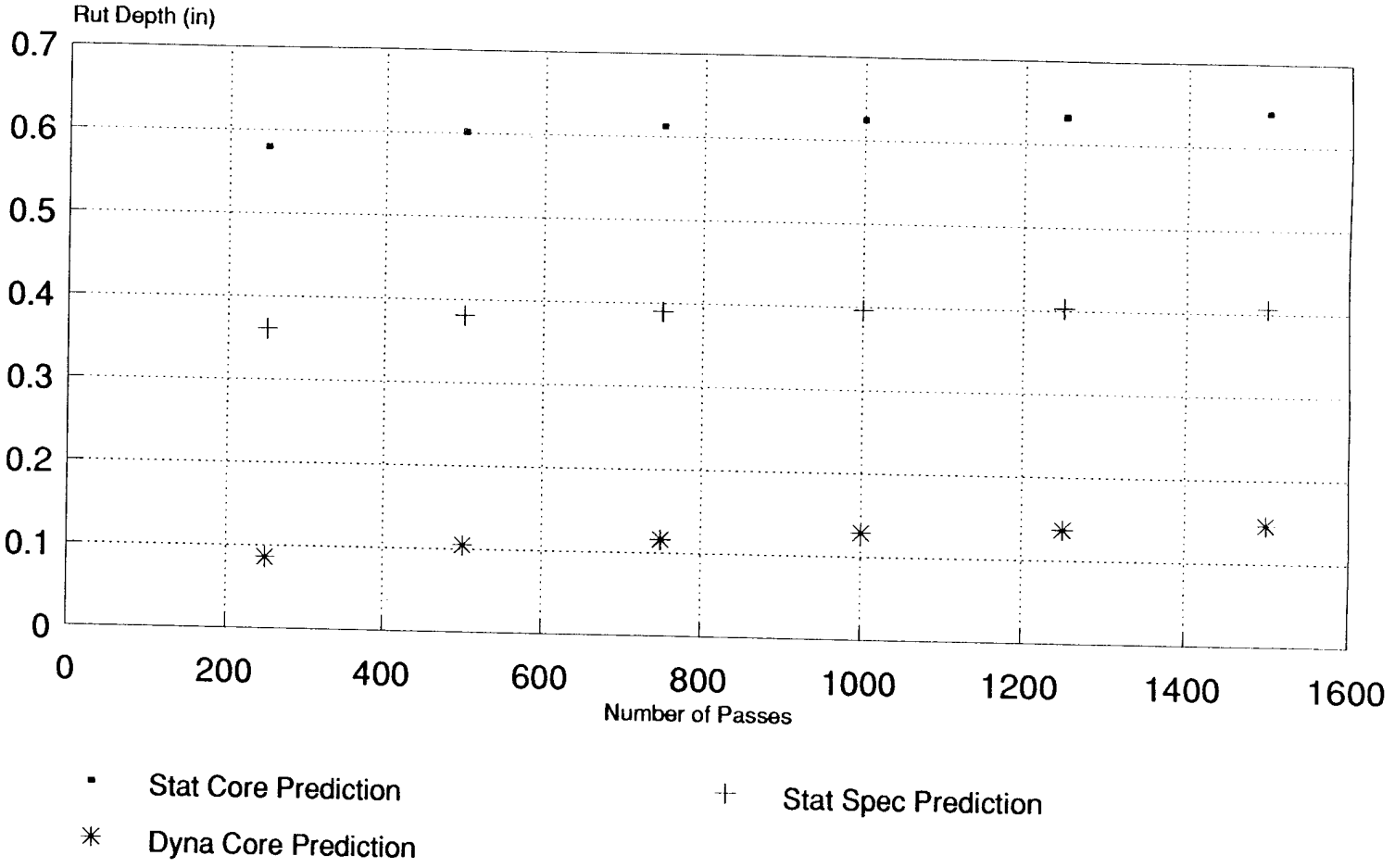

Figure 54. Rut Depth Predictions for Station C 2+57.

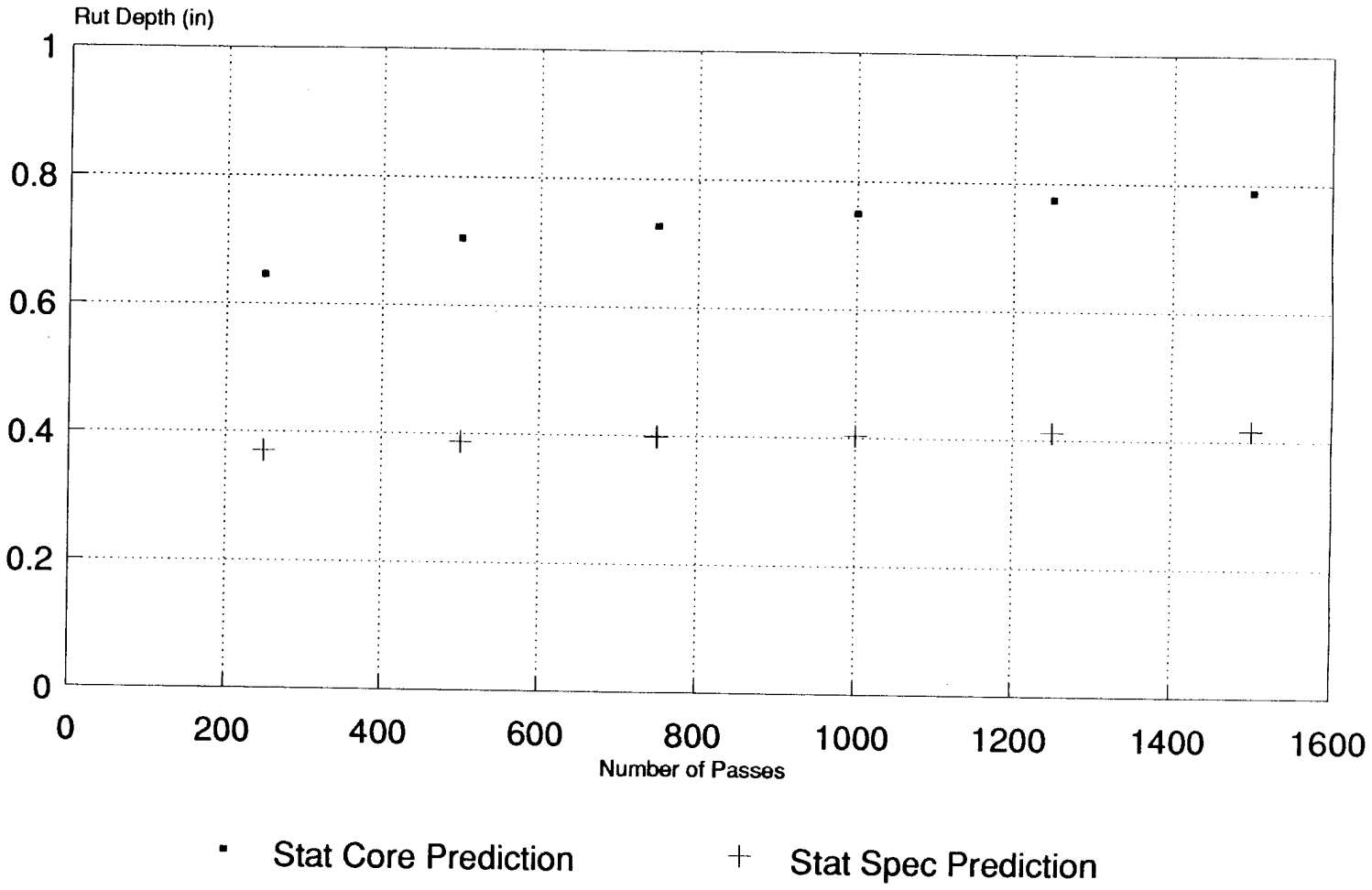

Figure 55. Rut Depth Predictions for Station C 2+85.

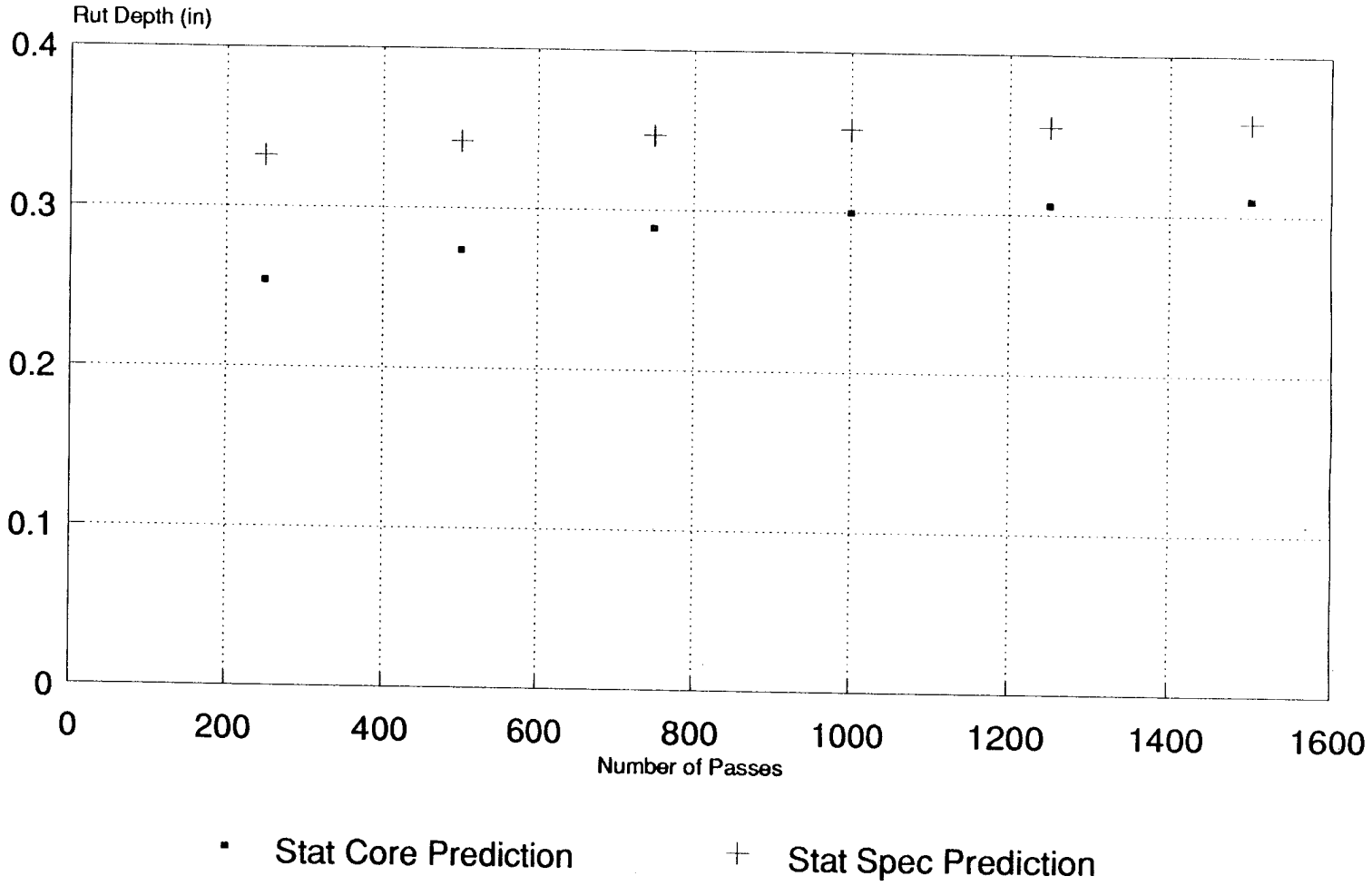

Figure 56. Rut Depth Predictions for Station C 3+25.

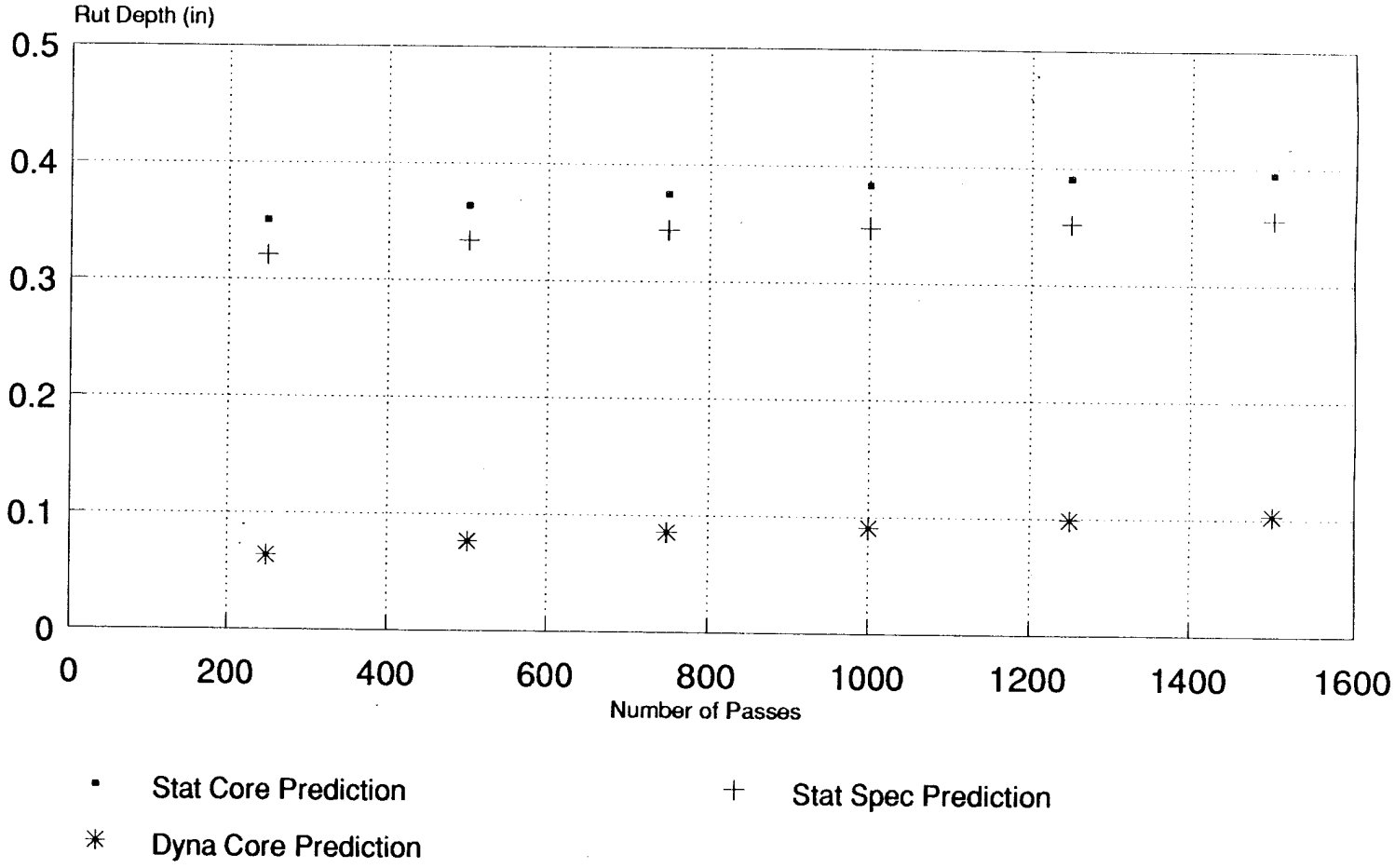

Figure 57. Rut Depth Predictions for Station C 3+69.

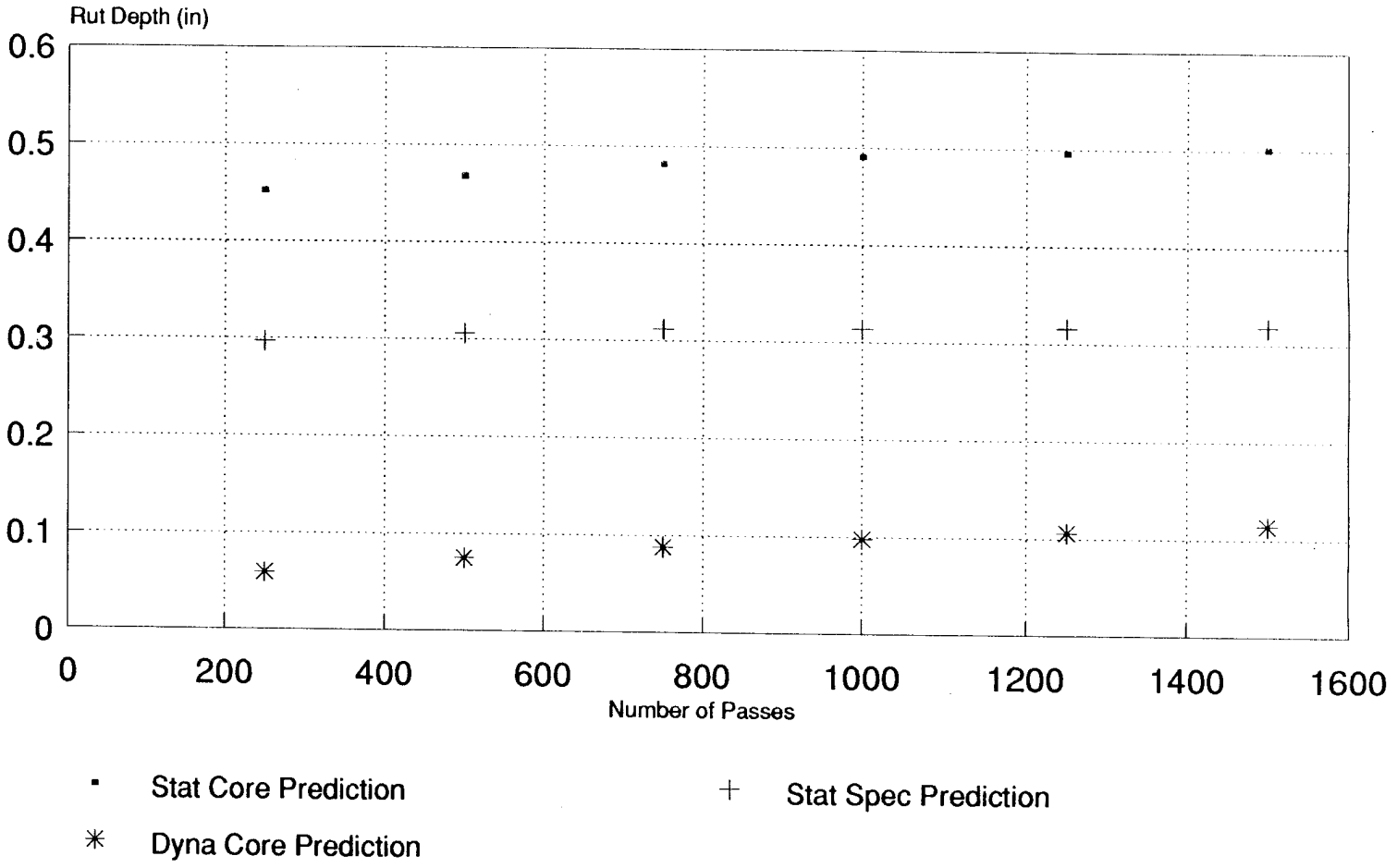

Figure 58. Rut Depth Predictions for Station C 4+15.

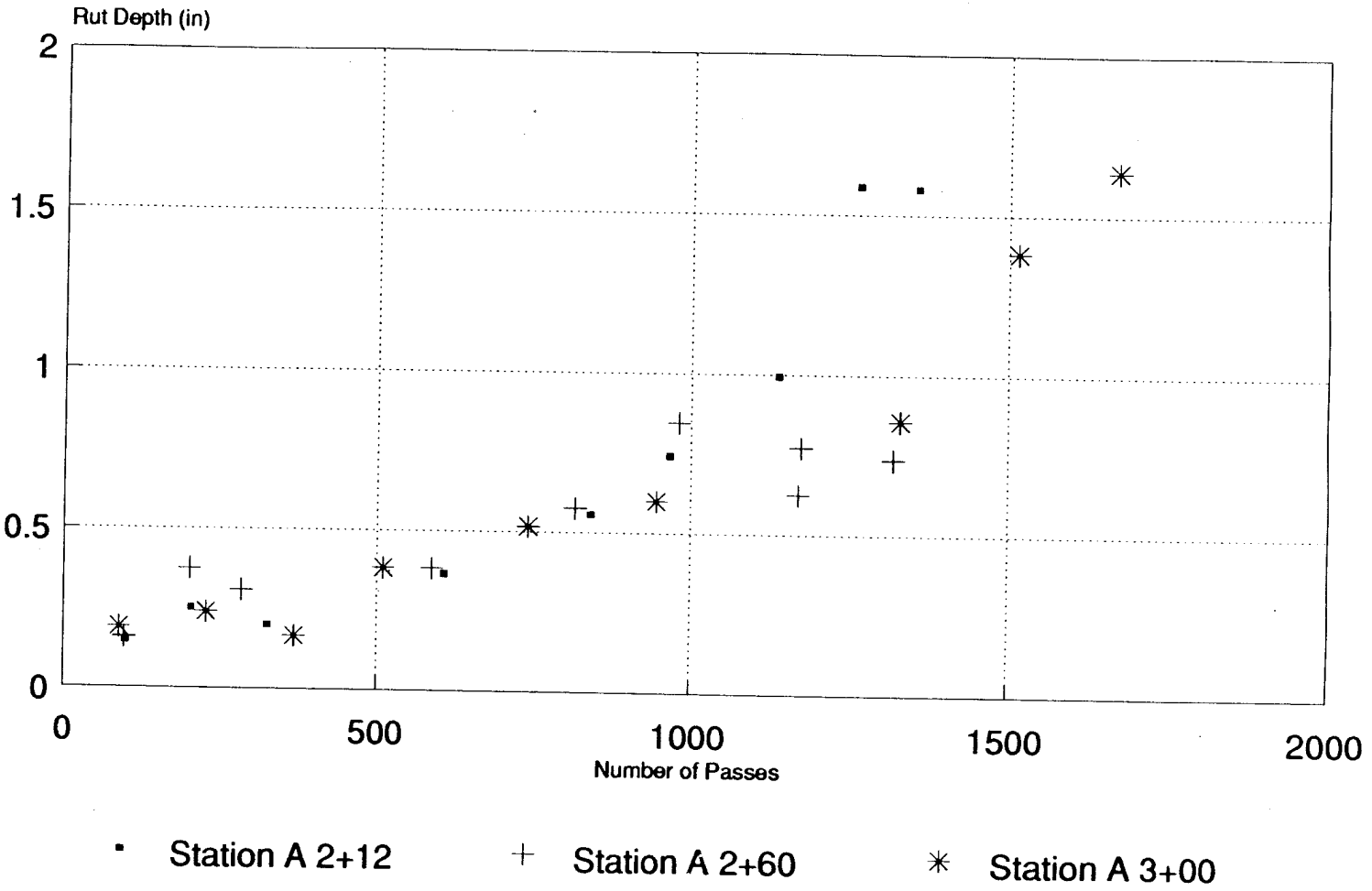

Figure 59. Rut Depth Measurements for Fully Loaded F-15 Section 3.

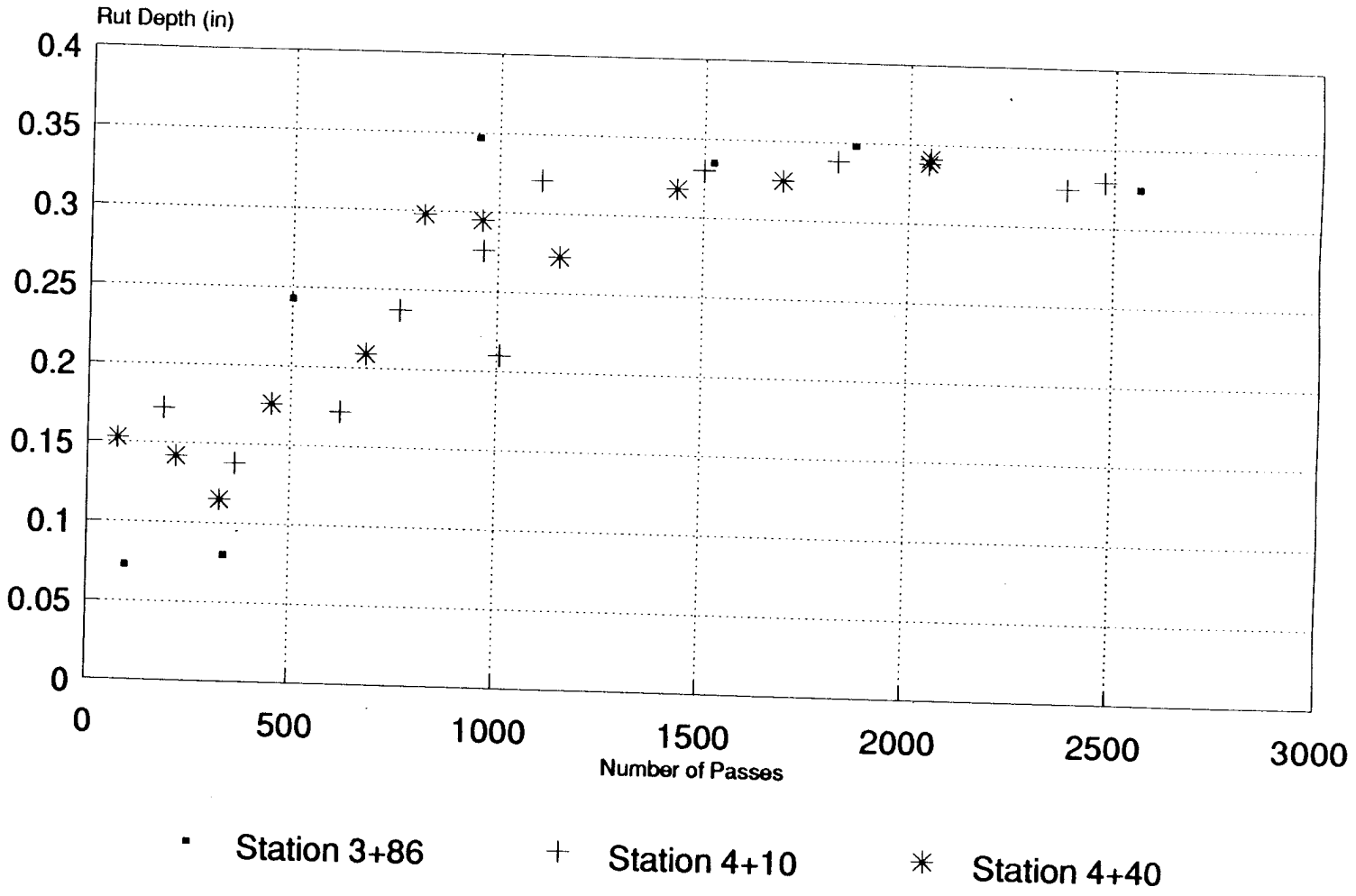

Figure 60. Rut Depth Measurements for Fully Loaded F-15 Section 4.

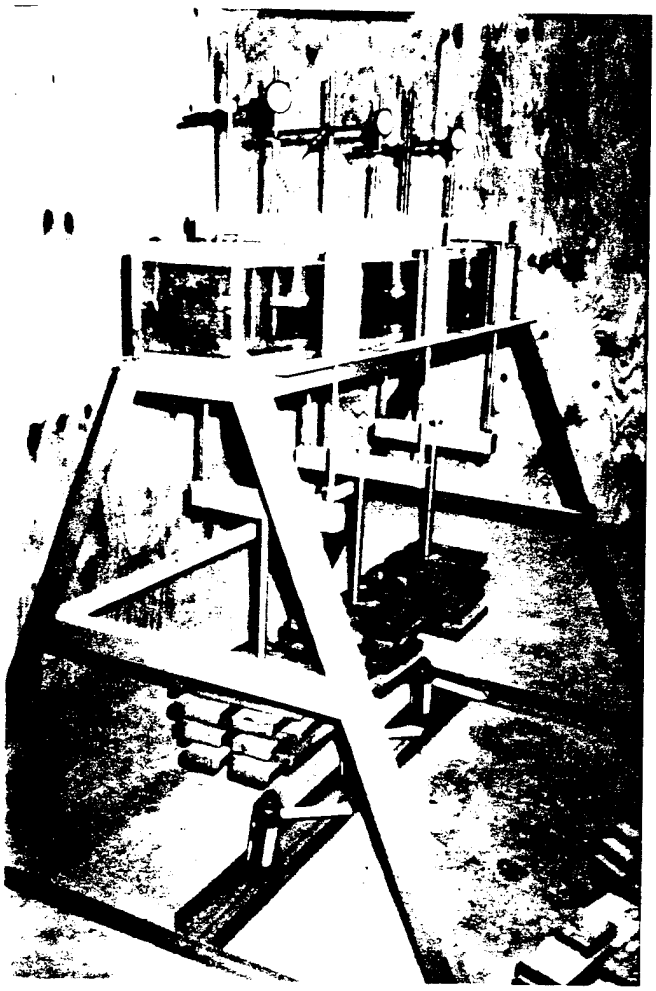

Figure A-1. Static Creep Test Machine.

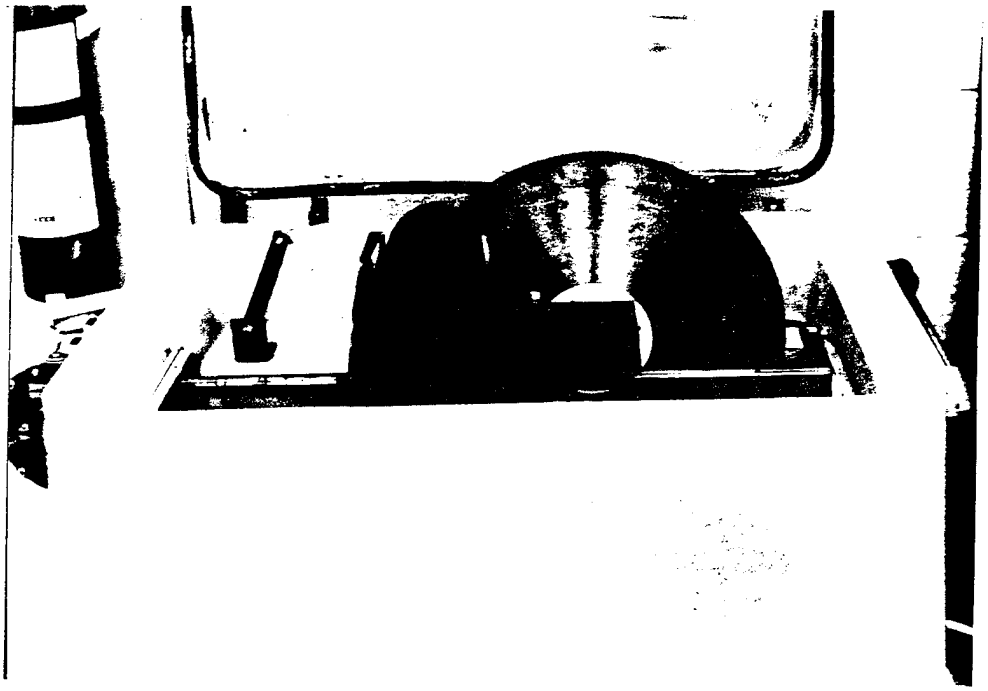

Figure A-2. Core-Cutting Saw.

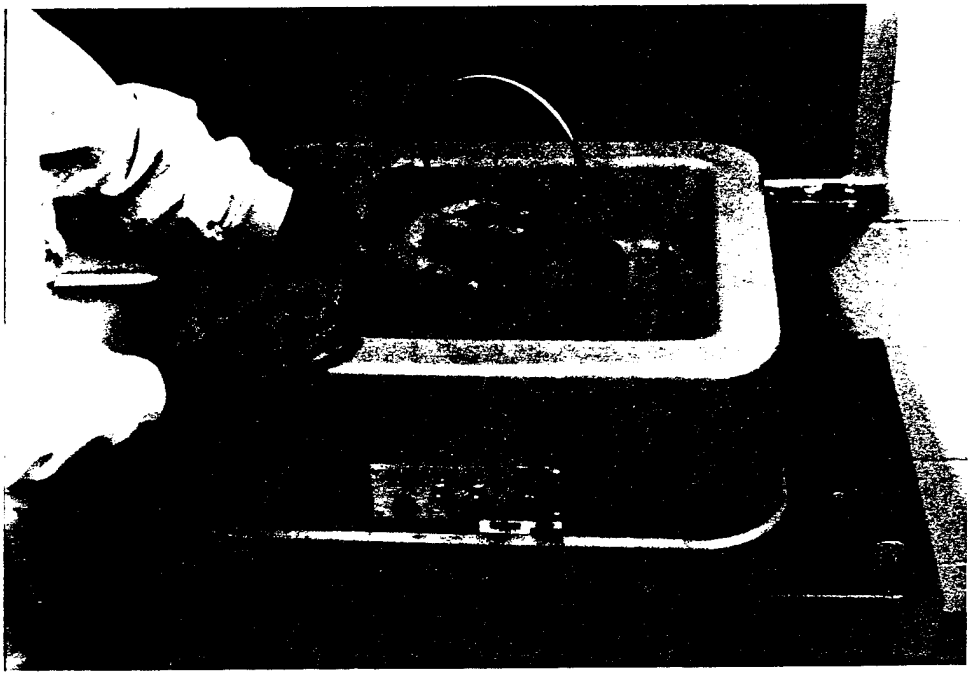

Figure A-3. Thin Section Grinder.

Figure A-4. Preparation of Test Specimen (Static Creep Test).

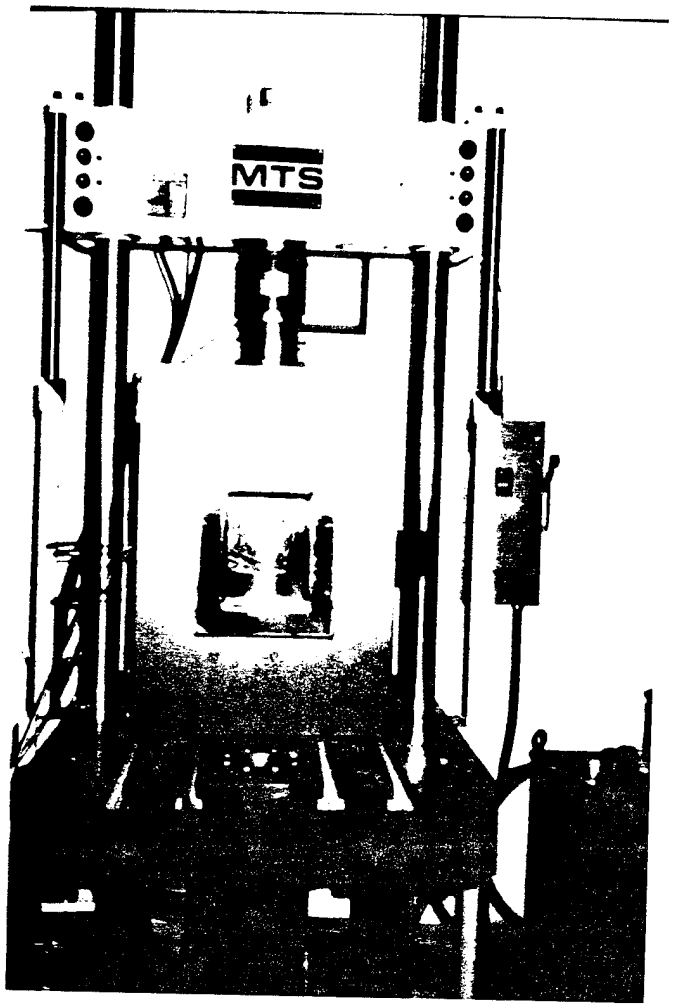

Figure B-1. MTS Machine (Dynamic Creep Test).

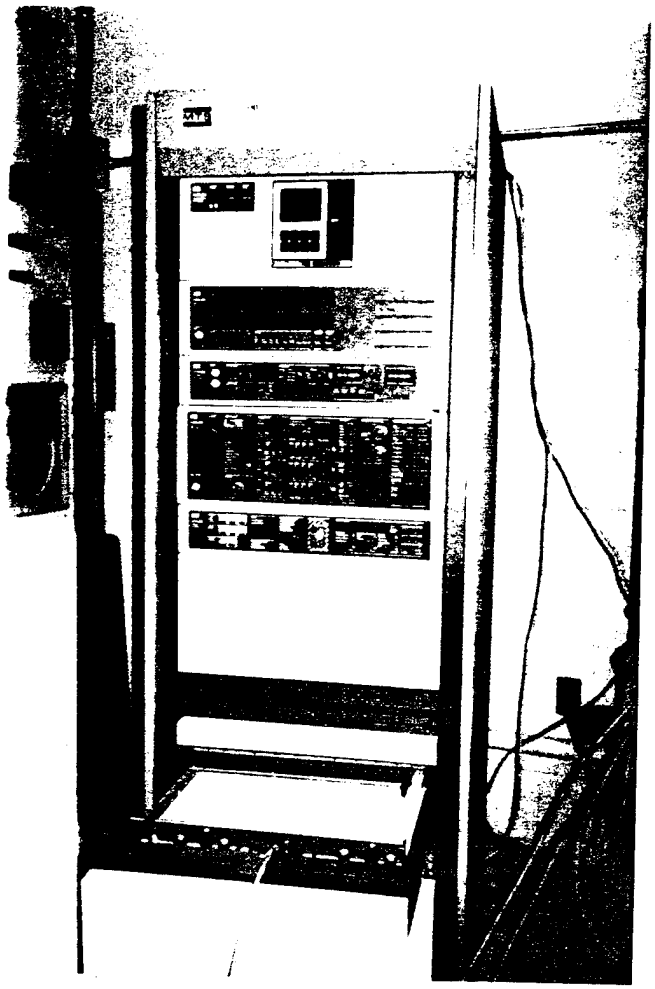

Figure B-2. MTS Machine Control Panel.

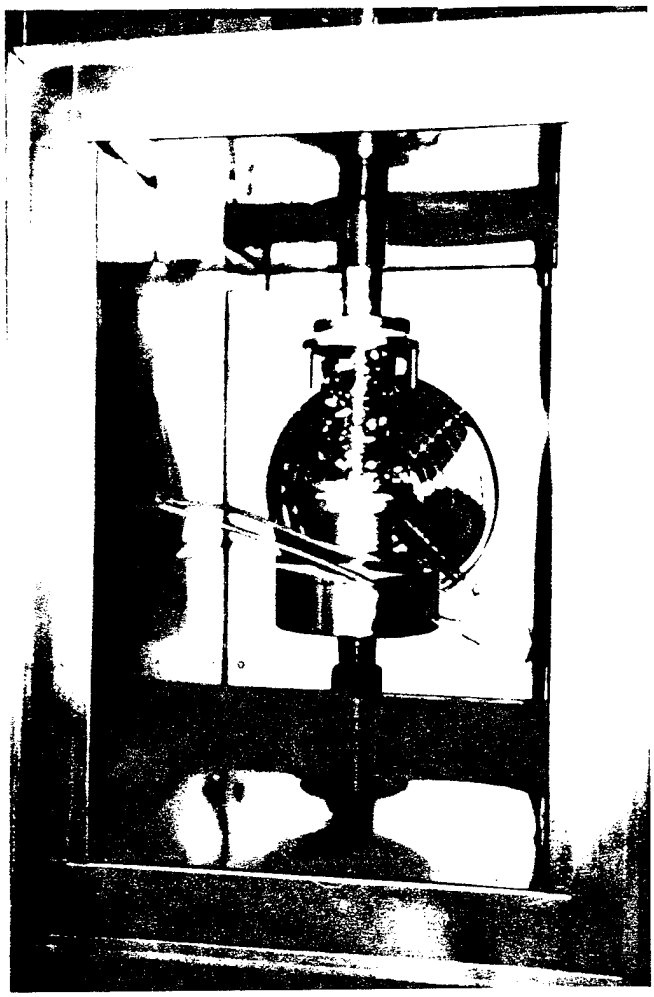

Figure B-3. Environmental Chamber for MTS Machine.

TABLE 1. PAVEMENT PROFILE DATA

Section No.	Base Course	Method of Compaction	Thickness of Asphalt Cement Concrete (in.)
1 & 7	Aggregate	Marshall	4
2 & 8	Aggregate	Marshall	6
3 & 9	Portland Cement Concrete	Marshall	6
4 & 10	Portland Cement Concrete	Gyratory	6
5 & 11	Aggregate	Gyratory	6
6 & 12	Aggregate	Gyratory	4

TABLE 2. CORRECTION FACTORS FOR DYNAMIC EFFECT (4) (6)

Mix Type		C_m
Open	Sand sheet and lean sand mixes Lean open asphaltic concrete	1.6-2.0
	Lean bitumen macadam	1.5-1.8
	Asphaltic concrete Gravel sand asphalt Dense bitumen macadam	1.2-1.6
Dense	Mastic types GuBasphalt Hot rolled asphalt	1.0-1.3

TABLE 3. STATIC CREEP DATA FOR DRILLED CORES
FULLY LOADED F-15 SECTION 1

Elapsed Time (min.)	Unit Strain ($x10^{-3}$in/in)	S_{mix} (N/m^2)	S_{mix} (N/m^2)
A 0+25			
2	10.29	9.72×10^6	4.6×10^2
5	10.87	9.20×10^6	2.0×10^2
10	11.30	8.85×10^6	1.0×10^2
15	11.57	8.64×10^6	7.5×10
30	11.87	8.42×10^6	4.0×10
45	12.07	8.29×10^6	3.0×10
60	12.60	7.94×10^6	2.0×10
A 0+49			
2	10.37	9.64×10^6	4.6×10^2
5	10.80	9.26×10^6	2.0×10^2
10	11.27	8.87×10^6	1.0×10^2
15	11.50	8.70×10^6	7.5×10
30	11.90	8.40×10^6	4.0×10
45	12.20	8.20×10^6	3.0×10
60	12.40	8.06×10^6	2.0×10

TABLE 4. STATIC CREEP DATA FOR DRILLED CORES
FULLY LOADED F-15 SECTION 2

Elapsed Time (min.)	Unit Strain ($x10^{-3}$in/in)	S_{mix} (N/m^2)	S_{bit} (N/m^2)
A 0+95			
2	9.90	1.01×10^7	4.6×10^2
5	10.57	9.46×10^6	2.0×10^2
10	11.03	9.07×10^6	1.0×10^2
15	11.27	8.87×10^6	7.5×10
30	11.73	8.53×10^6	4.0×10
45	11.93	8.38×10^6	3.0×10
60	12.17	8.22×10^6	2.0×10
A 1+41			
2	13.00	7.69×10^6	4.6×10^2
5	13.70	7.30×10^6	2.0×10^2
10	14.50	6.90×10^6	1.0×10^2
15	14.90	6.71×10^6	7.5×10
30	15.50	6.45×10^6	4.0×10
45	15.90	6.29×10^6	3.0×10
60	16.10	6.21×10^6	2.0×10

TABLE 5. STATIC CREEP DATA FOR DRILLED CORES
FULLY LOADED F-15 SECTION 3

Elapsed Time (min.)	Unit Strain ($\times 10^{-3}$ in/in)	S_{mix} (N/m^2)	S_{bit} (N/m^2)
A 2+13			
2	9.10	1.10×10^7	4.6×10^2
5	10.00	1.00×10^7	2.0×10^2
10	10.40	9.62×10^6	1.0×10^2
15	10.50	9.52×10^6	7.5×10
30	11.00	9.09×10^6	4.0×10
45	11.20	8.93×10^6	3.0×10
60	11.20	8.93×10^6	2.0×10
A 2+57			
2	10.40	9.62×10^6	4.6×10^2
5	10.90	9.17×10^6	2.0×10^2
10	11.40	8.77×10^6	1.0×10^2
15	11.80	8.47×10^6	7.5×10
30	12.30	8.13×10^6	4.0×10
45	12.60	7.94×10^6	3.0×10
60	12.80	7.81×10^6	2.0×10
A 3+05			
2	14.68	6.81×10^6	4.6×10^2
5	15.84	6.31×10^6	2.0×10^2
10	17.00	5.88×10^6	1.0×10^2
15	17.41	5.74×10^6	7.5×10
30	17.89	5.59×10^6	4.0×10
45	18.13	5.52×10^6	3.0×10
60	18.41	5.43×10^6	2.0×10

TABLE 6. STATIC CREEP DATA FOR DRILLED CORES
FULLY LOADED F-15 SECTION 4

Elapsed Time (min.)	Unit Strain ($x10^{-3}$in/in)	S_{mix} (N/m^2)	S_{bit} (N/m^2)
A 3+69			
2	8.90	1.12×10^7	4.6×10^2
5	9.30	1.08×10^7	2.0×10^2
10	9.80	1.02×10^7	1.0×10^2
15	10.10	9.90×10^6	7.5×10
30	10.70	9.35×10^6	4.0×10
45	11.20	8.93×10^6	3.0×10
60	11.30	8.85×10^6	2.0×10
A 4+15			
2	8.30	1.20×10^7	4.6×10^2
5	8.60	1.16×10^7	2.0×10^2
10	9.00	1.11×10^7	1.0×10^2
15	9.30	1.08×10^7	7.5×10
30	9.70	1.03×10^7	4.0×10
45	10.10	9.90×10^6	3.0×10
60	10.30	9.71×10^6	2.0×10
A 4+45			
2	9.08	1.10×10^7	4.6×10^2
5	9.63	1.04×10^7	2.0×10^2
10	10.01	9.99×10^6	1.0×10^2
15	10.81	9.25×10^6	7.5×10
30	11.59	8.63×10^6	4.0×10
45	11.85	8.44×10^6	3.0×10
60	12.02	8.32×10^6	2.0×10

TABLE 7. STATIC CREEP DATA FOR DRILLED CORES
FULLY LOADED F-15 SECTION 5

Elapsed Time (min.)	Unit Strain ($\times 10^{-3}$ in/in)	S_{mix} (N/m^2)	S_{bit} (N/m^2)
A 4+97			
2	8.40	1.19×10^7	4.6×10^2
5	8.83	1.13×10^7	2.0×10^2
10	9.23	1.08×10^7	1.0×10^2
15	9.63	1.04×10^7	7.5×10
30	10.00	1.00×10^7	4.0×10
45	10.13	9.87×10^6	3.0×10
60	10.30	9.71×10^6	2.0×10
A 5+10			
2	9.50	1.05×10^7	4.6×10^2
5	9.90	1.01×10^7	2.0×10^2
10	10.33	9.68×10^6	1.0×10^2
15	10.93	9.15×10^6	7.5×10
30	11.13	8.98×10^6	4.0×10
45	11.30	8.85×10^6	3.0×10
60	11.43	8.75×10^6	2.0×10

TABLE 8. STATIC CREEP DATA FOR DRILLED CORES
FULLY LOADED F-15 SECTION 6

Elapsed Time (min.)	Unit Strain ($x10^{-3}$in/in)	S_{mix} (N/m^2)	S_{bit} (N/m^2)
A 5+67			
2	9.23	1.08×10^7	4.6×10^2
5	9.80	1.02×10^7	2.0×10^2
10	10.30	9.71×10^6	1.0×10^2
15	10.57	9.46×10^6	7.5×10
30	10.97	9.12×10^6	4.0×10
45	11.13	8.98×10^6	3.0×10
60	11.20	8.93×10^6	2.0×10
A 5+91			
2	9.07	1.10×10^7	4.6×10^2
5	9.57	1.04×10^7	2.0×10^2
10	10.23	9.78×10^6	1.0×10^2
15	10.43	9.59×10^6	7.5×10
30	10.97	9.12×10^6	4.0×10
45	11.07	9.03×10^6	3.0×10
60	11.07	9.03×10^6	2.0×10

TABLE 9. STATIC CREEP DATA FOR COMPACTED SPECIMENS FULLY LOADED F-15 SECTION 1

Elapsed Time (min.)	Unit Strain ($\times 10^{-3}$ in/in)	S_{mix} (N/m^2)	S_{bit} (N/m^2)
TA 13-2			
2	8.60	1.16×10^7	4.6×10^2
5	8.91	1.12×10^7	2.0×10^2
10	9.10	1.10×10^7	1.0×10^2
15	9.20	1.09×10^7	7.5×10
30	9.40	1.06×10^7	4.0×10
45	9.50	1.05×10^7	3.0×10
60	9.60	1.04×10^7	2.0×10
TA 14-1			
2	9.40	1.06×10^7	4.6×10^2
5	9.85	1.02×10^7	2.0×10^2
10	10.24	9.77×10^6	1.0×10^2
15	10.49	9.53×10^6	7.5×10
30	10.75	9.30×10^6	4.0×10
45	10.89	9.18×10^6	2.0×10
60	11.10	9.01×10^6	2.0×10

TABLE 10. STATIC CREEP DATA FOR COMPACTED SPECIMENS FULLY LOADED F-15 SECTION 2

Elapsed Time (min.)	Unit Strain ($\times 10^{-3}$ in/in)	S_{mix} (N/m^2)	S_{bit} (N/m^2)
TA 11-3			
2	9.40	1.06×10^7	4.6×10^2
5	9.80	1.02×10^7	2.0×10^2
10	10.10	9.90×10^6	1.0×10^2
15	10.22	9.78×10^6	7.5×10
30	10.50	9.52×10^6	4.0×10
45	10.70	9.35×10^6	3.0×10
60	10.80	9.26×10^6	2.0×10
TA 12-2			
2	9.16	1.09×10^7	4.6×10^2
5	9.75	1.03×10^7	2.0×10^2
10	10.20	9.80×10^6	1.0×10^2
15	10.45	9.57×10^6	7.5×10
30	10.90	9.17×10^6	4.0×10
45	11.20	8.93×10^6	3.0×10
60	11.45	8.73×10^6	2.0×10

TABLE 11. STATIC CREEP DATA FOR COMPACTED SPECIMENS
FULLY LOADED F-15 SECTION 3

Elapsed Time (min.)	Unit Strain ($x10^{-3}$in/in)	S_{mix} (N/m^2)	S_{bit} (N/m^2)
TA 8-1			
2	13.00	7.69×10^6	4.6×10^2
5	13.70	7.30×10^6	2.0×10^2
10	14.35	6.97×10^6	1.0×10^2
15	14.60	6.85×10^6	7.5×10
30	15.16	6.60×10^6	4.0×10
45	15.50	6.45×10^6	3.0×10
60	15.70	6.37×10^6	2.0×10
TA 9-1			
2	10.20	9.80×10^6	4.6×10^2
5	10.83	9.23×10^6	2.0×10^2
10	11.31	8.84×10^6	1.0×10^2
15	11.50	8.70×10^6	7.5×10
30	11.99	8.34×10^6	4.0×10
45	12.29	8.14×10^6	3.0×10
60	12.47	8.02×10^6	2.0×10
TA 10-1			
2	8.60	1.16×10^7	4.6×10^2
5	9.20	1.09×10^7	2.0×10^2
10	9.60	1.04×10^7	1.0×10^2
15	9.85	1.02×10^6	7.5×10
30	10.30	9.71×10^6	4.0×10
45	10.60	9.43×10^6	2.0×10
60	10.80	9.26×10^6	2.0×10
TA 10-2			
2	8.55	1.17×10^7	4.6×10^2
5	9.05	1.10×10^7	2.0×10^2
10	9.40	1.06×10^7	1.0×10^2
15	9.65	1.04×10^7	7.5×10
30	10.00	1.00×10^7	4.0×10
45	10.20	9.80×10^6	3.0×10
60	10.45	9.57×10^6	2.0×10

TABLE 12. STATIC CREEP DATA FOR COMPACTED SPECIMENS FULLY LOADED F-15 SECTION 4

Elapsed Time (min.)	Unit Strain ($x10^{-3}$in/in)	S_{mix} (N/m^2)	S_{bit} (N/m^2)
TA 5-2			
2	7.23	1.38×10^7	4.6×10^2
5	7.53	1.33×10^7	2.0×10^2
10	7.70	1.30×10^7	1.0×10^2
15	7.82	1.28×10^7	7.5×10
30	8.00	1.25×10^7	4.0×10
45	8.12	1.23×10^7	3.0×10
60	8.20	1.22×10^7	2.0×10
TA 6-2			
2	8.20	1.22×10^7	4.6×10^2
5	8.60	1.16×10^7	2.0×10^2
10	8.80	1.14×10^7	1.0×10^2
15	9.00	1.11×10^7	7.5×10
30	9.20	1.09×10^7	4.0×10
45	9.38	1.07×10^7	3.0×10
60	9.45	1.06×10^7	2.0×10
TA 7-1			
2	8.20	1.22×10^7	4.6×10^2
5	8.60	1.16×10^7	2.0×10^2
10	8.90	1.12×10^7	1.0×10^2
15	9.10	1.10×10^7	7.5×10
30	9.50	1.05×10^7	4.0×10
45	9.70	1.03×10^7	3.0×10
60	9.80	1.02×10^7	2.0×10
TA 7-2			
2	7.85	1.27×10^7	4.6×10^2
5	8.10	1.23×10^7	2.0×10^2
10	8.35	1.20×10^7	1.0×10^2
15	8.50	1.18×10^7	7.5×10
30	8.70	1.15×10^7	4.0×10
45	8.80	1.14×10^7	3.0×10
60	8.90	1.12×10^7	2.0×10

TABLE 13. STATIC CREEP DATA FOR COMPACTED SPECIMENS FULLY LOADED F-15 SECTION 5

Elapsed Time (min.)	Unit Strain ($x10^{-3}$in/in)	S_{mix} (N/m^2)	S_{bit} (N/m^2)
TA 3-1			
2	9.80	1.02×10^7	4.6×10^2
5	10.12	9.88×10^6	2.0×10^2
10	10.50	9.52×10^6	1.0×10^2
15	10.69	9.35×10^6	7.5×10
30	10.87	9.20×10^6	4.0×10
45	11.03	9.07×10^6	3.0×10
60	11.12	8.99×10^6	2.0×10
TA 4-2			
2	8.70	1.15×10^7	4.6×10^2
5	9.10	1.10×10^7	2.0×10^2
10	9.40	1.06×10^7	1.0×10^2
15	9.60	1.04×10^7	7.5×10
30	9.90	1.01×10^7	4.0×10
45	10.00	1.00×10^7	3.0×10
60	10.25	9.76×10^6	2.0×10

TABLE 14. STATIC CREEP DATA FOR COMPACTED SPECIMENS FULLY LOADED F-15 SECTION 6

Elapsed Time (min.)	Unit Strain ($x10^{-3}$in/in)	S_{mix} (N/m^2)	S_{bit} (N/m^2)
TA 2-1			
2	7.35	1.36×10^7	4.6×10^2
5	7.80	1.28×10^7	2.0×10^2
10	8.15	1.23×10^7	1.0×10^2
15	8.40	1.19×10^7	7.5×10
30	8.80	1.14×10^7	4.0×10
45	9.00	1.11×10^7	3.0×10
60	9.20	1.09×10^7	2.0×10

TABLE 15. STATIC CREEP DATA FOR DRILLED CORES
UNARMED F-15 SECTION 7

Elapsed Time (min.)	Unit Strain ($\times 10^{-3}$ in/in)	S_{mix} (N/m^2)	S_{bit} (N/m^2)
C 0+25			
2	14.42	6.93×10^6	4.6×10^2
5	15.71	6.37×10^6	2.0×10^2
10	16.96	5.90×10^6	1.0×10^2
15	17.55	5.70×10^6	7.5×10
30	18.58	5.38×10^6	4.0×10
45	19.15	5.22×10^6	3.0×10
60	19.46	5.14×10^6	2.0×10
C 0+49			
2	15.34	6.52×10^6	4.6×10^2
5	16.48	6.07×10^6	2.0×10^2
10	17.68	5.66×10^6	1.0×10^2
15	18.28	5.47×10^6	7.5×10
30	19.33	5.17×10^6	4.0×10
45	19.82	5.05×10^6	3.0×10
60	20.21	4.95×10^6	2.0×10

TABLE 16. STATIC CREEP DATA FOR DRILLED CORES
UNARMED F-15 SECTION 8

Elapsed Time (min.)	Unit Strain ($\times 10^{-3}$ in/in)	S_{mix} (N/m^2)	S_{bit} (N/m^2)
C 0+95			
2	10.97	9.12×10^6	4.6×10^2
5	11.65	8.58×10^6	2.0×10^2
10	12.98	7.70×10^6	1.0×10^2
15	13.73	7.28×10^6	7.5×10
30	14.61	6.84×10^6	4.0×10
45	15.18	6.59×10^6	3.0×10
60	15.40	6.49×10^6	2.0×10
C 1+41			
2	14.06	7.11×10^6	4.6×10^2
5	14.91	6.71×10^6	2.0×10^2
10	15.58	6.42×10^6	1.0×10^2
15	15.98	6.26×10^6	7.5×10
30	16.27	6.15×10^6	4.0×10
45	16.66	6.00×10^6	3.0×10
60	16.77	5.96×10^6	2.0×10

TABLE 17. STATIC CREEP DATA FOR DRILLED CORES
UNARMED F-15 SECTION 9

Elapsed Time (min.)	Unit Strain ($x10^{-3}$in/in)	S_{mix} (N/m^2)	S_{bit} (N/m^2)
C 2+13			
2	13.16	7.60×10^6	4.6×10^2
5	14.03	7.13×10^6	2.0×10^2
10	14.75	6.78×10^6	1.0×10^2
15	15.08	6.63×10^6	7.5×10
30	15.54	6.44×10^6	4.0×10
45	15.95	6.27×10^6	3.0×10
60	16.16	6.19×10^6	2.0×10
C 2+57			
2	13.17	7.59×10^6	4.6×10^2
5	14.18	7.05×10^6	2.0×10^2
10	14.82	6.75×10^6	1.0×10^2
15	15.23	6.57×10^6	7.5×10
30	15.72	6.36×10^6	4.0×10
45	15.89	6.29×10^6	3.0×10
60	16.11	6.21×10^6	2.0×10
C 2+85			
2	18.18	5.50×10^6	4.6×10^2
5	19.85	5.04×10^6	2.0×10^2
10	20.89	4.79×10^6	1.0×10^2
15	22.12	4.52×10^6	7.5×10
30	23.27	4.30×10^6	4.0×10
45	25.09	3.99×10^6	3.0×10
60	25.34	3.95×10^6	2.0×10

TABLE 18. STATIC CREEP DATA FOR DRILLED CORES
UNARMED F-15 SECTION 10

Elapsed Time (min.)	Unit Strain ($\times 10^{-3}$ in/in)	S_{mix} (N/m^2)	S_{bit} (N/m^2)
C 3+25			
2	7.24	1.38×10^7	4.6×10^2
5	7.84	1.28×10^7	2.0×10^2
10	8.74	1.14×10^7	1.0×10^2
15	9.04	1.11×10^7	7.5×10
30	9.34	1.07×10^7	4.0×10
45	9.88	1.01×10^7	3.0×10
60	9.96	1.00×10^7	2.0×10
C 3+69			
2	8.47	1.18×10^7	4.6×10^2
5	8.90	1.12×10^7	2.0×10^2
10	9.42	1.06×10^7	1.0×10^2
15	9.72	1.03×10^7	7.5×10
30	10.03	9.97×10^6	4.0×10
45	10.17	9.83×10^6	3.0×10
60	10.17	9.83×10^6	2.0×10
C 4+15			
2	10.19	9.81×10^6	4.6×10^2
5	10.64	9.40×10^6	2.0×10^2
10	10.91	9.17×10^6	1.0×10^2
15	11.33	8.83×10^6	7.5×10
30	11.72	8.53×10^6	4.0×10
45	11.81	8.47×10^6	3.0×10
60	12.08	8.28×10^6	2.0×10

TABLE 19. STATIC CREEP DATA FOR DRILLED CORES
UNARMED F-15 SECTION 11

Elapsed Time (min.)	Unit Strain ($\times 10^{-3}$ in/in)	S_{mix} (N/m^2)	S_{bit} (N/m^2)
C 4+97			
2	9.23	1.08×10^7	4.6×10^2
5	9.97	1.00×10^7	2.0×10^2
10	11.08	9.03×10^6	1.0×10^2
15	11.58	8.64×10^6	7.5×10
30	12.51	7.99×10^6	4.0×10
45	12.78	7.82×10^6	3.0×10
60	13.01	7.69×10^6	2.0×10
C 5+10			
2	11.52	8.68×10^6	4.6×10^2
5	12.19	8.20×10^6	2.0×10^2
10	13.38	7.47×10^6	1.0×10^2
15	13.75	7.27×10^6	7.5×10
30	14.26	7.01×10^6	4.0×10
45	14.42	6.93×10^6	3.0×10
60	15.07	6.64×10^6	2.0×10

TABLE 20. STATIC CREEP DATA FOR DRILLED CORES
UNARMED F-15 SECTION 12

Elapsed Time (min.)	Unit Strain ($x10^{-3}$in/in)	S_{mix} (N/m^2)	S_{bit} (N/m^2)
C 5+67			
2	9.08	1.10×10^7	4.6×10^2
5	9.68	1.03×10^7	2.0×10^2
10	10.57	9.46×10^6	1.0×10^2
15	10.92	9.16×10^6	7.5 x 10
30	11.56	8.65×10^6	4.0 x 10
45	11.97	8.35×10^6	3.0 x 10
60	12.12	8.25×10^6	2.0 x 10
C 5+91			
2	9.69	1.03×10^7	4.6×10^2
5	10.30	9.71×10^6	2.0×10^2
10	11.31	8.84×10^6	1.0×10^2
15	11.72	8.53×10^6	7.5 x 10
30	12.42	8.05×10^6	4.0 x 10
45	13.04	7.67×10^6	3.0 x 10
60	13.35	7.49×10^6	2.0 x 10

TABLE 21. STATIC CREEP DATA FOR COMPACTED SPECIMENS UNARMED F-15 SECTION 7

Elapsed Time (min.)	Unit Strain ($x10^{-3}$in/in)	S_{mix} (N/m^2)	S_{bit} (N/m^2)
TC 2-2			
2	11.30	8.85×10^6	4.6×10^2
5	12.00	8.33×10^6	2.0×10^2
10	12.47	8.02×10^6	1.0×10^2
15	12.73	7.86×10^6	7.5×10
30	13.13	7.62×10^6	4.0×10
45	13.33	7.50×10^6	3.0×10
60	13.50	7.41×10^6	2.0×10
TC 3-2			
2	11.53	8.67×10^6	4.6×10^2
5	12.37	8.08×10^6	2.0×10^2
10	13.10	7.63×10^6	1.0×10^2
15	13.30	7.52×10^6	7.5×10
30	13.77	7.26×10^6	4.0×10
45	14.13	7.08×10^6	3.0×10
60	14.40	6.94×10^6	2.0×10

TABLE 22. STATIC CREEP DATA FOR COMPACTED SPECIMENS UNARMED F-15 SECTION 8

Elapsed Time (min.)	Unit Strain ($x10^{-3}$in/in)	S_{mix} (N/m^2)	S_{bit} (N/m^2)
TC 4-2			
2	8.63	1.16×10^7	4.6×10^2
5	9.13	1.10×10^7	2.0×10^2
10	9.53	1.05×10^7	1.0×10^2
15	9.73	1.03×10^7	7.5×10
30	10.03	9.97×10^6	4.0×10
45	10.10	9.90×10^6	3.0×10
60	10.20	9.80×10^6	2.0×10
TC 5-2			
2	11.57	8.64×10^6	4.6×10^2
5	12.30	8.13×10^6	2.0×10^2
10	12.87	7.77×10^6	1.0×10^2
15	13.13	7.62×10^6	7.5×10
30	13.47	7.42×10^6	4.0×10
45	13.60	7.35×10^6	3.0×10
60	13.60	7.35×10^6	2.0×10

TABLE 23. STATIC CREEP DATA FOR COMPACTED SPECIMENS
UNARMED F-15 SECTION 9

Elapsed Time (min.)	Unit Strain ($\times 10^{-3}$ in/in)	S_{mix} (N/m^2)	S_{bit} (N/m^2)
TC 6-3			
2	9.53	1.05×10^7	4.6×10^2
5	10.03	9.97×10^6	2.0×10^2
10	10.43	9.59×10^6	1.0×10^2
15	10.70	9.35×10^6	7.5×10
30	11.07	9.03×10^6	4.0×10
45	11.23	8.90×10^6	3.0×10
60	11.30	8.85×10^6	2.0×10
TC 7-2			
2	8.73	1.15×10^7	4.6×10^2
5	9.23	1.08×10^7	2.0×10^2
10	9.60	1.04×10^7	1.0×10^2
15	9.77	1.02×10^7	7.5×10
30	10.03	9.97×10^6	4.0×10
45	10.20	9.80×10^6	3.0×10
60	10.33	9.68×10^6	2.0×10
TC 8-1			
2	9.37	1.07×10^7	4.6×10^2
5	9.90	1.01×10^7	2.0×10^2
10	10.27	9.74×10^6	1.0×10^2
15	10.63	9.41×10^6	7.5×10
30	10.87	9.20×10^6	4.0×10
45	11.13	8.98×10^6	3.0×10
60	11.30	8.85×10^6	2.0×10

TABLE 24. STATIC CREEP DATA FOR COMPACTED SPECIMENS
UNARMED F-15 SECTION 10

Elapsed Time (min.)	Unit Strain ($x10^{-3}$in/in)	S_{mix} (N/m^2)	S_{bit} (N/m^2)
TC 9-2			
2	7.83	1.28×10^7	4.6×10^2
5	8.13	1.23×10^7	2.0×10^2
10	8.37	1.19×10^7	1.0×10^2
15	8.50	1.18×10^7	7.5×10
30	8.60	1.16×10^7	4.0×10
45	8.73	1.15×10^7	3.0×10
60	8.80	1.14×10^7	2.0×10
TC 10-1			
2	7.70	1.30×10^7	4.6×10^2
5	8.23	1.22×10^7	2.0×10^2
10	8.50	1.18×10^7	1.0×10^2
15	8.70	1.15×10^7	7.5×10
30	8.87	1.13×10^7	4.0×10
45	9.00	1.11×10^7	3.0×10
60	9.07	1.10×10^7	2.0×10
TC 10-3			
2	7.03	1.42×10^7	4.6×10^2
5	7.37	1.36×10^7	2.0×10^2
10	7.43	1.35×10^7	1.0×10^2
15	7.50	1.33×10^7	7.5×10
30	7.60	1.32×10^7	4.0×10
45	7.70	1.30×10^7	3.0×10
60	7.70	1.30×10^7	2.0×10
TC 11-3			
2	6.53	1.53×10^7	4.6×10^2
5	6.66	1.50×10^7	2.0×10^2
10	6.67	1.50×10^7	1.0×10^2
15	6.83	1.46×10^7	7.5×10
30	6.97	1.43×10^7	4.0×10
45	7.13	1.40×10^7	3.0×10
60	7.27	1.38×10^7	2.0×10

TABLE 25. STATIC CREEP DATA FOR COMPACTED SPECIMENS
UNARMED F-15 SECTION 11

Elapsed Time (min.)	Unit Strain ($x10^{-3}$in/in)	S_{mix} (N/m^2)	S_{bit} (N/m^2)
TC 12-2			
2	7.87	1.27×10^7	4.6×10^2
5	8.20	1.22×10^7	2.0×10^2
10	8.17	1.22×10^7	1.0×10^2
15	8.27	1.21×10^7	7.5×10
30	8.47	1.18×10^7	4.0×10
45	8.50	1.17×10^7	3.0×10
60	8.50	1.17×10^7	2.0×10
TC 13-1			
2	8.60	1.16×10^7	4.6×10^2
5	9.20	1.09×10^7	2.0×10^2
10	9.70	1.03×10^7	1.0×10^2
15	9.87	1.01×10^7	7.5×10
30	10.17	9.83×10^6	4.0×10
45	10.37	9.64×10^6	3.0×10
60	10.77	9.29×10^6	2.0×10
TC 13-2			
2	7.87	1.27×10^7	4.6×10^2
5	8.43	1.19×10^7	2.0×10^2
10	9.13	1.10×10^7	1.0×10^2
15	9.30	1.08×10^7	7.5×10
30	9.77	1.02×10^7	4.0×10
45	9.97	1.00×10^7	3.0×10
60	10.10	9.90×10^6	2.0×10

TABLE 26. STATIC CREEP DATA FOR COMPACTED SPECIMENS UNARMED F-15 SECTION 12

Elapsed Time (Min.)	Unit Strain ($x10^{-3}$in/in)	S_{mix} (N/m^2)	S_{bit} (N/m_2)
TC 14-2			
2	8.57	1.17×10^7	4.6×10^2
5	8.83	1.13×10^7	2.0×10^2
10	9.17	1.09×10^7	1.0×10^2
15	9.37	1.07×10^7	7.5×10
30	9.60	1.04×10^7	4.0×10
45	9.67	1.03×10^7	3.0×10
60	9.90	1.01×10^7	2.0×10
TC 15-1			
2	7.17	1.39×10^7	4.6×10^2
5	7.43	1.35×10^7	2.0×10^2
10	7.57	1.32×10^7	1.0×10^2
15	7.67	1.30×10^7	7.5×10
30	8.13	1.23×10^7	4.0×10
45	8.27	1.21×10^7	3.0×10
60	8.27	1.21×10^7	2.0×10

TABLE 27. DYNAMIC CREEP DATA FOR DRILLED CORES
FULLY LOADED F-15 SECTION 2

Station A 0+95 Thickness of ACC = 5.99 in.

Elapsed Time (sec.)	Unit Strain ($\times 10^{-3}$ in/in)	S_{mix} (N/m^2)	S_{bit} (N/m^2)
10	1.73	5.78×10^7	4.0×10^3
50	2.41	4.15×10^7	1.0×10^3
100	2.80	3.57×10^7	5.0×10^2
500	3.85	2.60×10^7	1.0×10^2
1000	4.56	2.19×10^7	5.0×10
3600	7.03	1.42×10^7	2.0×10

TABLE 28. DYNAMIC CREEP DATA FOR DRILLED CORES
FULLY LOADED F-15 SECTION 3

Elapsed Time (sec.)	Unit Strain ($x10^{-3}$in/in)	S_{mix} (N/m^2)	S_{bit} (N/m^2)
Station A 2+13		Thickness of ACC = 6.39 in.	
10	1.19	8.40×10^7	4.0×10^3
50	2.62	3.82×10^7	1.0×10^3
100	3.52	2.84×10^7	5.0×10^2
500	6.06	1.65×10^7	1.0×10^2
1000	7.68	1.30×10^7	5.0×10
3600	10.44	9.58×10^6	2.0×10
Station A 2+57		Thickness of ACC = 6.75 in.	
10	1.25	8.03×10^7	4.0×10^3
50	1.99	5.03×10^7	1.0×10^3
100	2.38	4.20×10^7	5.0×10^2
500	3.52	2.84×10^7	1.0×10^2
1000	4.14	2.42×10^7	5.0×10
3600	6.22	1.61×10^7	2.0×10
Station A 3+00		Thickness of ACC = 6.38 in.	
10	0.93	1.073×10^8	4.0×10^3
50	2.24	4.464×10^7	1.0×10^3
100	3.01	3.322×10^7	5.0×10^2
500	4.69	2.132×10^7	1.0×10^2
1000	5.80	1.724×10^7	5.0×10
3600	7.52	1.33×10^7	2.0×10

TABLE 29. DYNAMIC CREEP DATA FOR DRILLED CORES
FULLY LOADED F-15 SECTION 4

Elapsed Time (sec.)	Unit Strain ($x10^{-3}$in/in)	S_{mix} (N/m^2)	S_{bit} (N/m^2)
Station A 3+84		Thickness of ACC = 6.15 in.	
10	0.53	1.89×10^8	4.0×10^2
50	0.86	1.16×10^8	1.0×10^3
100	0.95	1.05×10^8	5.0×10^2
500	1.56	6.41×10^7	1.0×10^2
1000	2.12	4.72×10^7	5.0×10
3600	5.10	1.96×10^7	2.0×10
Station A 4+15		Thickness of ACC = 6.39 in.	
10	0.72	1.38×10^8	4.0×10^3
50	1.06	9.43×10^7	1.0×10^3
100	1.27	7.87×10^7	5.0×10^2
500	2.04	4.89×10^7	1.0×10^2
1000	2.67	3.74×10^7	5.0×10
3600	6.07	1.65×10^7	2.0×10

TABLE 30. DYNAMIC CREEP DATA FOR DRILLED CORES
FULLY LOADED F-15 SECTION 5

Station A 4+97 Thickness of ACC = 5.86 in.

Elapsed Time (sec.)	Unit Strain ($\times 10^{-3}$ in/in)	S_{mix} (N/m^2)	S_{bit} (N/m^2)
10	0.86	1.16×10^8	4.0×10^3
50	1.31	7.63×10^7	1.0×10^3
100	1.55	6.45×10^7	5.0×10^2
500	2.21	4.52×10^7	1.0×10^2
1000	2.68	3.73×10^7	5.0×10
3600	3.93	2.55×10^7	2.0×10

TABLE 31. DYNAMIC CREEP DATA FOR DRILLED CORES
UNARMED F-15 SECTION 8

Station C 0+95 Thickness of ACC = 6.21 in.

Elapsed Time (sec.)	Unit Strain ($x10^{-3}$in/in)	S_{mix} (N/m^2)	S_{bit} (N/m^2)
10	1.62	6.17×10^7	4.0×10^3
50	2.49	4.02×10^7	1.0×10^3
100	2.96	3.38×10^7	5.0×10^2
500	4.24	2.36×10^7	1.0×10^2
1000	5.00	2.00×10^7	5.0×10
3600	6.94	1.44×10^7	2.0×10

TABLE 32. DYNAMIC CREEP DATA FOR DRILLED CORES
UNARMED F-15 SECTION 9

Elapsed Time (sec.)	Unit Strain ($x10^{-3}$in/in)	S_{mix} (N/m^2)	S_{bit} (N/m^2)
Station C 2+13		Thickness of ACC = 6.47 in.	
10	1.99	5.02×10^7	4.0×10^3
50	3.02	3.31×10^7	1.0×10^3
100	3.54	2.82×10^7	5.0×10^2
500	4.87	2.05×10^7	1.0×10^2
1000	5.75	1.74×10^7	5.0×10
3600	8.07	1.24×10^7	2.0×10
Station C 2+57		Thickness of ACC = 6.30 in.	
10	1.91	5.22×10^7	4.0×10^3
50	3.12	3.12×10^7	1.0×10^3
100	3.82	2.62×10^7	5.0×10^2
500	5.66	1.77×10^7	1.0×10^2
1000	6.68	1.50×10^7	5.0×10
3600	9.24	1.08×10^7	2.0×10

TABLE 33. DYNAMIC CREEP DATA FOR DRILLED CORES
UNARMED F-15 SECTION 10

Elapsed Time (sec.)	Unit Strain ($\times 10^{-3}$ in/in)	S_{mix} (N/m^2)	S_{bit} (N/m^2)
Station C 3+69		Thickness of ACC = 6.25 in.	
10	1.42	7.04×10^7	4.0×10^3
50	2.18	4.59×10^7	1.0×10^3
100	2.58	3.88×10^7	5.0×10^2
500	3.77	2.65×10^7	1.0×10^2
1000	4.43	2.26×10^7	5.0×10
3600	6.31	1.58×10^7	2.0×10
Station C 4+15		Thickness of ACC = 6.53 in.	
10	1.35	7.41×10^7	4.0×10^3
50	2.37	4.22×10^7	1.0×10^3
100	2.97	3.37×10^7	5.0×10^2
500	4.82	2.07×10^7	1.0×10^2
1000	5.91	1.69×10^7	5.0×10
3600	9.57	1.04×10^7	2.0×10

TABLE 34. DYNAMIC CREEP DATA FOR DRILLED CORES
UNARMED F-15 SECTION 11

Station C 4+97 Thickness of ACC = 6.08 in.

Elapsed Time (sec.)	Unit Strain ($x10^{-3}$in/in)	S_{mix} (N/m^2)	S_{bit} (N/m^2)
10	1.02	9.80×10^7	4.0×10^3
50	1.63	6.13×10^7	1.0×10^3
100	2.01	4.98×10^7	5.0×10^2
500	3.44	2.91×10^7	1.0×10^2
1000	4.58	2.18×10^7	5.0×10
3600	10.98	9.11×10^6	2.0×10

TABLE 35. OTHER PERTINENT DATA*

Property of Asphalt Cement:

Type of asphalt cement used:	AC-20
Softening point:	128°F or 53.3°C
Penetration index:	-0.082

Modulus of Elasticity:

E_1	= 5.91×10^4 psi	(Marshall cores)
E_1	= 9.87×10^4 psi	(Gyratory cores)
E_2	= 4.60×10^6 psi	(Portland Cement Concrete)
E_2	= 8.00×10^4 psi	(Aggregate base)

Time of Loading (t_o):

Fully Loaded F-15C/D

Wheel load = 29,500 lbs.
Tire pressure = 355 psi = 2.448×10^6 N/m²
Area of tire impact = 29,500/355 = 83 in².
Equivalent radius of tire print:
πR^2 = 83 in².
R = 5.1 in.

Actual tire imprint:
Width of tire imprint = 7.75 in.
Length of tire imprint = 14.5 in. = 1.21 ft.
Average wheel speed = 11 mph = 16.13 ft./sec.
Time of loading (t_o) = 0.075 sec.

Unarmed F-15C/D

Wheel load = 19,500 lbs.
Tire pressure = 195 psi = 1.345×10^6 N/m²
Area of tire impact = 19,000/195 = 97 in².
Equivalent radius of tire print:
πR^2 = 97 in².
R = 5.6 in.

Actual tire imprint:
Width of tire imprint = 7.35 in.
Length of tire imprint = 14.3 in. = 1.19 ft.
Average wheel speed = 11 mph = 16.13 ft./sec.
Time of loading (t_o) = 0.074 sec.

* Data furnished by the Air Force.

TABLE 36. COMPARISON OF RUT DEPTH PREDICTIONS AND FIELD MEASUREMENTS AT VARIOUS NUMBER OF WHEEL PASSES FOR FULLY LOADED F-15 SECTION 3

Station	Passes Over Peak Rut Location	Static Cores (in.)	Static Specimens (in.)	Dynamic Cores (in.)	Field* Measurements (in.)
A 2+12	100	0.512	0.479	0.071	0.150
A 2+12	206	0.543	0.505	0.079	0.253
A 2+12	326	0.565	0.523	0.097	0.201
A 2+12	607	0.588	0.552	0.124	0.367
A 2+12	841	0.598	0.560	0.135	0.557
A 2+12	967	0.608	0.569	0.149	0.742
A 2+12	1137	0.619	0.574	0.160	0.990
A 2+12	1263	0.624	0.578	0.167	1.589
A 2+12	1356	0.629	0.588	0.172	1.583
A 2+60	98	0.620	0.611	0.065	0.159
A 2+60	203	0.647	0.642	0.082	0.375
A 2+60	285	0.664	0.659	0.092	0.309
A 2+60	588	0.701	0.689	0.111	0.383
A 2+60	816	0.721	0.708	0.122	0.576
A 2+60	981	0.728	0.715	0.128	0.846
A 2+60	1169	0.742	0.721	0.135	0.625
A 2+60	1173	0.742	0.721	0.135	0.773
A 2+60	1319	0.746	0.743	0.140	0.737
A 3+00	90	0.786	0.742	0.053	0.190
A 3+00	230	0.863	0.786	0.076	0.240
A 3+00	368	0.895	0.814	0.087	0.167
A 3+00	510	0.918	0.832	0.102	0.383
A 3+00	742	0.942	0.852	0.118	0.517
A 3+00	946	0.967	0.867	0.128	0.600
A 3+00	1330	0.987	0.884	0.146	0.857
A 3+00	1515	0.995	0.893	0.153	0.383
A 3+00	1669	1.002	0.895	0.159	1.639

* Data furnished by the Air Force.

TABLE 37. COMPARISON OF RUT DEPTH PREDICTIONS AND FIELD MEASUREMENTS AT VARIOUS NUMBER OF WHEEL PASSES FOR FULLY LOADED F-15 SECTION 4

Station	Passes Over Peak Rut Location	Static Cores (in.)	Static Specimens (in.)	Dynamic Cores (in.)	Field* Measurements (in.)
A 3+86	97	0.483	0.469	0.020	0.073
A 3+86	340	0.525	0.503	0.032	0.080
A 3+86	501	0.539	0.519	0.037	0.243
A 3+86	529	0.539	0.519	0.038	0.150
A 3+86	659	0.548	0.527	0.041	0.235
A 3+86	952	0.566	0.531	0.048	0.347
A 3+86	1041	0.570	0.533	0.049	0.312
A 3+86	1263	0.575	0.539	0.053	0.330
A 3+86	1523	0.585	0.548	0.057	0.335
A 3+86	1869	0.595	0.552	0.061	0.348
A 3+86	2563	0.611	0.561	0.068	0.325
A 4+10	188	0.478	0.509	0.040	0.172
A 4+10	365	0.509	0.527	0.048	0.138
A 4+10	622	0.523	0.543	0.057	0.172
A 4+10	765	0.539	0.547	0.062	0.237
A 4+10	965	0.548	0.556	0.067	0.276
A 4+10	1008	0.552	0.552	0.068	0.210
A 4+10	1104	0.557	0.560	0.071	0.321
A 4+10	1499	0.565	0.569	0.078	0.330
A 4+10	1826	0.573	0.574	0.083	0.338
A 4+10	2385	0.578	0.583	0.091	0.324
A 4+10	2477	0.588	0.585	0.093	0.329
A 4+40	75	0.416	0.421		0.153
A 4+40	221	0.464	0.437		0.142
A 4+40	329	0.484	0.444		0.115
A 4+40	453	0.498	0.449		0.176
A 4+40	683	0.518	0.455		0.209
A 4+40	821	0.525	0.464		0.298
A 4+40	961	0.534	0.466		0.295
A 4+40	1150	0.543	0.471		0.273
A 4+40	1434	0.557	0.477		0.318
A 4+40	1693	0.565	0.481		0.325
A 4+40	2048	0.575	0.485		0.338
A 4+40	2052	0.575	0.485		0.341

* Data furnished by the Air Force.

TABLE 38. RUT DEPTH PREDICTIONS AT VARIOUS NUMBER OF WHEEL PASSES FOR UNARMED F-15 SECTION 9

Station	Passes Over Peak Rut Location	Static		Dynamic
		Cores (in.)	Specimens (in.)	Cores (in.)
C 2+13	250	0.570	0.411	0.090
	500	0.597	0.429	0.109
	750	0.611	0.440	0.119
	1000	0.626	0.448	0.132
	1250	0.631	0.456	0.139
	1500	0.638	0.460	0.147
C 2+57	250	0.580	0.361	0.086
	500	0.602	0.381	0.105
	750	0.613	0.390	0.116
	1000	0.625	0.396	0.129
	1250	0.633	0.403	0.137
	1500	0.641	0.406	0.146
C 2+85	250	0.646	0.371	
	500	0.705	0.388	
	750	0.727	0.399	
	1000	0.750	0.404	
	1250	0.775	0.412	
	1500	0.788	0.417	

TABLE 39. RUT DEPTH PREDICTIONS AT VARIOUS NUMBER OF WHEEL PASSES FOR UNARMED F-15 SECTION 10

Station	Passes Over Peak Rut Location	Static Cores (in.)	Static Specimens (in.)	Dynamic Cores (in.)
C 3+25	250	0.254	0.332	
	500	0.274	0.342	
	750	0.289	0.347	
	1000	0.300	0.352	
	1250	0.306	0.355	
	1500	0.310	0.358	
C 3+69	250	0.351	0.321	0.064
	500	0.364	0.334	0.077
	750	0.375	0.344	0.086
	1000	0.384	0.347	0.091
	1250	0.391	0.352	0.099
	1500	0.395	0.356	0.103
C 4+15	250	0.452	0.297	0.059
	500	0.468	0.306	0.075
	750	0.482	0.312	0.088
	1000	0.491	0.314	0.098
	1250	0.496	0.316	0.106
	1500	0.501	0.318	0.114